OPTIMIZATION OF TYPES, NUMBERS AND LOCATIONS OF SENSORS AND ACTUATORS USED IN MODAL ANALYSIS OF AIRCRAFT STRUCTURES USING GENETIC ALGORITHM

A THESIS SUBMITTED TO
THE GRADUATE SCHOOL OF NATURAL AND APPLIED SCIENCES
OF
MIDDLE EAST TECHNICAL UNIVERSITY

BY
NIMA PEDRAMASL

IN PARTIAL FULFILLMENT OF THE REQUIREMENTS
FOR
THE DEGREE OF MASTER OF SCIENCE
IN
AEROSPACE ENGINEERING

January 2017

Approval of the thesis:

OPTIMIZATION OF TYPES, NUMBERS AND LOCATIONS OF SENSORS AND ACTUATORS USED IN MODAL ANALYSIS OF AIRCRAFT STRUCTURES USING GENETIC ALGORITHM

Submitted by NIMA PEDRAMASL in partial fulfillment of the requirements for the degree of Master of Science in Aerospace Engineering Department, Middle East Technical University by,

Prof. Dr. Gülbin Dural Ünver
Dean, Graduate School of Natural and Applied Sciences ____________________

Prof. Dr. Ozan Tekinalp
Head of Department, Aerospace Engineering ____________________

Assoc. Prof. Dr. Melin Şahin
Supervisor, Aerospace Engineering Dept., METU ____________________

Assoc. Prof. Dr. Erdem Acar
Co-Supervisor, Mechanical Engineering Dept., TOBB ETU ____________________

Examining Committee Members:

Prof. Dr. Yavuz Yaman
Aerospace Engineering Dept., METU ____________________

Assoc. Prof. Dr. Melin Şahin
Aerospace Engineering Dept., METU ____________________

Assoc. Prof. Dr. Erdem Acar
Mechanical Engineering Dept., TOBB ETU ____________________

Asst. Prof. Dr. Ercan Gürses
Aerospace Engineering Dept., METU ____________________

Prof. Dr. Mehmet A. Güler
Mechanical Engineering Dept., TOBB ETU ____________________

Date: 26/01/2017

I hereby declare that all the information in this document has been obtained and presented in accordance with academic rules and ethical conduct. I also declare that, as required by these rules and conduct, I have fully cited and referenced all material and results that are not original to this work.

Name, Last Name: NIMA PEDRAMASL

ABSTRACT

OPTIMIZATION OF TYPES, NUMBERS AND LOCATIONS OF SENSORS AND ACTUATORS USED IN MODAL ANALYSIS OF AIRCRAFT STRUCTURES USING GENETIC ALGORITHM

PEDRAMASL, Nima
M.Sc., Department of Aerospace Engineering
Supervisor : Assoc. Prof. Dr. Melin ŞAHIN
Co-Supervisor : Assoc. Prof. Dr. Erdem ACAR

January 2017, 126 pages

Aircraft structures are exposed to dynamic loads under service conditions and therefore, it is necessary to determine their dynamic characteristics. Dynamic characteristics of a structure can be determined using simulation-based methods such as finite element analysis (FEA) or test-based methods such as experimental modal analysis (EMA). In order to perform an EMA with reliable and high quality results, test equipment must be lightweight and have high accuracy. In addition, the sensors and actuators must be positioned in an optimum pattern to extract dynamic characteristics (e.g., natural frequencies, mode shapes) of structure as correct as possible. In this study, a trapezoidal fin-like structure and an Unmanned Aerial Vehicle (UAV) wing are used as test structures, and it is aimed to find the optimum locations, types and numbers of transducers used in modal test which result in minimum mass loading error in natural frequency predictions, minimum mode shape observability error, minimum exciter errors (double hit with impact hammer and shaker-structure interaction with modal shaker) and minimum total sensor and actuator cost using a multi-objective optimization approach. The multi-objective genetic algorithm (MOGA) solver of the Global Optimization Toolbox in MATLAB is utilized to solve optimization problem. MSC©NASTRAN finite element solver is utilized to predict dynamic characteristics the structure. It is found that minimization of the mass loading error is achieved by locating the sensors near areas with minimum modal constant in all modes of interest and near clamped region of structures. It is also found that minimization of mode shape observability error is obtained by locating the sensors to the points with large displacements and avoiding nodal lines. With the inclusion of the optimum driving point error, the optimization results for the total error are also presented and validated with the experimental modal analyses.

Keywords: Modal Test, Pre-test Planning, Fin-like Structure, Genetic Algorithm, Multi-Objective Optimization, Pareto Frontier Curves

ÖZ

UÇAK YAPILARININ MODAL ANALİZLERİNDE KULLANILACAK ALGILAYICI VE UYARICILARIN TİP, ADET VE KONUMLARININ GENETİK ALGORİTMA İLE OPTİMİZASYONU

PEDRAMASL, Nima
Yüksek Lisans, Havacılık ve Uzay Mühendisliği Bölümü
Tez Yöneticisi : Doç.Dr. Melin Şahin
Yardımcı Tez Yöneticisi: Doç.Dr. Erdem Acar

Ocak 2017, 126 sayfa

Uçak yapıları gerçek çalışma koşulları altında dinamik yüklere maruz kalmakta ve bu nedenle tasarımlarının yapılabilmesi için dinamik özelliklerinin belirlenmesi gerekmektedir. Yapının dinamik özellikleri sonlu elemanlar yöntemi gibi benzetim tabanlı yöntemler kullanılarak tahmin edilebileceği gibi, deneysel modal analizi (DMA) teknikleri uygulanarak da belirlenebilir. Bir DMA sisteminin yapının dinamik performansı üzerinde olumsuz etkisinin olmaması için, bu sistemin hafif ve güvenilir olması gerekmektedir. Ayrıca, yapının dinamik karakteristiklerinin en doğru şekilde belirlenebilmesi için, sistemdeki algılayıcıların ve uyarıcının yapıya optimum şekilde yerleştirilmiş olması gerekmektedir. Literatürde DMA sistemlerindeki algılayıcıların yapıya optimum şekilde yerleştirilmesi üzerine birçok çalışma bulunmaktadır. Bu çalışmalarda çoğunlukla algılayıcı/uyarıcı verilerindeki hataların en küçültülmesi amaçlanmış olup, çoğunlukla algılayıcı tipleri önceden belirlenerek adetleri ve

konumları optimize edilmiştir. Ancak, proje yöneticisinin ve araştırmacısının bilgisi dahilinde, bir DMA sistemindeki algılayıcıların tiplerinin, adetlerinin ve konumlarının eşzamanlı olarak belirlenmesi üzerine bir çalışma bulunmamaktadır. Bu projede, DMA sistemlerindeki algılayıcıların tiplerinin, adetlerinin ve konumlarının eşzamanlı optimizasyonu gerçekleştirilecek, böylelikle literatürdeki kritik bir boşluk dolduracaktır. Ayrıca, literatürdeki çalışmalarda, optimizasyon problemindeki amaç fonksiyonu algılayıcı/uyarıcı verilerindeki hatayı karakterize eden bir metrik olup, bu hata metriğinin en küçüklenmesi amaçlanmıştır. Bu projede, amaç fonksiyonu olarak hem algılayıcı/uyarıcı verilerindeki hata hem de algılayıcı/uyarıcı maliyeti kullanılmak üzere Pareto eniyi tasarımlar elde edilerek literatüre katkıda bulunulacaktır. Projede karmaşıklık derecesi giderek artan uçak yapıları ele alınacak, bu yapıların dinamik özelliklerinin belirlenmesinde kullanılan DMA sistemindeki algılayıcıların/uyarıcıların adetleri, tipleri ve konumları eşzamanlı olarak optimizasyon yöntemleriyle belirlenecektir. Yapının dinamik özellikleri MSC/Nastran sonlu elemanlar programları ile belirlenecektir. Optimizasyon probleminin çözümünde MATLAB Global Optimizasyon Araç kutusu içindeki çok-amaçlı genetik algoritma MOGA çözücüsü kullanılacaktır. Elde edilen optimizasyon sonuçları deneysel modal analiz yapılarak da doğrulanacaktır.

Anahtar Kelimeler: Modal Test, Deney Öncesi Planlama, Kanat Gibi Yapı, Genetik Algoritma, Çok Amaçlı Optimizasyon, Pareto Sınır Eğrileri

To my family and friends

ACKNOWLEDGEMENTS

I would like to express my deepest gratitude to my supervisor Assoc. Prof. Dr. Melin Şahin and Co-Supervisor Assoc. Prof. Dr. Erdem Acar for their guidance, support, encouragement and criticism. I also appreciate Asst. Prof. Dr. Tuncay Yalçinkaya for providing extra computational power for this study.

I would also want to thank my friends Onur Akın, İlhan Ozan Tüncoz, Yoseph Yang, Chadi Amer, Yunus Tansu Aksoy, Harun Tıraş, Uğur Kalkan, Ramin Rouzbar, Pınar Arslan, Kourosh Ghahramanimarangalou, Burak Pehlivan and Erdal Bozkurt for their support during my master study and for their awesome friendship which worth more than anything. Last but not least, my family. They were always there for me no matter what.

I also gratefully acknowledge the funding provided by The Scientific and Technological Research Council of Turkey (TUBITAK) with project 112M845.

TABLE OF CONTENTS

LIST OF TABLES

LIST OF FIGURES

LIST OF SYMBOLS

EMA	Experimental modal analysis
$F(\omega)$	Force in frequency domain
FEM	Finite element model
h	Structural damping
i	Imaginary number
k	Stiffness
m	Mass
$X(t)$	Displacement (time domain)
$X(\omega)$	Displacement (frequency domain)
$\dot{X}(t)$	Velocity (time domain)
$\dot{X}(\omega)$	Velocity (frequency domain)
$\ddot{X}(t)$	Acceleration (time domain)
$\ddot{X}(\omega)$	Acceleration (frequency domain)
$\alpha(\omega)$	Receptance
ω	Frequency
$\emptyset_R$	Mass normalized modal matrix of reduced FEM
$\emptyset_F$	Mass normalized modal matrix of full FEM

LIST OF ABBREVIATIONS

FEA	Finite Element Analysis
FEM	Finite Element Model
IH	Impact Hammer
METU	Middle East Technical University
ML	Mass Loading
MSO	Mode Shape Observability
ODP	Optimum Driving Point
UAV	Unmanned Aerial Vehicle

CHAPTER 1

INTRODUCTION

1.1 Motivation of the Study

In an aircraft design, there are several disciplines which are applied to get best performance with minimum energy consumption. The major ones are aerodynamic performance, control stability and structural integrity. In structural integrity there are two major analysis parts. One is static analysis and the other is dynamic analysis. In dynamic analysis, the structure of aircraft is evaluated for several different performance criteria. One of them is to avoid excessive vibration which can damage structure and degrade handling quality of aircraft when structure is under operational loads (e.g. during flight). These loads in case of aircraft are mostly aerodynamic loads. Therefore structure is designed in a way which it its local and global modal frequencies are away from frequency spectrum of operational loads during flight. Conceptual design which is done using computer aided design/engineering (CAD, CAE) software packages and this design is analyzed for its dynamic characteristics using finite element analysis (FEA) packages. After applying an iterative process in which structure topology and materials are optimized for better dynamic characteristics, a final optimized model is obtained. In final stage optimized model is used to create a prototype of final structure and a ground vibration test is performed on prototype to verify and validate finite element results.

Test engineers usually face with problems during test phase which are listed as follows. Distributing transducers over areas which affect modal masses of structure in a minimum way. (This leads to minimum error in resonance frequency extraction from test results)

Placing transducers over areas which will capture all mode shapes of interest.
Getting all of required high quality test data with minimum time spent and minimum transducers used in test. (This means lower test costs)
All of these problems are discussed and solved in this thesis study.

1.2 Layout of the Study

Chapter 2 begins with a literature study and shows similar studies which are done in literature by other researchers. It also shows that how this study is different from other studies done in literature.

Chapter 3 gives a mathematical background of methods and concepts which are discussed and used in this study. It starts with describing what is pre-test analysis and concepts which are studied in this analysis. After that it gives a brief introduction to finite element model reduction technique which is utilized in this study. In this study there two test structures which are used to test validity of developed algorithms and codes.

In Chapter 4, fin-like trapezoidal plate geometrical dimensions, material properties are described. Its mesh convergence analysis, finite element analysis and modal test are also explained. At the end of chapter finite element model was updated to ensure that it represents real structure correctly.

Chapter 5 explains all of multi objective optimization components in this study which are objective functions, constraint functions and design variables. It gives an in depth explanation of optimization cases which were performed and the obtained final results.

Chapter 6 verifies the validity of numerical results obtained in chapter 5 by performing a classical modal analysis. It compares results of different optimization cases which are obtained in previous chapters.

In Chapter 7, same pipeline in chapter 4 was followed for the second test structure which is wing of an unmanned aerial vehicle (UAV). Chapter 8 and 9 are same as chapter 5 and 6 but test structure is UAV wing.

Finally, in Chapter 10 the concluding marks of this study are explained and possible further development paths of this study are also mentioned.

CHAPTER 2

LITERATURE SURVEY

2.1 Literature Review

In literature, studies related to finding optimum location of transducers in modal test can be traced back to the end of 1970s. Shah and Udwadia [1] assumed that the error in prediction of dynamic parameters of a system follows Gaussian distribution. They also assumed that correlation between errors of transducers was proportional to distance between them, and the mean value of error was taken as zero. They constructed a correlation matrix which embed correlated error between transducers. Using a random search optimization algorithm, a norm (trace, determinant, etc.) of this matrix was minimized for a given number and types of transducers. The other works done in 1990s, instead of correlated error matrix Fisher information matrix was used in optimization and a norm of this matrix (trace, determinant, etc.) was maximized, because maximum norm value of Fisher information matrix corresponds to minimum norm value of correlated error matrix for optimum location of transducers. While Kammer [2], Yao [3] and Udwadia [4] did not include the correlated error between transducers, Kirkegaard and Brinckera [5] included transducers' correlated error in their optimization. Kammer [2], Udwadia [4] and Kirkegaard and Brinkcker [5] used local search optimization algorithm, whereas Yao [3] used genetic algorithm. Based on Fisher information matrix, there were two commonly used methods which were effective independence (EI) and modal kinetic energy (MKE). In effective independence method the effect of transducers location on orthogonality of interested mode shapes was studied and in modal kinetic energy, the amount of added kinetic energy to modes of interest by transducers' location was studied. Penny [6] compared the Fisher information matrix and Guyan reduction methods and found that Fisher information matrix was more effective. In all of above studies, it was tried to find optimal location of a specific set of transducers and there were no functional relation between modal characteristics of structure with the type or number of transducers. Even though most of these studies used genetic algorithm for optimization, particle swarm optimization (PSO) method was also used. There also exist other studies where a hybrid optimization algorithm was used. For example, Rao and Anandakumar [7] used PSO as global optimization routine and Nelder-Mead method as local optimization routine.

In all of above studies dynamic characteristics of structure were found using fully analytical or semi analytical methods. There also exist other studies that used finite element solver. Langehove and Brughmans [8] used MSC©NASTRAN and LMS/PRETEST software packages to find optimal location of transducers over NASA’s X33 suborbital spaceplane. Similarly, Peck and Torrers [9] used DMAP (Direct Matrix Abstraction Program) which is scripting language of MSC©NASTRAN. They used effective independence and average kinetic energy methods to reduce number of initial candidate transducers’ location to optimum ones. In literature, usually it was tried find optimum location for a set of candidate transducer location. Types of transducers has also importance on quality of measured data. For example, using a tri-axial accelerometer may correspond to using three uniaxial accelerometers to capture desired mode shape. In this way mass loading error of transducers could be reduced due to the use of one instead of three transducers. Selection of transducer type also helps in using high quality accelerometers which have lower biased error in their readings.

2.2 Objectives of This Study

To the best of the author's knowledge, the sensor positioning studies in literature have been focused on optimal positioning of a given number of sensors of given type, whereas simultaneous optimization of the number of sensors, sensor types and sensor positions have not been investigated. The main objective of this study is to fill this gap in literature. To simplify the analysis, the error in prediction of the dynamic characteristics of the structure is limited to the mass loading error (error in the predictions of the first three natural frequencies of the structure caused by the sensor mass) and mode shape observability error in this study. The paper is structured as follows. The importance of pre-test analysis in modal testing is discussed first and a brief introduction to theoretical concepts is given. Next, finite element analysis (FEA) of the fin-like structure is presented. In finite element model, transducers are modelled as lumped mass over nodes. Since FEA solutions does not usually represent dynamic characteristics of modelled structure exactly, a modal test is performed to validate FEA results. Using FEA results and test results, a correlation analysis is performed to evaluate reliability of numerical model.

Due to some discrepancies between numerical and test models, a model updating is performed to increase the accuracy of the numerical model. Then, design variables, objective and constraint functions used in optimization problem are defined. Since optimization requires repeated generation of the finite element model many times, a script is developed in MATLAB [10] which is capable of handling communications between the optimizer (MATLAB genetic algorithm toolbox module) and finite element solver (MSC©NASTRAN [11]). To speed-up the optimization process, a parallel processing algorithm is also implemented using distributed computing toolbox in MATLAB. To validate results obtained thorough optimization, modal tests are performed for various selected optimum configurations over Pareto frontier set. Finally, the paper culminates with concluding remarks followed by potential future research directions.

CHAPTER 3

THEORY

This chapter will give a brief theoretical introduction to topics mentioned in following chapters.

3.1 Pretest Analysis

In a modal test, location of excitation, suspension and measurement on the structure have a vital importance in quality of test results. Therefore, before performing a modal test, it is required to find optimum locations. Considering the motion equation of a structure with hysteresis damping model in time domain and assuming that the response would be harmonic for a linear structure when the excitation given to the structure is harmonic, the receptance ($\alpha(\omega)$) can be shown in Equation 1.

$$\alpha(\omega) = \frac{X(\omega)}{F(\omega)} = \frac{1}{-m\omega^2 + i\omega h + k} \tag{1}$$

Where X and F are the displacement and force vectors in frequency domain respectively, m is the mass, h is the hysteresis damping and k is the stiffness matrices and ω is the excitation frequency.

The receptance matrix can also be written in terms of mass normalized eigenvectors (ϕ_{jr})and the system natural frequencies (ω_r) in Equation 2.

$$\alpha_{jk}(\omega) = \sum_{r=1}^{m} \frac{\phi_{jr}\phi_{kr}}{\omega_r^2 - \omega^2 + ih\omega_r\omega} \tag{2}$$

If a structure is excited around one of its natural frequencies, response of structure would be mostly dominated by that mode term in receptance so its approximate response is as following (Equation 3).

$$X(\omega_r) = \alpha(\omega_r)F(\omega_r) \cong \frac{\phi_{jr}\phi_{kr}}{ih\omega_r^2}F(\omega_r) \tag{3}$$

From Equation 3, it can be concluded that amplitude of response of a structure is proportional to modal matrix constants and frequencies at that mode (Equation 4).

$$X(\omega_r) \propto \frac{\phi_{jr}\phi_{kr}}{\omega_r^2} \tag{4}$$

From relation between displacement, velocity and acceleration following equations are also derived (Equation 5).

$$\begin{gathered} X(t) = X(\omega)e^{i\omega t}X(\omega_r) \propto \frac{\phi_{jr}\phi_{kr}}{\omega_r^2} \\ \dot{X}(t) = i\omega X(t)\dot{X}(\omega_r) \propto \frac{\phi_{jr}\phi_{kr}}{\omega_r} \\ \ddot{X}(t) = -\omega^2 X(t)\ddot{X}(\omega_r) \propto \phi_{jr}\phi_{kr} \end{gathered} \tag{5}$$

These response amplitudes can be summed for a set of interested modes. If response and measurement are at same location, average driving degree of freedom displacement (ADDOFD), velocity (ADDOFV) and acceleration (ADDOFA) [12-13] are derived respectively in Equation 6.

$$\begin{gathered} ADDOFD(j) = \sum_{r=1}^{m} \frac{\emptyset_{jr}^2}{\omega_r^2} \quad m = 1,2,3,..,n \ \ (modes\ of\ interest) \\ ADDOFV(j) = \sum_{r=1}^{m} \frac{\emptyset_{jr}^2}{\omega_r} \quad m = 1,2,3,..,n \ \ (modes\ of\ interest) \\ ADDOFA(j) = \sum_{r=1}^{m} \emptyset_{jr}^2 \quad m = 1,2,3,..,n \ \ (modes\ of\ interest) \\ \emptyset_{jr} = modal\ constant\ at\ jth\ DOF\ of\ rth\ mode \end{gathered} \tag{6}$$

3.1.1 Suspension Location

In a free-free test when a structure is suspended from locations near nodal lines of a particular mode, it does not restrain structure motion. Therefore to select optimum suspension locations, the minimum value of average driving degree of freedom displacement (ADDOFD) for all interested modes can be used. Since in this study plate is clamped from bottom edge, it is a fixed-free problem and there is no need for suspending structure.

3.1.2 Excitation Location

Energy transfer to a structure during modal test is done by exciting structure from single or multiple locations. There are three main aspects that must be taken into account while selecting excitation point; the frequency content of the force, the amplitude of the force, and avoiding the adverse effect of the excitation equipment on test results.

"The frequency content of the force" will ensure that all modes of interest are excited. With impact hammer this option can be controlled by selection of transducer head, namely; aluminum, plastic or rubber head. Since the impact force amplitude and bandwidth depend on stiffness of impact hammer head, there will be several wide band excitation with different frequency spectrum. Aluminum tip will have wider spectrum than plastic and rubber tips. But tester must be careful to not damage structure when high amplitude force is required. In the case of shaker, a sine sweep or white noise signal is used to excite structure within interested frequency spectrum.

"The amplitude of the applied force" will ensure the transfer of sufficient energy to structure. In case of energy transfer, it is good to excite structure from locations with highest modal constant (more of impact energy will be transferred into kinetic/strain energy rather than into heat and sound) in all modes of interest but this will have a downside which is double-hit or shaker-structure interaction. So it is a good practice to excite structure from locations close to nodal lines since these are regions with lowest velocity and acceleration. However, this requires forces with higher amplitude to deliver sufficient energy into structure.

The last but not the least is “the excitation equipment’s adverse effect on test results”. In case of impact hammer it is double hit issue which happens when exciting structure from locations with high velocity amplitude and in case of modal shaker it is structure-shaker interaction issue (force transducer attached to structure which introduce extra mass to system) which happens when exciting structure from locations with high acceleration amplitude.

Therefore it is a good approach to excite structure from regions near to nodal lines and this can achieved by finding the location with minimum average driving point velocity and acceleration and the contour plots of ADDOFV and ADDOFA are shown in Figure 1.

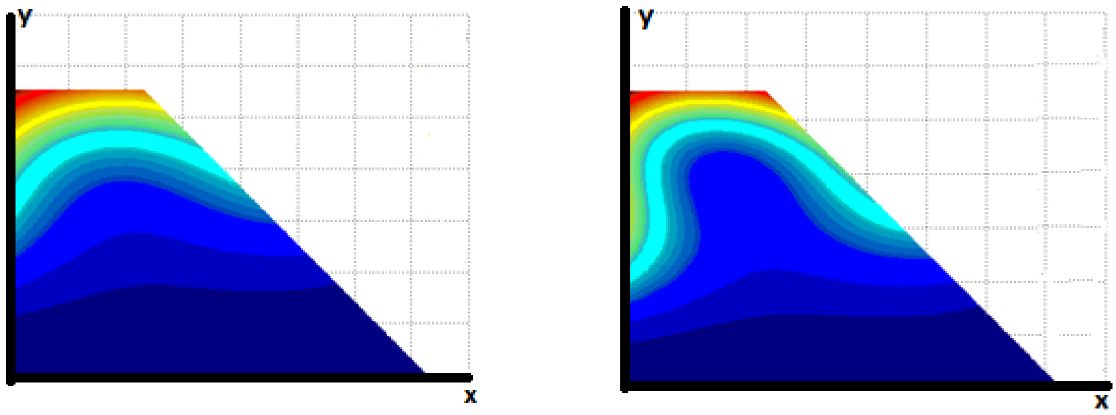

(a) (b)

Figure 1 Contour Plots for minimum (a) ADDOFV (b) ADDOFA

3.1.3 Measurement Location

Optimum locations of accelerometers on test structure provides test engineer with an advantage of being able to distinguish mode shapes of interest in minimum amount of time. Also it will ensure maximum signal to noise ratio. Usually locations on structure with highest acceleration (Figure 2) in all modes of interest will have highest signal to noise ratio. Therefore, maximum values of ADDOFA (Equation 6) can be used as an indicator to find optimum locations of accelerometers.

3.2 Finite Element Model Reduction

In order to validate or update a finite element model using a reference test model a correlation is performed beforehand. This correlation is possible if number of degrees of freedom of both finite element model (node points) and test model (test points) are same. Usually finite element model has more degrees of freedom than a test model. There are several techniques to reduce finite element model degrees of freedom or expand test model degrees of freedom. In this study, a FEM reduction technique used is called as Guyan reduction. Guyan or static reduction is a model reduction technique [14][15][16] which is suitable for static structural analysis. Because it assumes there is no acceleration (zero frequency), therefore inertial terms would automatically drop in the equation of a motion of a system. Damping is also dropped because it usually has negligible effect over natural frequencies (shift) and amplitude of response (decrease). Since in a reduction algorithm like Guyan, the number of DOF decreases, some DOF are retained (master DOF) and the rest are discarded (as slave DOF). Using the reduced stiffness and mass matrices, an eigenvalue problem can be solved in order to find natural frequencies and mode shapes of system. These results are usually a bit higher than the ones derived from original system and that is because of exclusion of inertial terms. Since in Guyan reduction inertial terms of equation of motion are dropped and it is assumed there is no loading on slave DOF, the accuracy of reduced finite element model is highly dependent on selection of locations of master DOF[17].

In the selection of master DOF, accuracy, completeness and the practicality should be considered accordingly. Accuracy is an assessment technique in which shows how exact are structure characteristics found from reduced finite element model (natural frequencies and mode shapes). Completeness is another assessment technique which checks whether all modes of interest are existent in reduced finite element model results. Neglecting some degrees of freedom may make some mode shapes not distinguishable in reduced FEM results. Occasionally some DOF are under load or their response is required. In that case those DOF must retained in master DOF set. An indicator which will ensure high accuracy and completeness of reduced FEM results is cross modal assurance criteria (xMAC) matrix (Equation 7) [18]. It is an indicator which checks correlation between two eigenvectors or modal matrices. If master DOF are placed on optimal locations, diagonal elements of xMAC matrix would be close to unity and off-diagonal close to zero which is a sign of completeness and high accuracy.

$$\text{Cross MAC Matrix} = \frac{|[\emptyset_{\mathrm{R}}]^T[\emptyset_{\mathrm{F}}]|^2}{|[\emptyset_{\mathrm{R}}]^T[\emptyset_{\mathrm{R}}]||[\emptyset_{\mathrm{F}}]^T[\emptyset_{\mathrm{F}}]|}$$

$$[\emptyset_{\mathrm{F}}] = \text{Mass Normalized Modal Matrix of Full FEM} \qquad (7)$$

$$[\emptyset_{\mathrm{R}}] = \text{Mass Normalized Modal Matrix of Reduced FEM}$$

CHAPTER 4

FIN-LIKE PLATE

Fin-like plates are usually used as devices to change direction of airflow to attain desired flight direction of an aircraft (e.g. vertical and horizontal stabilizers or control fins on missiles) in aerospace industry. Fin-like plates are lightweight and flexible which makes them more vulnerable to vibration problems. As a result when they are under excessive dynamic loads, they will have poor dynamic performance and may fail due to fatigue. In this paper, a 2 mm thick aluminum trapezoidal plate (Figure 2) is used as a test structure and its properties are listed in Table 1.

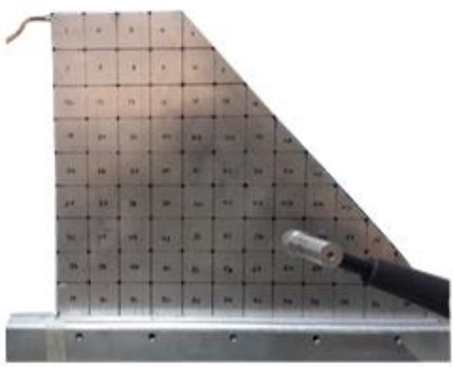

Figure 2 Fin-Like Plate Used In This Study

Table 1 Material Properties of Fin-like Plate

Material	Poisson Ratio	Density (kg/m3)	Youngs' Modulus (GPa)
Aluminum	0.33	2768	69

4.1 Numerical Model of Fin-Like Plate

4.1.1 Finite Element Modelling and Analysis

Plate structure is modelled and meshed using MSC©PATRAN [19] (Figure 3). Modal characteristics of the plate (i.e. the natural frequencies and the corresponding mode shapes) are determined by MSC©NASTRAN using SOL103 module and are shown in Figure 4. Mesher function is chosen as hybrid as on some areas on geometry of plate when mesher is unable to create QUAD shell elements with QUAD4 topology, it will create TRIA shell elements with TRI3 topology by avoiding QUAD4 elements with aspect ratio error. A mesh convergence analysis is also performed to obtain a fine enough mesh density with reasonable accuracy and computing time.

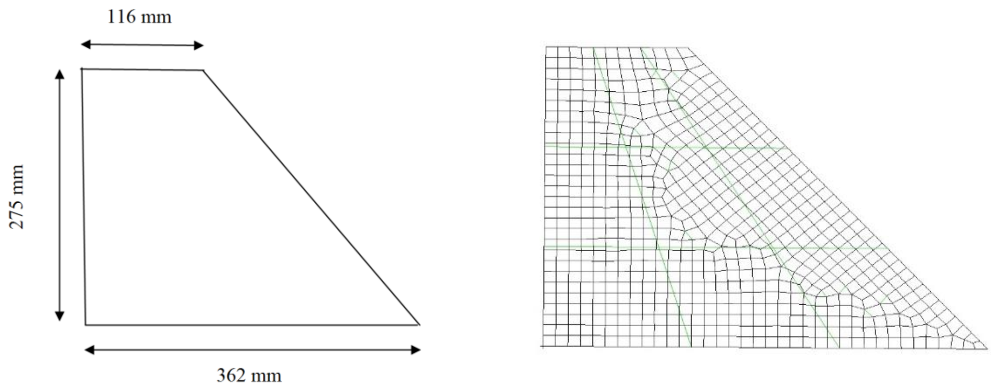

Figure 3 Dimensions of Fin-like Plate and the mesh used in MSC©PATRAN

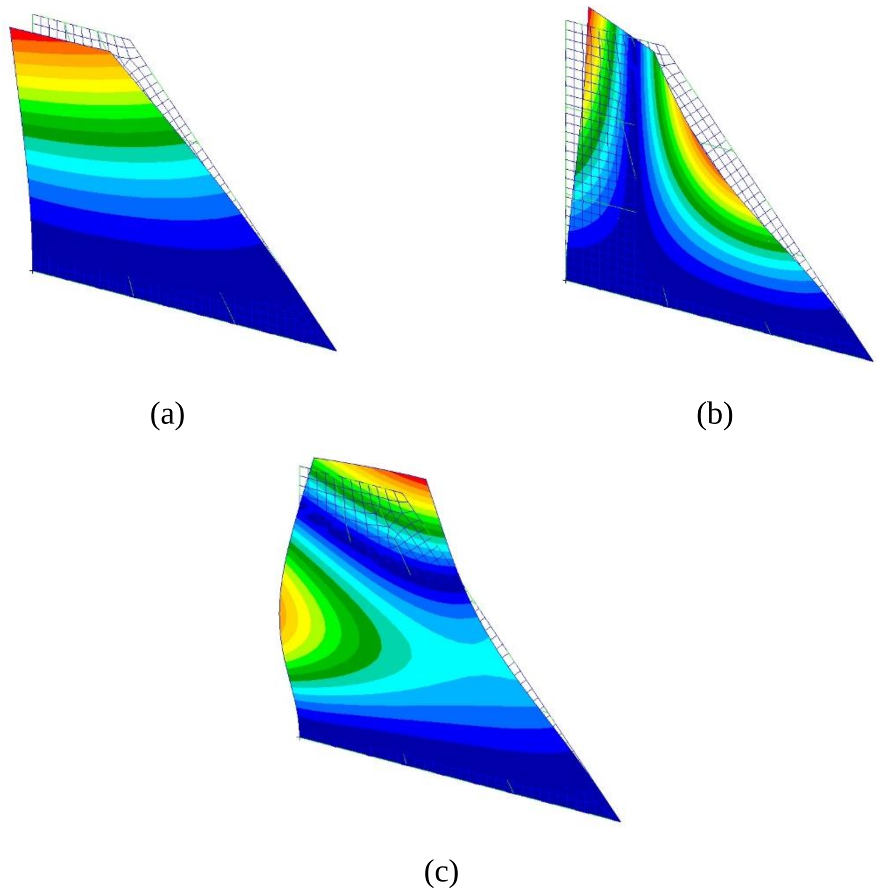

Figure 4 Mode Shapes obtained via FEA corresponding to (a) 1st Out-of-Plane Bending, (b) 1st Torsion, and (c) 2nd Out-of-Plane Bending

4.1.2 Mesh Convergence Analysis

A mesh convergence analysis is also performed to obtain a fine enough mesh density with reasonable accuracy and computing time. Different mesh densities are depicted in Figure 5 and mesh convergence analysis results are tabulated in Table 2.

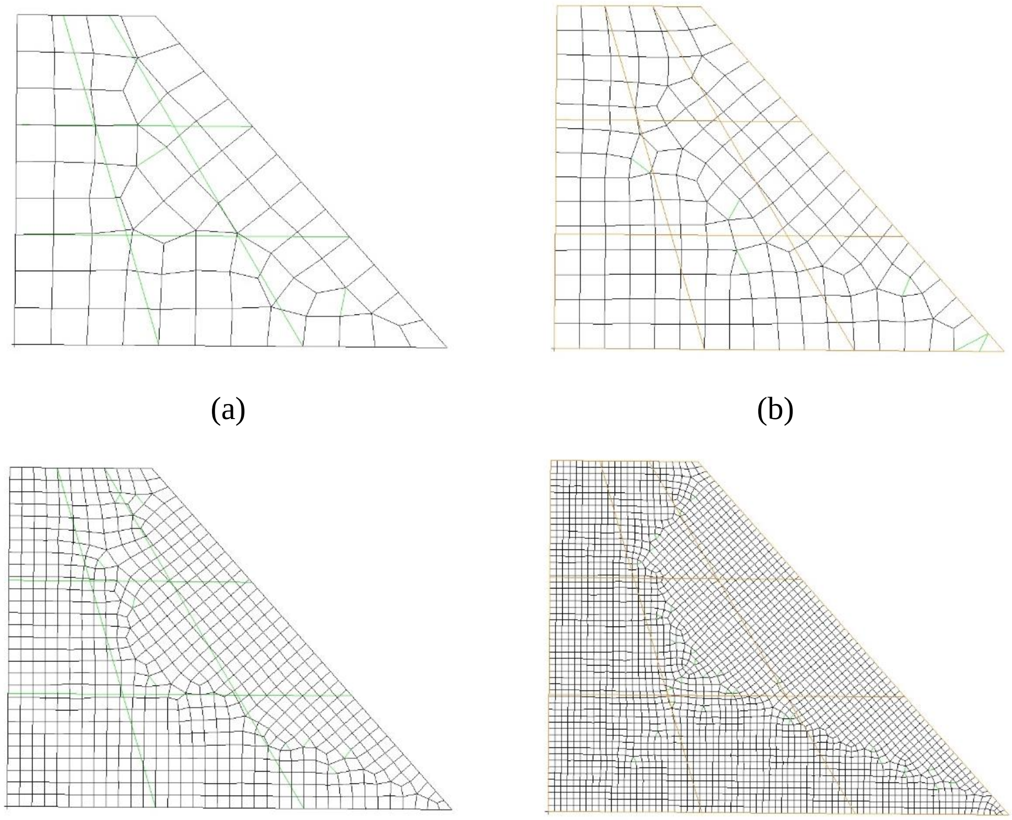

(a) (b) (c) (d)

Figure 5 Four Different Mesh Densities. (a) 0.03 m (b) 0.02 m (c) 0.01 m (d) 0.005 m

Table 2 Mesh Convergence Analysis for Fin-Like Plate

Mode Shape (Element Edge Length)	**1st Mesh (0.03 m)**	**2nd Mesh (0.02 m)**	**3rd Mesh (0.01 m)**	**4th Mesh (0.005 m)**
1st Out-of-Plane Bending [Hz]	27.29	27.41	27.48	27.49
1st Torsion [Hz]	86.37	88.02	89.12	89.38
2nd Out-of-Plane Bending [Hz]	142.29	144.47	145.61	145.9
# of Elements	73	164	658	2618
# of Nodes	91	190	711	2714

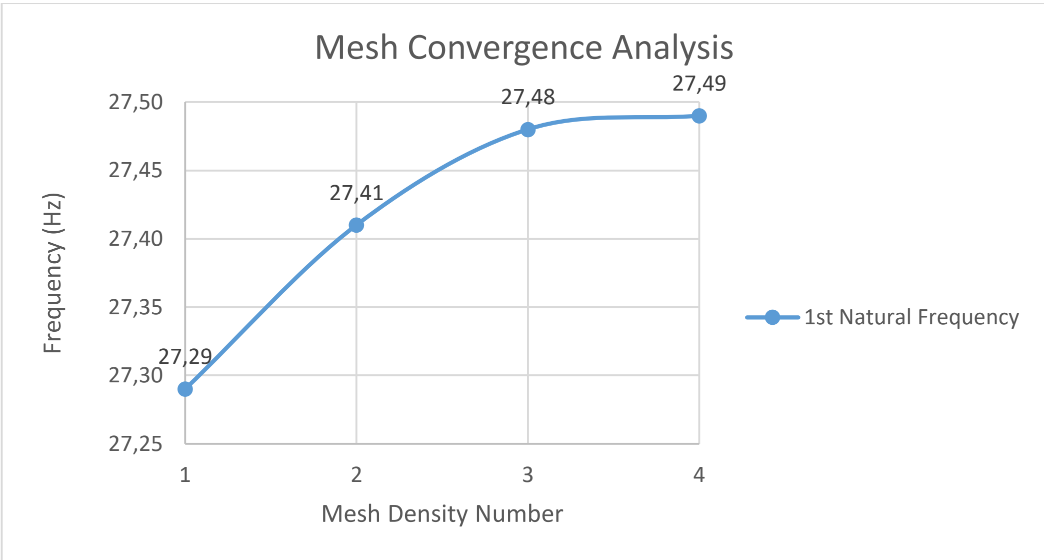

(a)

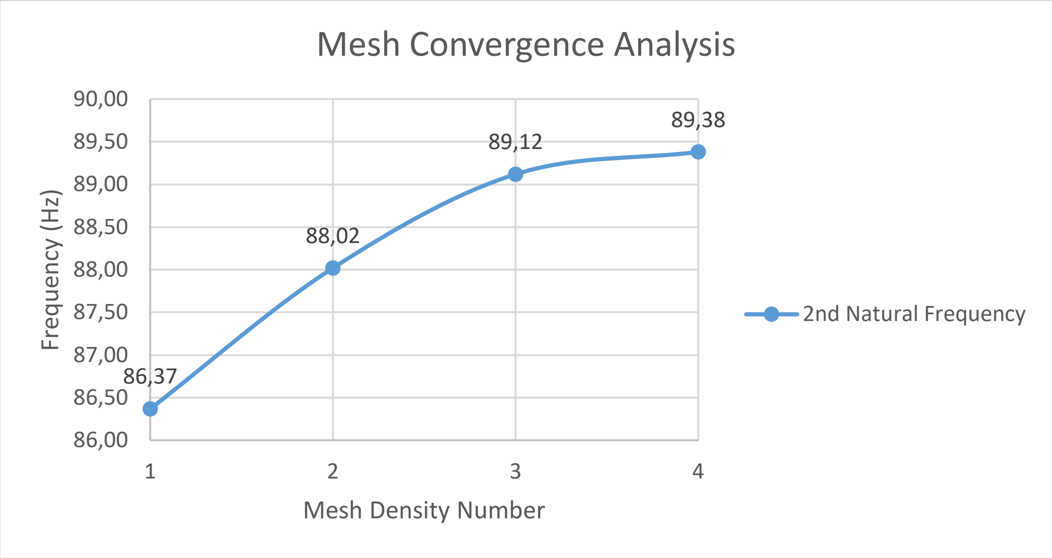

(b)

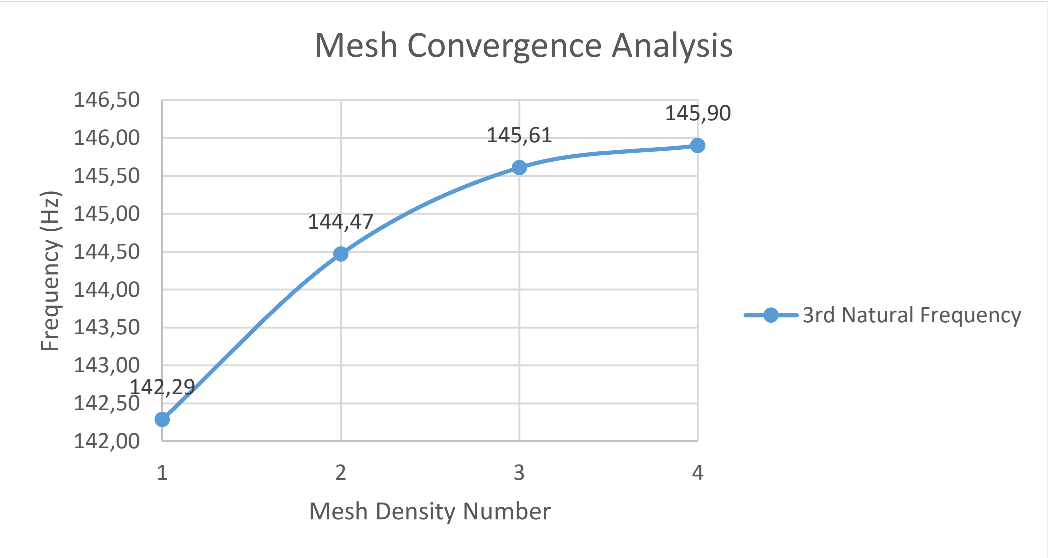

(c)

Figure 6 Mesh Convergence Analysis Diagrams of Fin-Like Pates (a) 1st Natural Frequency (b) 2nd Natural Frequency (c) 3rd Natural Frequency

It can interpreted from Table 2 and Figure 6 and Figure that increase in mesh density over 0.01 (3^{rd} Mesh Density) results in differences in frequencies smaller than 0.3% in predictions (stopping criteria set before), therefore 3^{rd} mesh density (0.01 m) is decided to be used in this study.

4.2 Parametric Model of Fin-Like Plate

During optimization, a new set of locations of transducers in each iteration is generated. To determine the new modal characteristics of the fin-like plate, re-meshing of existing finite element model is mandatory. Re-meshing is performed using a MATLAB script by changing existing finite element model mesh. This script first creates zero dimensional point elements on candidate transducers' locations, and then assigns a lumped mass property to these locations which carry mass information of transducers. It also selects these locations as master degrees of freedom (ASET) to use in Guyan model reduction.

Since genetic algorithm mimics nature evolutionary behavior, it evolves in each iteration. Therefore, there must be an automated process which evaluates objective and constraint functions for each solution of population. The objective function related with the error in prediction of the modal characteristics of the plate is evaluated by re-meshing and re-analysis of baseline FEM. A distributed computing cluster was setup using parallel computing toolbox of MATLAB and 6 computers were selected as workers. Therefore, by help of cluster, a fourfold increase in computation power is observed.

Global optimization toolbox of MATLAB was used for optimization. Genetic algorithm code sends out design variables of each member to objective and constraint functions by taking into account limits of design variables. In these objective and constraint functions there are calls to external finite element solver (MSC©NASTRAN). Result from solver is fed back into these functions by help of regular expression library in MATLAB. At the end these functions return objective values and constraint violations of each member to genetic algorithm main code.

4.3 Test Model of Fin-Like Plate

In order to obtain dynamic test model of the fin-like plate, classical modal analysis (CMA) is performed. Impact Hammer (B&K 8206) [20] with aluminum tip is used as an exciter and a miniature accelerometer (B&K 4517-002) [21] is attached to tip of the plate and the Frequency Response Functions (FRFs) are calculated by roving hammer process (Figure 7).

B&K Pulse/Labshop [22] software is used to gather experimental data from data acquisition device (B&K Modal Test Consultant 7753 with 6 channels) [23] and B&K Pulse/Reflex [24] software was used to perform the modal analysis by using obtained accelerance FRFs (Figure 7). The experimentally obtained resonance frequencies and the corresponding mode shapes are shown in Figure 8.

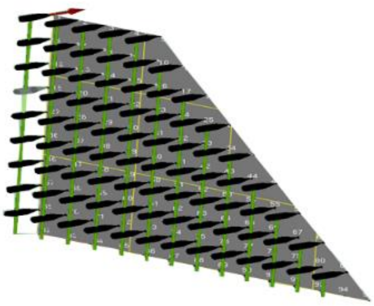

(a)

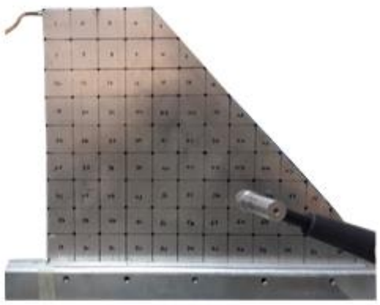

(b)

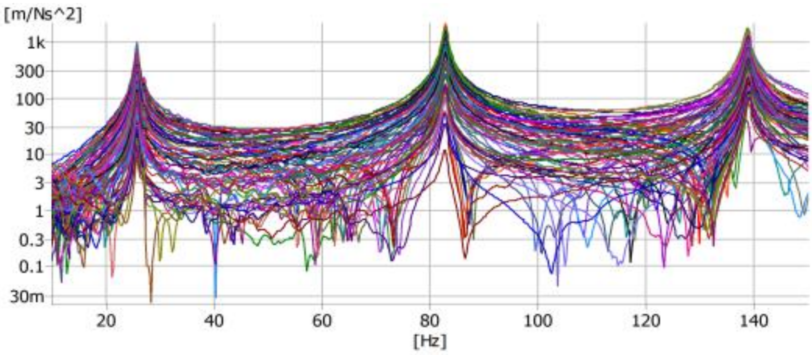

(c)

Figure 7 (a,b) Measurement Locations and (c) Accelerance FRFs Plots (Roving Hammer Test)

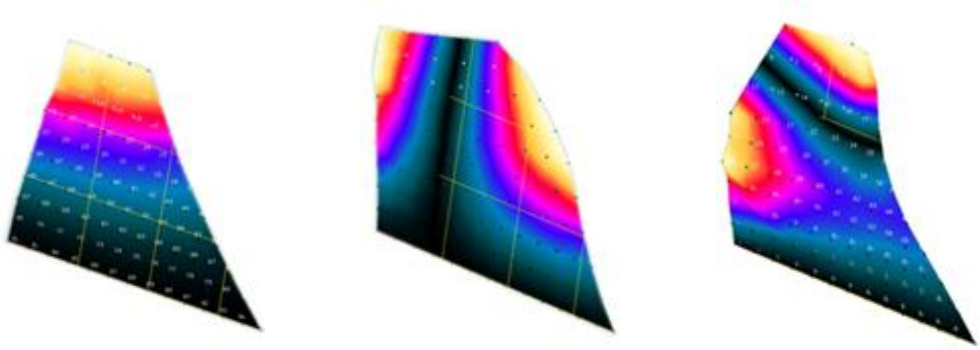

(a) (b) (c)

Figure 8 Mode Shapes obtained via EMA. (a) 1st Out-of-Plane Bending (b) 1st Torsion, (c) 2nd Out-of-Plane Bending

4.3.1 Validation and Model Updating

Finite element models which are numerical models of real structure most of the time are not perfect representation of real structure. There are several reasons which lead to this discrepancy.

- Incorrect material properties
- Bad boundary condition modelling
- Neglecting local material properties changes

- Inaccurate model dimensions
- Modelling nonlinear behavior of structure with linear finite elements

Among above causes, incorrect material properties can be fixed to some extend by applying a model updating in which global material stiffness and mass values are changed. Also bad boundary condition modeling and neglecting local material property changes (e.g. attachment of extra mass like an accelerometer) can be fixed by applying a model updating targeting local material stiffness and mass values.

Since FEM usually do not represent the real structure dynamic characteristics exactly, a correlation analysis is performed to make a comparison between the modal characteristics of two different models, namely FEM and the test model. The model updating is done using FEMTools [25] software. Since exact material properties of fin-like test specimen are not known while modelling. Standard values of aluminum were used. Therefore in model updating plates' global material properties (stiffness, density) are chosen as changing parameters and natural frequencies are chosen as response parameters. These changing parameters are changing within reasonable limit which are found in literature (Table 3). After several iterations, the obtained natural frequencies of FE model are closer to those of test model. The results of the model updating are tabulated in Table 4.

Table 3 Range of Material Properties for Aluminum Plate

Properties	***Selected Value***	***Range***
Stiffness	*69 GPa*	*68.9-73.1 GPa*
Density	*2768 kg/m^3*	*2660-2851 kg/m^3*

Table 4 Model Updating Results For Fin-Like Plate

Mode Shape	FE Natural Frequencies–Before(Hz)	FE Natural Frequencies-After(Hz)	EMA Resonance Frequencies(Hz)	% $\Delta\omega$ Before	%$\Delta\omega$ After
1st Out-of Plane Bending	27.48	27.06	25.58	6.91	5.46
1st Torsion	89.12	87.75	82.70	7.20	5.75
2nd Out-of Plane Bending	145.61	143.37	138.61	4.80	3.32

CHAPTER 5

MULTI-OBJECTIVE GENETIC ALGORITHM OPTIMIZATION OF PLATE

Genetic algorithm (GA) is a heuristic evolutionary optimization algorithm which is a mathematical representation of Darwinian evolution [26-27]. In Darwinian evolution, a population composed of individuals fight with each other in order to survive. After fight individuals with highest fitness (survived ones) are chosen for mating with other fit individuals. In this way less fit individuals die and most fit individuals mate and produces offspring which inherit part of their DNA strands. A mathematical representation of this nature's behavior is used in optimization problems in mathematics and engineering sciences. First of all a random initial population is created which is composed of several individuals (chromosomes). Each individual contains all design variables of optimization problem in one of encoding formats (binary encoding is the most commonly used one). Each individual is evaluated by using objective function and constraint function (if there is any). A fitness value is assigned to each individual which is used in selection of individuals for next generation. Usually half of population is discarded during selection. The discarded half is replaced with new offspring created by most fit half of population. This trend continues in each generation until one of stopping criteria hit.

5.1 Objective Functions

As noted earlier, simultaneous optimization of the number of transducers, transducer types and transducer positions is formulated as a multi-objective optimization problem in this study. The objective functions to be minimized are chosen as: (1) the error in the predictions of the first three natural frequencies of the fin-like plate due to mass loading of sensors, (2) the mode shape observability error, (3) the optimum driving point error and the total transducer cost for each aforementioned case.

5.1.1 Mass Loading Error

In spite of advances in manufacturing of lightweight and accurate transducers, mass of transducer will change modal masses of a dynamic structure. This will result in a change in modal parameters obtained during modal survey. The location of this extra mass which is introduced by transducer into system is important. Areas closer to nodal lines of all modes of interests are the most suitable locations, because addition of mass in those areas results in minimum modal mass alteration. Mass loading error is calculated using summation of squared difference between first three natural frequencies of structure with and without transducers.

$$\text{Mass Loading Error} = \sum_{k=1}^{3} ({\omega^{nt}}_k - {\omega^{t}}_k)^2 \tag{8}$$

$${\omega^{nt}}_\mathrm{k} = \mathrm{k'th\ Natural\ Frequency\ w/o\ transducer}$$

$${\omega^{\mathrm{t}}}_\mathrm{k} = \mathrm{k'th\ natural\ frequency\ w/\ transducer}$$

5.1.2 Mode Shape Observability Error

In order to be able to detect/distinguish mode shapes of interest in test results, it is of vital importance to place accelerometers on areas on structure which have highest movement and avoid nodal lines in all modes of interest. In finite element order reduction algorithms like Guyan reduction, active degrees of freedom must usually be selected from areas with highest modal constant in all modes of interest in order to have highest possible correlation of mode shapes between reduced and full finite element model. To achieve this, full finite element model is reduced using candidate accelerometers locations as master degree of freedom by Guyan reduction scheme and a cross correlation performed between mode shapes of full finite element model and reduced one using cross MAC (Modal Assurance Criterion) matrix. Inverse of trace of cross MAC matrix is used as mode shape observability error.

$$\text{Cross MAC Matrix} = \frac{\left|\emptyset_{\mathrm{R}}^{\mathrm{T}}\emptyset_{\mathrm{F}}\right|^{2}}{\left|\emptyset_{\mathrm{R}}^{\mathrm{T}}\emptyset_{\mathrm{R}}\right|\left|\emptyset_{\mathrm{F}}^{\mathrm{T}}\emptyset_{\mathrm{F}}\right|}$$

$$\emptyset_{\mathrm{F}} = \text{Mass Normalized Modal Matrix of Full FEM} \tag{9}$$

$$\emptyset_{\mathrm{R}} = \text{Mass Normalized Modal Matrix of Reduced FEM}$$

$$\text{Mode Shape Observability Error} = \frac{1}{\text{trace(CrossMACMatrix)}}$$

5.1.3 Optimum Driving Point Error

While exciting structure via impact hammer or modal shaker, there are several aspects which needs to be taken care of. When modal shake is attached to structure, its stinger will hinder motion of structure at that point by introducing extra stiffness. Also since force transducer has a mass, it will introduce new inertial forces into systems. It is beneficial to excite structure from places with minimum acceleration in all modes of interest. When impact hammer is used, location with higher velocity must avoided since the probability of double impact is high. So for excitation locations, areas with minimum acceleration and velocity in all modes of interest is preferred. To find those locations, minimum value of ADDOFV and ADDOFA are used (Equation 6) for error of impact hammer and modal shaker respectively.

5.2 Constraint Function

Five constraints which are used in all of optimizations are listed below. In following equations these binary valued arrays are used.

$$y_i = its\ elements\ shows\ whether$$
$$that\ specific\ transducers\ is\ selected\ or\ not$$
$$i = 1, .. , 15\ (number\ of\ available\ tranducers)$$

$$ACC_i = its\ elements\ shows\ whether$$
$$that\ specific\ transducers\ is\ accelerometer\ or\ not$$
$$i = 1, .. , 15\ (number\ of\ available\ tranducers)$$

$$FT_i = its\ elements\ shows\ whether$$
$$that\ specific\ transducers\ is\ force\ transducer\ or\ not$$
$$i = 1, .. , 15\ (number\ of\ available\ tranducers)$$

$$CH_i = its\ elements\ shows\ number$$
$$of\ occupied\ channels\ in\ data\ aquisition\ device\ by\ that\ transducer$$
$$i = 1, .. , 15\ (number\ of\ available\ tranducers)$$

In case of impedance head, FT and ACC are both one.

i. Distance of the candidate transducers from clamped part of plate must not exceed the diameter of the largest transducer.

$$v_i \geq \frac{D_{Largest}}{2}$$

$$v_i = 1..15 \begin{pmatrix} \text{vertical distance from middle of transducer to clamp} \\ 15 = \text{ number of available transducers} \end{pmatrix}$$

$$D_{Largest} = \ largest\ transudcer\ diameter$$

ii. At least one accelerometer and one force transducer must be selected.

$$\sum_{i=1}^{15} y_i * \ (ACC_i + FT_i) \geq 2$$

iii. Minimum distance between transducers must not exceed diameter of largest transducer.

$$\sum_{\substack{i=1\\j=1}}^{\substack{i=15\\j=15}} \sqrt{\left(x_i - x_j\right)^2 + \left(y_i - y_j\right)^2 \left(z_i - z_j\right)^2} \geq D_{Largest}$$

$$x_{i,j} = x\ coordinate\ of\ center\ of\ transducer$$

$$y_{i,j} = y\ coordinate\ of\ center\ of\ transducer$$

$$z_{i,j} = z\ coordinate\ of\ center\ of\ transducer$$

iv. Number of occupied channels by transducers must not exceed six. (data acquisition device has maximum of six channels)

$$\sum_{i=1}^{15} y_i *\ CH_i\ \leq 6$$

v. Only one force transducer must be selected, because the test setup (roving hammer) is a SIMO (single-input and multiple-output) system.

$$\sum_{i=13}^{15} y_i\ \leq 1$$

$$i = 13{,}14{,}15\ are\ indices\ of\ force\ transducers$$

5.3 Design Variables

There are fifteen available transducers used in this study. In Table 5, transducers' type, model, number, image, price, mass and channel usage are listed. For each of these transducers two design variables are assigned. One variable is a binary variable that shows the use of that transducer and is either one or zero. The other variables is a discrete variable which is node number of corresponding transducer. Therefore, there are 30 discrete design variables which are used in this optimization problem.

Table 5 Available Equipment for EMA

Transducer Type **Model (Number)**	**Price ($)**	**Image**	**# of Occupied Channels**	**Mass (gr)**
Single Axis Accelerometer **B&K 4517-002 (5)**	762		1	0.7
Single Axis **Accelerometer** **B&K 4508-B (5)**	630		1	4.8
Triple Axis **Accelerometer** **B&K 4524 (1)**	2197		3	4.8
Triple Axis **Accelerometer** **B&K 4506-B (1)**	1190		3	15.0
Modal Shaker's **Force Transducer** **B&K 8230-002 (1)**	1132		1	30.2
Impedance Head **B&K 8001 (1)**	3165		2	29.0
Impact Hammer's **Force Transducer** **B&K 8206 (1)**	1684		1	0.0 (Contactless)

5.4 Optimization Cases Considered

Four different multi objective optimization problems are considered in this study. In the first case, the summation of the mass loading error (MLE) and the total cost are minimized subject to constraints. In the second case, the summation the mode shape observability error (MSOE) and the total cost are minimized subject to constraints. In the third case, the summation of optimum driving point error (ODPE) and the total cost are minimized subject to constraints. In the fourth case, error is obtained by summing all these three error. This error and total cost are minimized subject to constraints. The optimization results corresponding to these four cases are presented and discussed in next section.

5.5 Optimization Results

In multi-objective optimization problem, there is no single optimum solution, instead there is a range of solutions in which several optima can reside. In this range, some solutions are dominated by other solutions (has higher values in all of objectives). Solutions which are not dominated by any other solutions (has lower values in all of objectives) are called non-dominant solutions. A curve passing through these non-dominant solutions is called Pareto frontier curve. In following figures, grey areas represent areas with low modal constant (near zero) value. Which are either an area close to clamped side of plate or nodal line of plate in any of first three mode shapes. Nodal lines are very thick and that is because of mesh density. Otherwise nodal lines would be thin lines with very fine mesh density.

5.5.1 Case 1: Minimization of the MLE and the Total Cost

The Pareto frontier curve obtained for Case 1 is shown in Figure 9. Three representative Pareto optimal solutions are chosen for depiction and listed in Table 6. It is observed from Table 6 and Figure 9 that the mass loading error is very small for the chosen representative Pareto optimal solutions. When the optimum configurations A and B are analyzed (see Figure 10) it is observed that transducers are placed very close to the region with minimum modal constant in all modes of interest (near clamp and rightmost area). For configuration C, on the other hand, one force transducer is located at the top portion of plate. Since the selected transducer is an impact hammer, its location does not affect modal masses of plate because it is not attached to structure like shaker's force transducer. Another important concept is that with increasing cost limit, the optimizer still chooses only one accelerometer and force transducer and that is because to keep mass loading as minimum as possible. With increasing price only type (therefore mass) of transducers is changed.

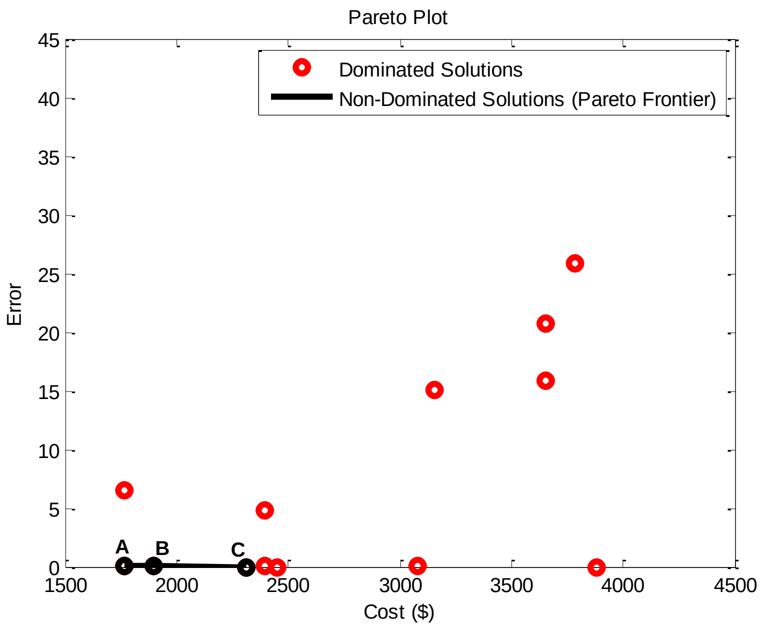

Figure 9 Pareto Frontier Curve and Selected Non-dominant Solutions (ML Error Only)

Table 6 Total Error and Cost of Pareto Frontier Solutions (ML Error Only) For Fin-Like Plate.

Configuration	*ML Error	Cost ($)
A	0.00049	1762
B	0.00045	1895
C	~0.00	2314

** ML: Mass Loading*

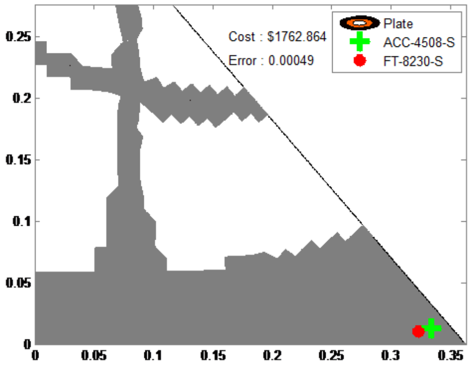

(a)

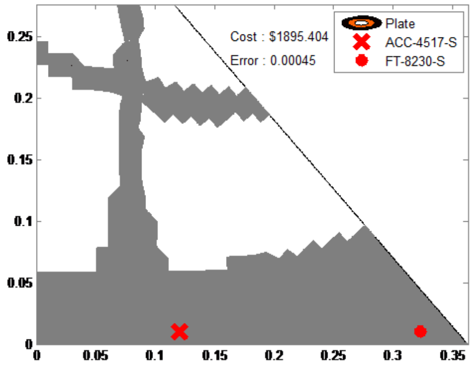

(b)

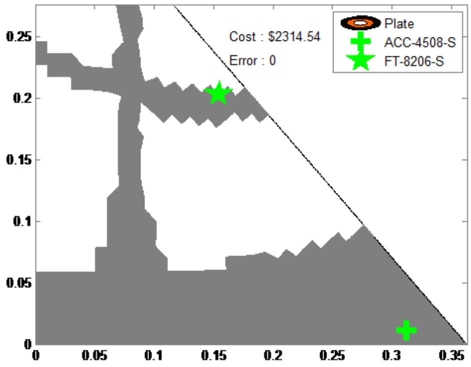

(c)

Figure 10 Locations of Transducers in Candidate Configurations from Pareto Frontier (ML Error Only). (a) Configuration A (b) Configuration B (c) Configuration C

5.5.2 Case 2: Minimization of the MSOE and the Total Cost

The Pareto frontier curve obtained for Case 2 is shown in Figure 11. Seven representative Pareto optimal solutions are chosen for depiction and listed in Table 7. It is evident from results that increase in number of accelerometers will lead to better mode shape observability. Figure 12 shows that for configuration A, since cost limit only allows for two accelerometers, optimizer locates the accelerometers side by side to capture first mode shape (1^{st} bending) and second mode shape (1^{st} torsion). Even in configuration B with an increase in price limit algorithm still cannot use third accelerometer (because of cost limit).

It only changed type of one of accelerometer with more expensive one (miniature 4517-002). In configuration C, this time algorithm is able to select three accelerometers and they are placed in a way to detect all three first mode shapes of plate. As it is expected with increasing price more accelerometers are added and they are usually placed in regions with high acceleration (at least in one mode shape). This optimization shows that for mode shape observability the more accelerometer you use, mode shapes are more distinguished with only one SIMO test (not roving) and of course their location has a vital importance in observability of mode shapes. For example with three accelerometers you can capture all three modes or only two and that depends on how you arrange accelerometers to capture torsion mode (triangular configuration).

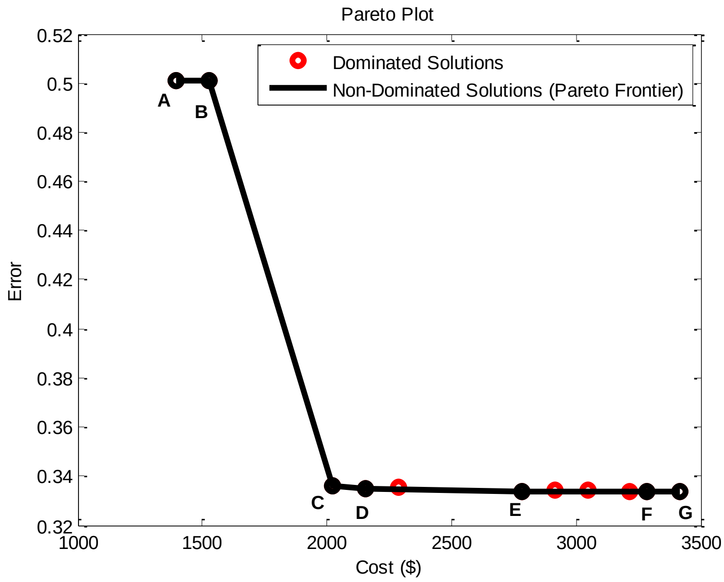

Figure 11 Pareto Frontier Curve and Selected Non-dominant Solutions (MSO Error Only).

Table 7 Total Error and Cost of Pareto Frontier Solutions (MSO Error Only) For Fin-Like Plate.

Configuration	***MSO Error**	**Cost ($)**
A	0.50073	1392
B	0.50072	1525
C	0.33615	2022
D	0.33504	2155
E	0.33373	2785
F	0.33358	3282
G	0.33354	3415

**MSO: Mode Shape Observability*

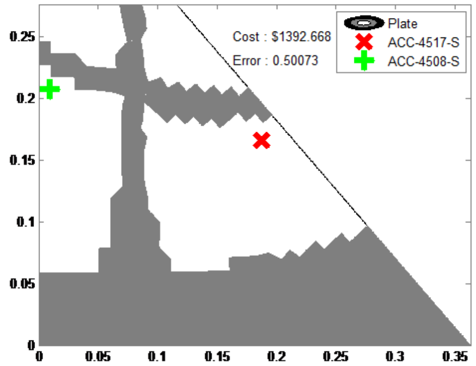

(a)

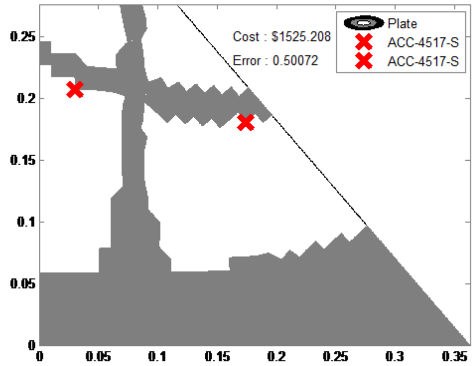

(b)

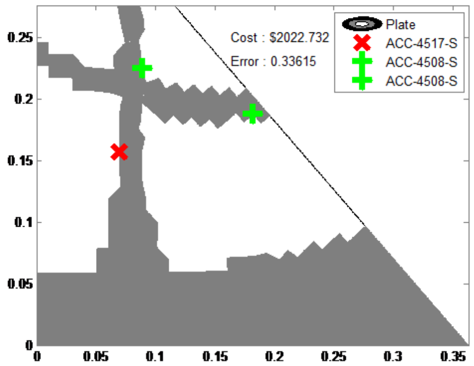

(c)

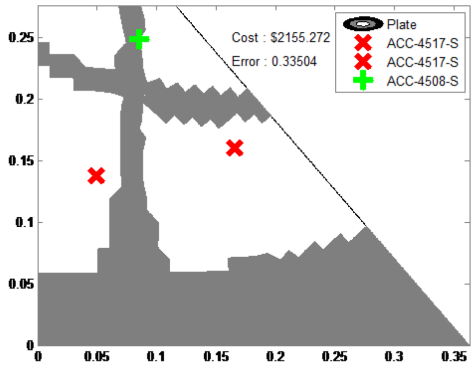

(d)

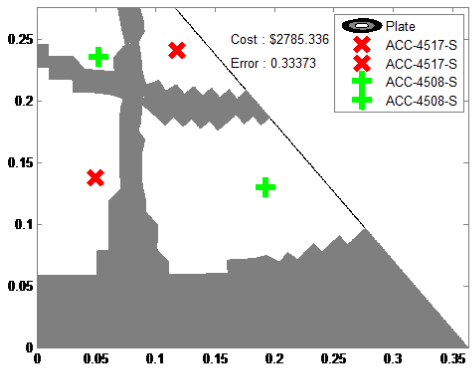

(e)

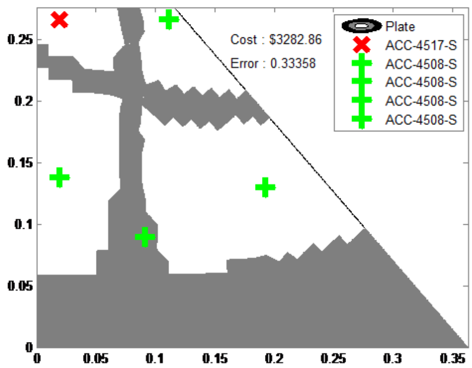

(f)

Figure continues on next page

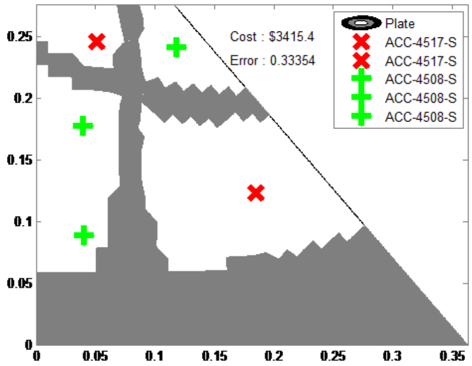

(g)

Figure 12 Locations of Transducers in Candidate Configurations from Pareto Frontier (MSO Error Only). (a) Configuration A (b) Configuration B (c) Configuration C (d) Configuration D (e) Configuration E (f) Configuration F (g) Configuration G

5.5.3 Case 3: Minimization of the ODPE and the Total Cost

When objective function is only dependent on optimum driving point error, the optimization problem reduces to the selection of the most appropriate location for the impact hammer or modal shaker. Since the shaker's force transducer is less expensive than the impact hammer, the optimum choice is the use of the shaker. It is found that the optimum solution is attaching the shaker to a point with minimum acceleration (Figure 13). The ODP error for this configuration is computed as 0.0001462.

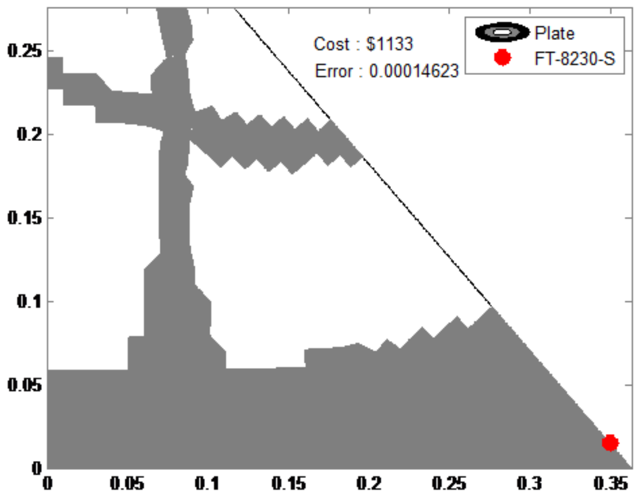

Figure 13 Optimum Location of the Shaker for minimum ODPE

5.5.4 Case 4: Minimization of the Overall Equivalent Error and the Total Cost

The Pareto frontier curve obtained for Case 4 is shown in Figure 14. Seven representative Pareto optimal solutions are chosen for depiction and listed in Table 8. Figure 15 shows that for configurations of all optimum solutions. When all of errors are combined together it can be concluded that all errors are tried to get minimized or kept at a minimum level. Since there is no weighting used in summation of errors, dominant error (MSO Error) is always tried to get minimized further as price increases. Also the other two non-dominant ones (ML and ODP Errors) are kept at a minimum level with increasing price. In configuration A, because of price limit only two accelerometers (cheapest one) and a shaker force transducer is used. As it was expected force transducer was located near clamping part of plate and accelerometer were placed side by side to capture 1st and 2nd mode shapes and to keep mass loading at a minimum level they are placed closer to clamped part of plate and near nodal line when compared to the case with only MSO error. In configuration B, with an increase in price limit algorithm added third accelerometer of the same type but still because these accelerometers are heavy (cheapest ones), they are placed near clamped area and nodal line but have a triangular configuration like the one in optimizations with only MSO error.

In configuration C, because of an increase in price limit algorithm changes one of those three accelerometers with lighter one (more expensive) and place it higher and near nodal line of torsion mode. By this means its mass will only affect modal mass of 1^{st} and 3^{rd} mode but since it is very light (mass=0.4 gram), ML errors has not increased (keeping ML error at minimum level). After another price limit increase in configuration D, another accelerometer was exchanged with lighter one. Therefore mass loading error decreased a little. In configuration E, all of three accelerometers are chosen as the lightest accelerometer (miniature 4517).

In configuration F, one of accelerometers were exchanged with previous heavy one (4508) and that is because force transducer is changed from shaker (less expensive) to impact hammer (more expensive). So price limit forced algorithm to change one of accelerometers. In configuration G because of an increase in price limit, all accelerometers are chosen as the lightest one (4517) and impact hammer is used which does not affect ML error. In this forth optimization which all of errors were included, it is obvious that algorithm decides that three accelerometers in triangular configuration are sufficient to capture all first three mode shapes of plate and because of mass loading error they are selected as the lightest accelerometers (miniature 4517) and impact hammer is chosen (no ML error). ODP error also make sure that plate is excited from a region near to clamped area (minimum velocity) to decrease possibility of double-hit error of impact hammer.

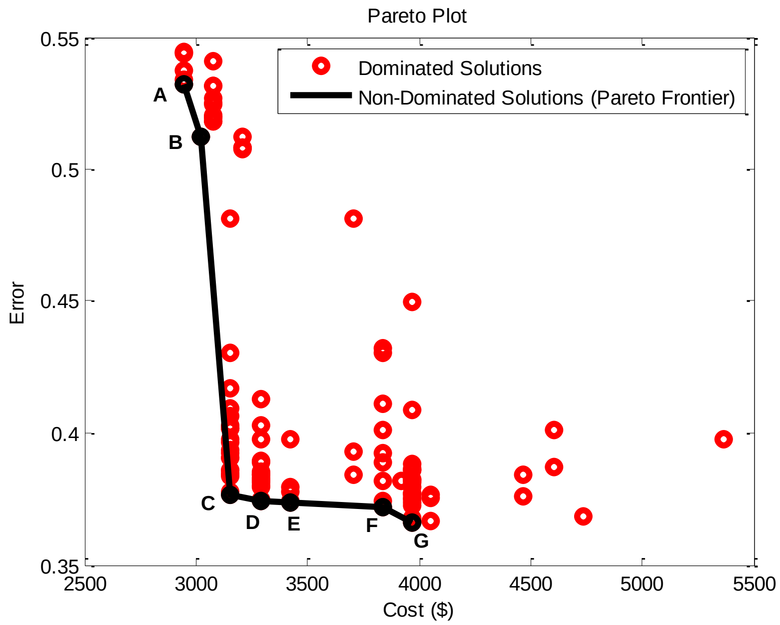

Figure 14 Pareto Frontier Curve and Selected Non-dominant Solutions (Total Error).

Table 8 Total Error and Cost of Pareto Frontier Solutions (Total Error) For-Like Plate.

Configuration	*ML Error	*MSO Error	*ODP Error	Total Error	Cost ($)
A	0.0061	0.5241	0.0016	0.5319	2,944
B	0.0410	0.4713	0.0000	0.5123	3,022
C	0.0092	0.3673	0.0001	0.3766	3,155
D	0.0043	0.3696	0.0000	0.3739	3,288
E	0.0061	0.3673	0.0001	0.3737	3,420
F	0.0056	0.3658	0.0002	0.3717	3,839
G	0.0067	0.3595	0.0000	0.3662	3,972

** ML: Mass Loading MSO: Mode Shape Observability ODP: Optimum Driving Point*

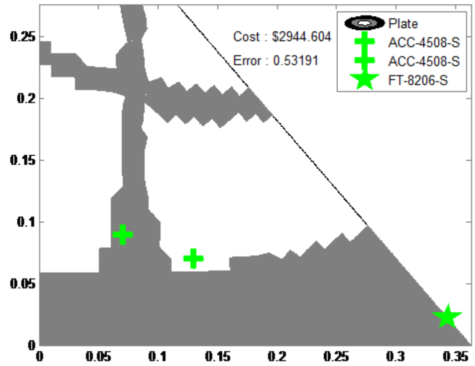

(a)

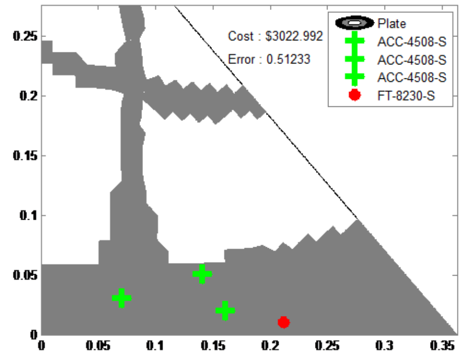

(b)

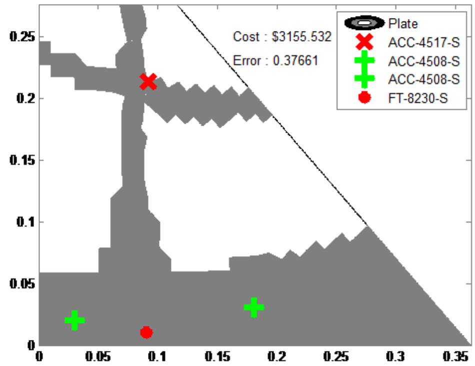

(c)

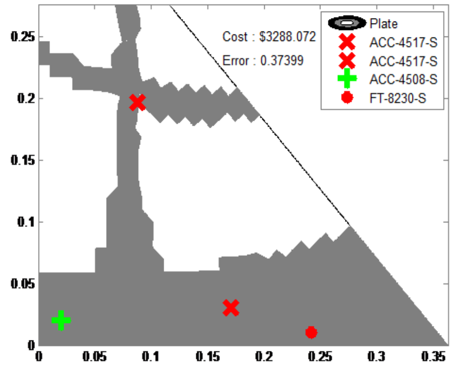

(d)

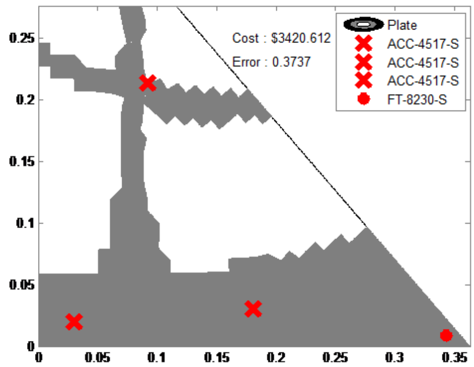

(e)

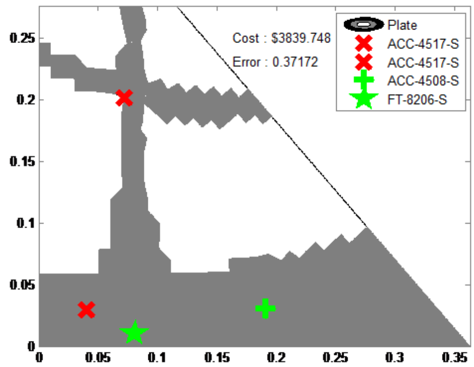

(f)

Figure continues on next page

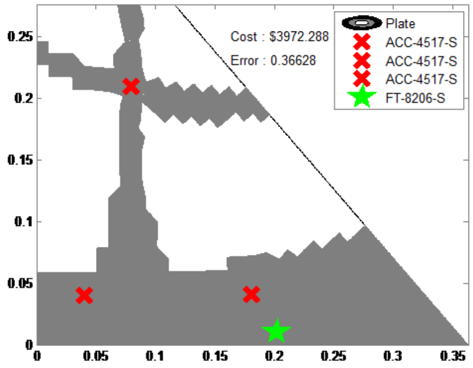

(g)

Figure 15 Locations of Transducers in Candidate Configurations from Pareto Frontier (Total Error).(a) Configuration A (b) Configuration B (c) Configuration C (d) Configuration D (e) Configuration E (f) Configuration F (g) Configuration G

CHAPTER 6

VALIDATION OF THE OPTIMIZATION RESULTS VIA MODAL TEST

In this part of the study, configurations of Pareto optimum set in all optimizations are verified using experimental modal analysis technique. The previously obtained optimal results are taken into consideration and the experimental modal analysis setups are designed. The sensor(s)/actuator pairs are selected from Table 5 and the FRFs are calculated for various configurations by using B&K Modal Test Consultant 7753 software with 6 channel spectrum analyzer. The configurations are selected in such a way that one corresponding to a minimum-error (the most expensive) and one for the maximum-error (the cheapest). In (Figure 16 till Figure 21) all of results are presented in terms of the configuration obtained from the optimization analyses (the upper left figure), corresponding B&K Modal Test Consultant plate configuration (the upper right figure), accelerance FRF in the frequency range of interest, photo of the experimental setup regarding sensor(s)/actuator pairs and test results for the first three modes. Additionally, figures showing whether the modes of interests are captured by the performed experimental analyses or not are also presented (the bottom figure). This figure is especially important from the performance comparison point of view of the Mode Shape Observability Error (MSOE) case with the other cases.

The verification results are presented in the order of the Mass Loading Error (MLE), the Mode Shape Observability Error (MSOE) and the Total Error (TE). As the MSOE case contains only sensors and no actuators, the result of the Optimum Driving Point Error (ODPE) is used in the determination of the actuator force traducer for these MSOE cases. In case 1 which was minimization of MLE and total cost, the first mode shape resonance frequency could not be extracted from the accelerance FRF plot because the accelerometer was placed near the clamped area of plate which has the minimum acceleration and provides very low signal to noise ratio that is therefore buried into noise in the first mode shapes. Regarding all the following tests where the accelerometers are located very close to the clamp end, the aforementioned low signal to noise ratio problem comes into picture especially in the accelerance FRF of the 1st out-of-plane mode.

6.1 Case 1: Minimization of the MLE and the Total Cost

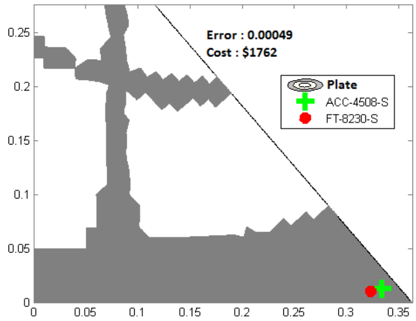

(a)

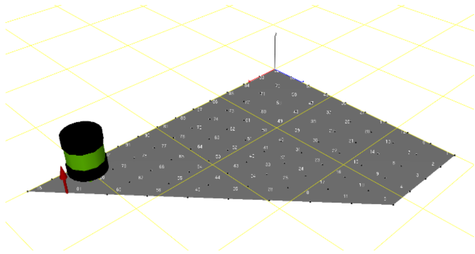

(b)

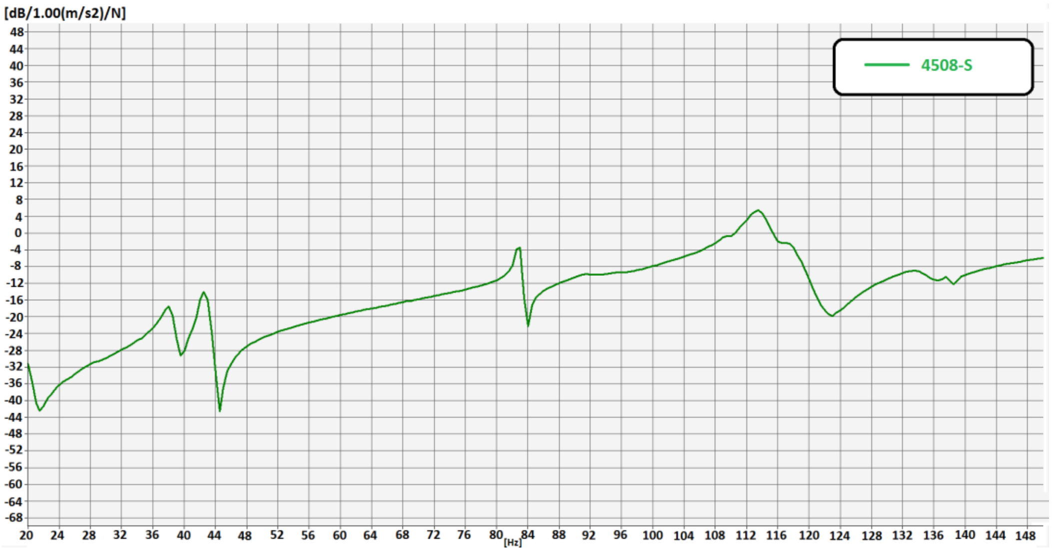

(c)

Figure continues on next page

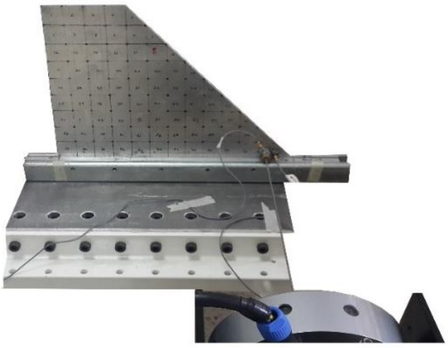

(d)

Configuration	Resonance Frequencies [Hz]		
	1st Mode	2nd Mode	3rd Mode
MLE (A)	-	79.5	137.5

(e)

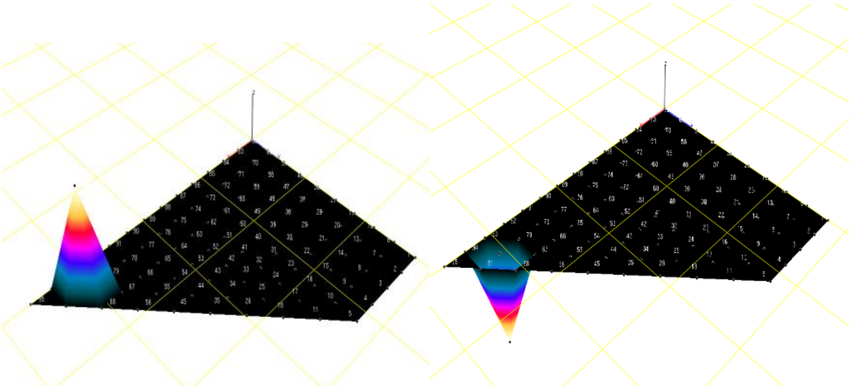

(f)

Figure 16 Mass Loading Error Configuration A (a) Configuration Obtained from Optimization (b) Configuration in B&K Modal Test Consultant (c) Accelerance FRF (d) Test Setup (e) Resonance Frequencies Obtained (f) Mode Shapes Observed from One Measurement

As it is evident from Figure 16 in the cheapest configuration of mass loading error optimization, a cheap accelerometer was placed near area with minimum acceleration so that it gives minimum mass loading error. This configuration will have minimum mass loading error but very bad mode shape observability. In part (f) of above figure, only the first mode shape is captured. Also because of the cost limit, modal shaker's force transducer was selected instead of an impact hammer.

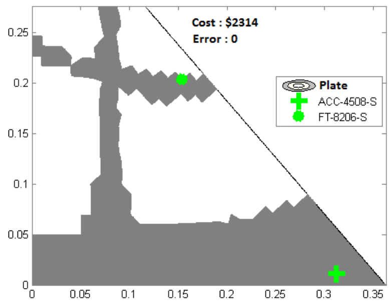

(a)

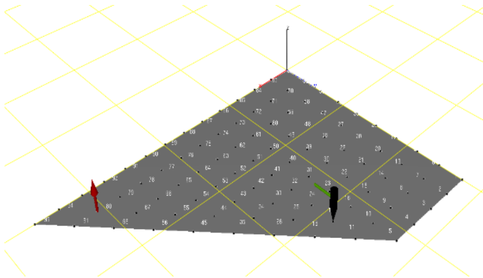

(b)

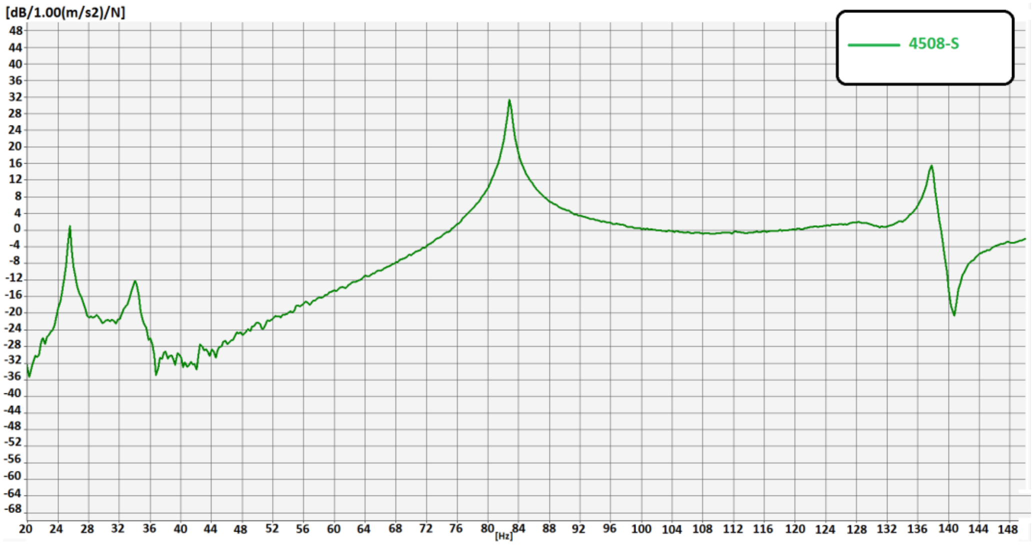

(c)

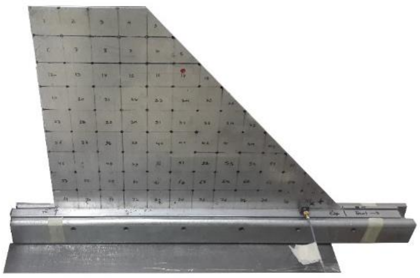

(d)

Configuration	Resonance Frequencies [Hz]		
	1st Mode	2nd Mode	3rd Mode
MLE (C)	25.50	82.75	137.80

(e)

Figure continues on next page

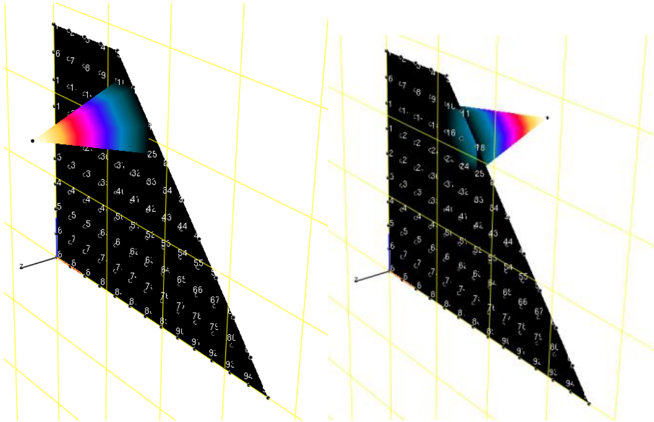

(f)

Figure 17 Mass Loading Error Configuration – C (a) Configuration Obtained from Optimization (b) Configuration in B&K Modal Test Consultant (c) Accelerance FRF (d) Test Setup (e) Resonance Frequencies Obtained (f) Mode Shapes Observed from One Measurement

In Figure 17, the most expensive case of mass loading error optimization is shown. As it was expected that the force transducer of impact hammer was selected and it is not mounted on structure, it does not change the modal masses of the plate. Therefore, impact hammer is located over the areas having more acceleration so that it delivers a force with high enough amplitude. On the hand, an accelerometer was placed near the clamped area having minimum acceleration in all mode shapes.

6.2 Case 2 and 3: Minimization of the MSOE and ODP and the Total Cost

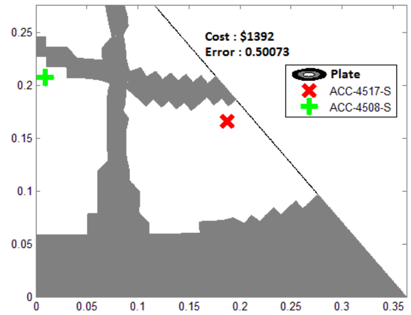

(a)

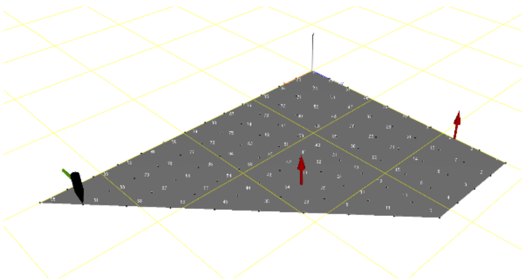

(b)

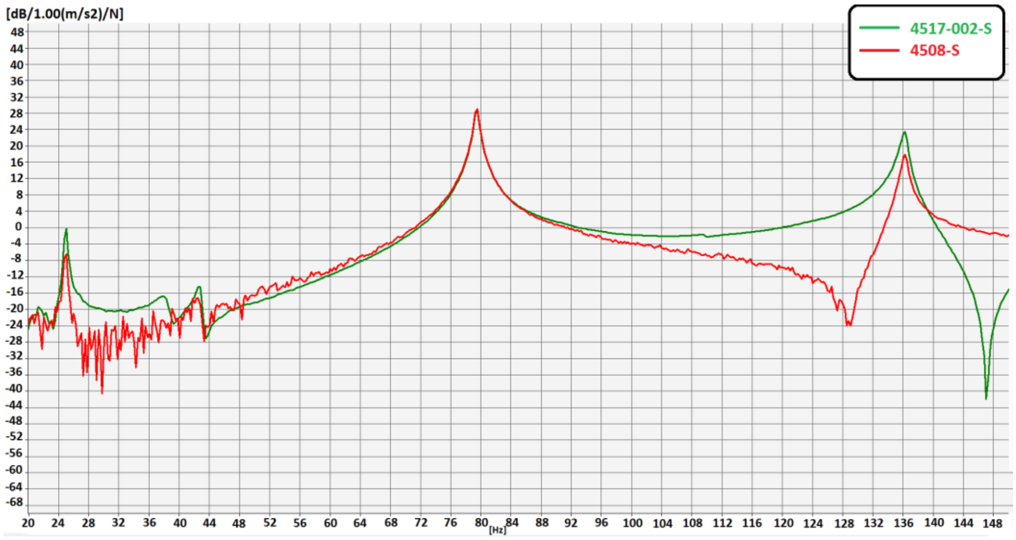

(c)

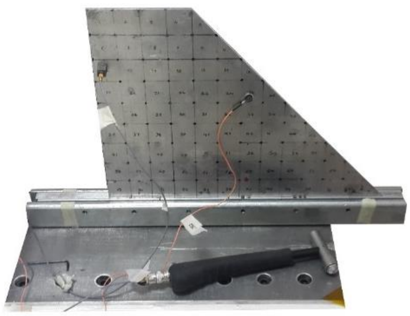

(d)

Configuration	Resonance Frequencies [Hz]		
	1st Mode	2nd Mode	3rd Mode
MSOE (A)	25.00	79.50	136.30

(e)

Figure continues on next page

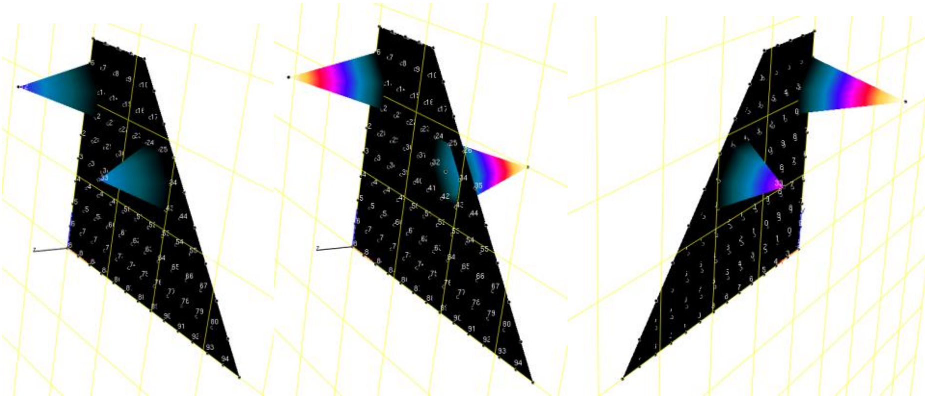

(f)

Figure 18 Mode Shape Observability Error - Configuration A (a) Configuration Obtained from Optimization (b) Configuration in B&K Modal Test Consultant (c) Accelerance FRF (d) Test Setup (e) Resonance Frequencies Obtained (f) Mode Shapes Observed from One Measurement

In mode shape observability case, the accelerometers were located in a way to capture all three mode shapes. Since this is the cheapest configuration only two accelerometers were selected and they were only able to capture the first bending and the first torsion mode shapes (Figure 18 part (f)).

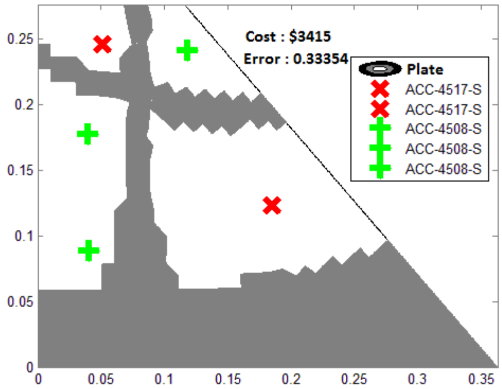

(a)

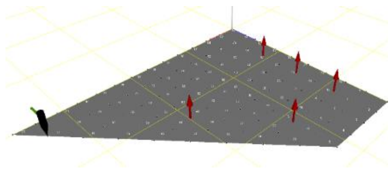

(b)

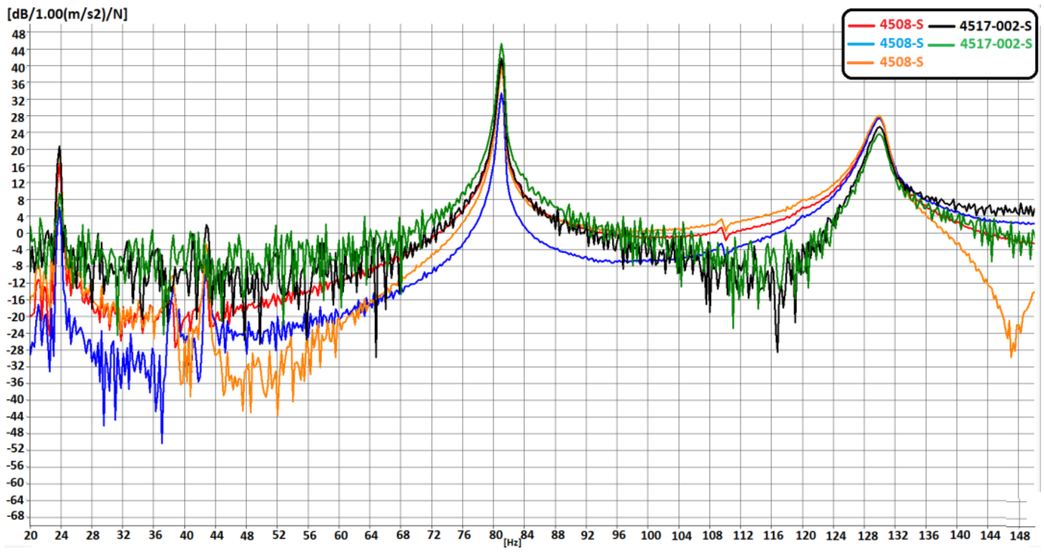

(c)

Figure continues on next page

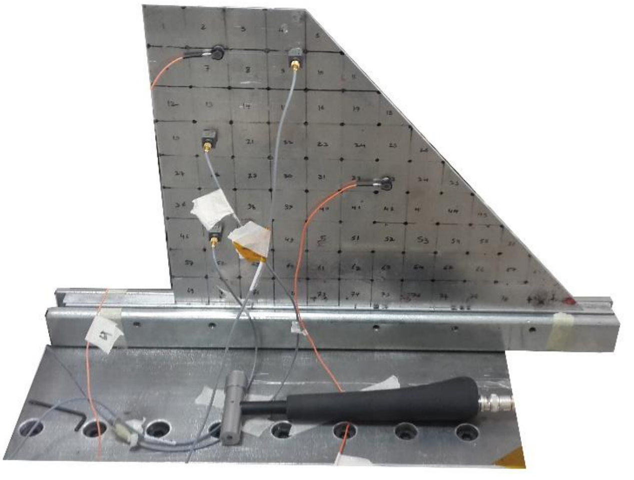

(d)

Configuration	Resonance Frequencies [Hz]		
	1st Mode	2nd Mode	3rd Mode
MSOE (G)	23.75	81.00	130.00

(e)

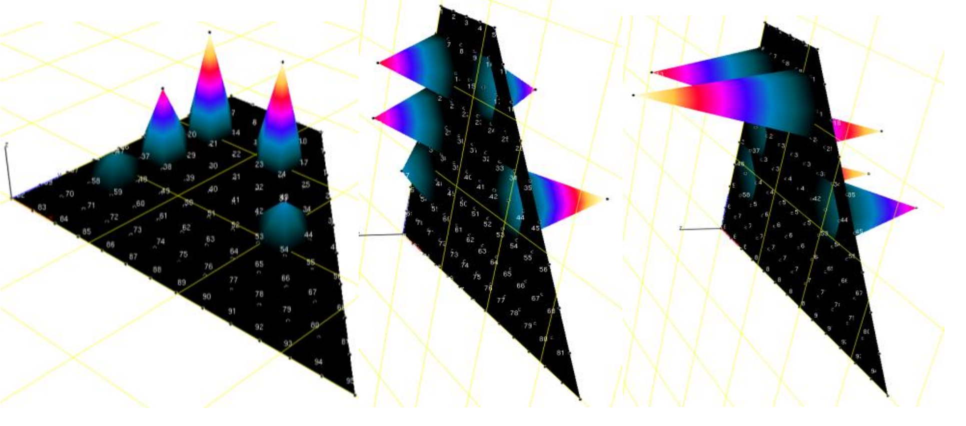

(f)

Figure 19. Mode Shape Observability Error - Configuration G (a) Configuration Obtained from Optimization (b) Configuration in B&K Modal Test Consultant (c) Accelerance FRF (d) Test Setup (e) Resonance Frequencies Obtained (f) Mode Shapes Observed from One Measurement

In the most expensive optimization case of mode shape observability shown in Figure 19, five accelerometers were selected which are strategically placed on locations where the first three mode shapes are captured in the best way possible. Since the mass loading error is not considered here, couple of heavy accelerometers are also selected which will introduce more mass to structure.

6.3 Case 4: Minimization of the Overall Equivalent Error and the Total Cost

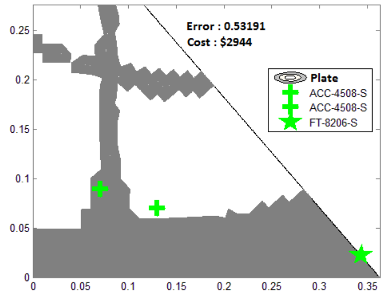

(a)

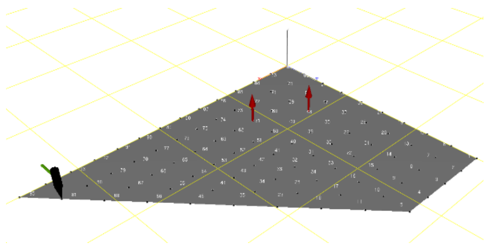

(b)

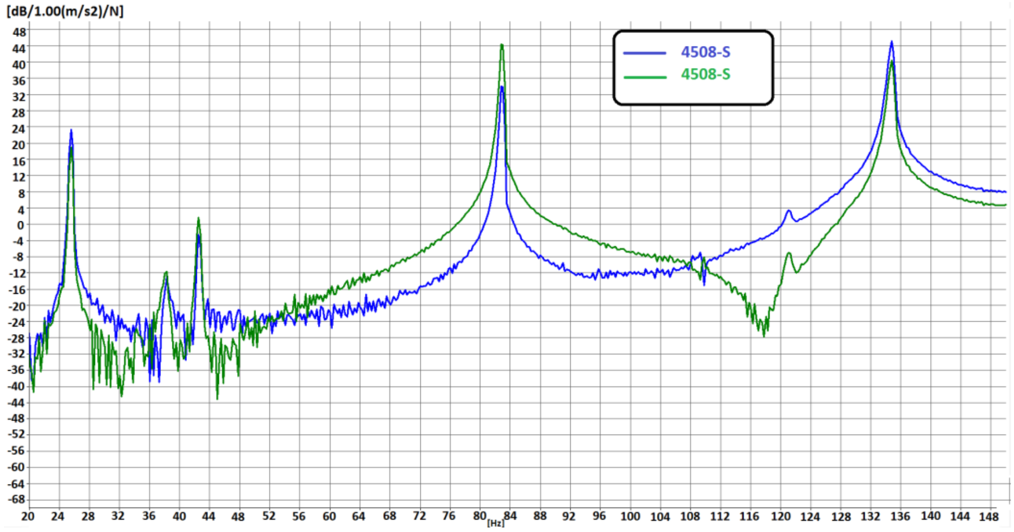

(c)

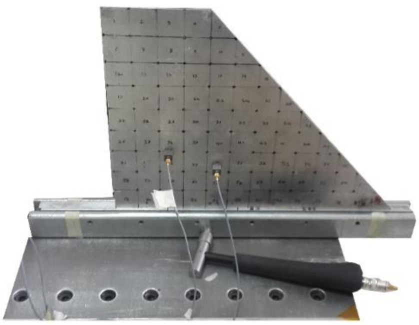

(d)

Configuration	Resonance Frequencies [Hz]		
	1st Mode	2nd Mode	3rd Mode
TE (A)	25.50	82.75	134.80

(e)

Figure continues on next page

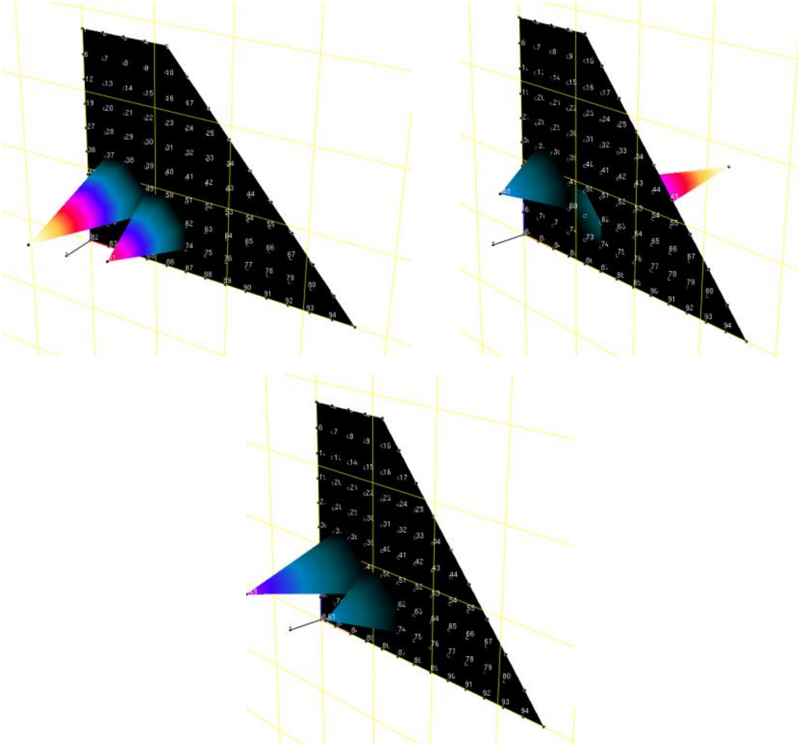

(f)

Figure 20 Total Error - Configuration A (a) Configuration Obtained from Optimization (b) Configuration in B&K Modal Test Consultant (c) Accelerance FRF (d) Test Setup (e) Resonance Frequencies Obtained (f) Mode Shapes Observed from One Measurement

In Figure 20, since all errors were considered, the algorithm tried to locate accelerometers on locations which can capture the first three mode shapes and they were tried to be located closer to the nodal lines as much as possible so that a minimum mass loading error is achieved.

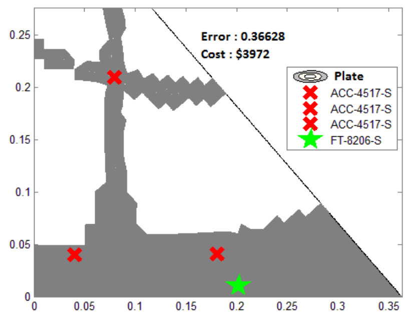

(a)

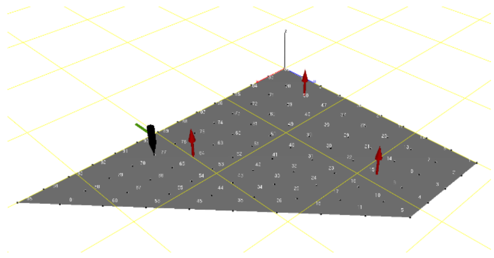

(b)

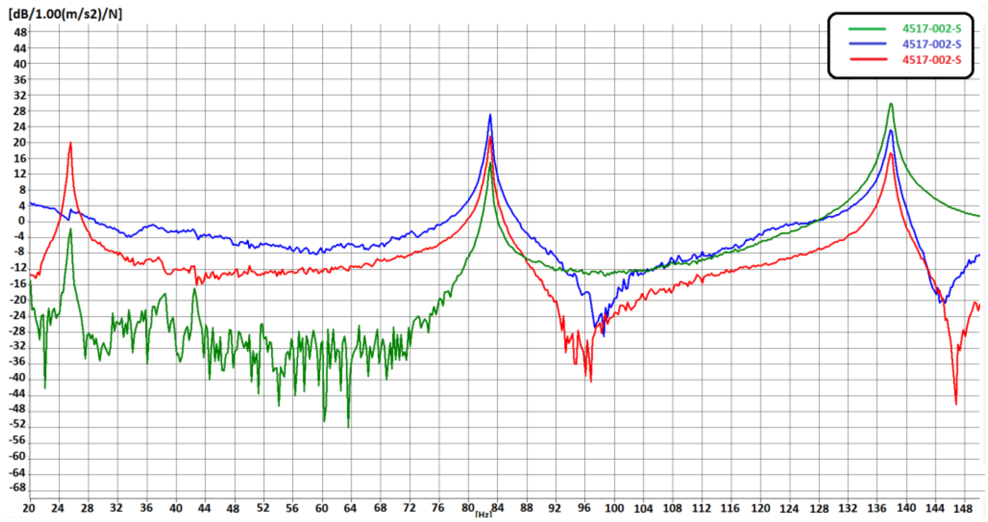

(c)

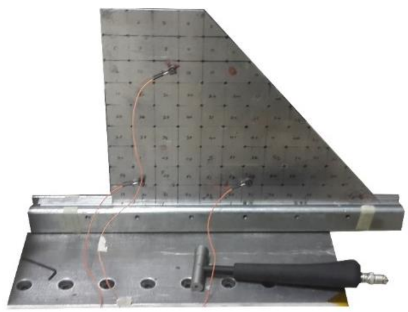

(d)

Configuration	Resonance Frequencies [Hz]		
	1st Mode	2nd Mode	3rd Mode
TE (G)	25.50	83.00	137.80

(e)

Figure continues on next page

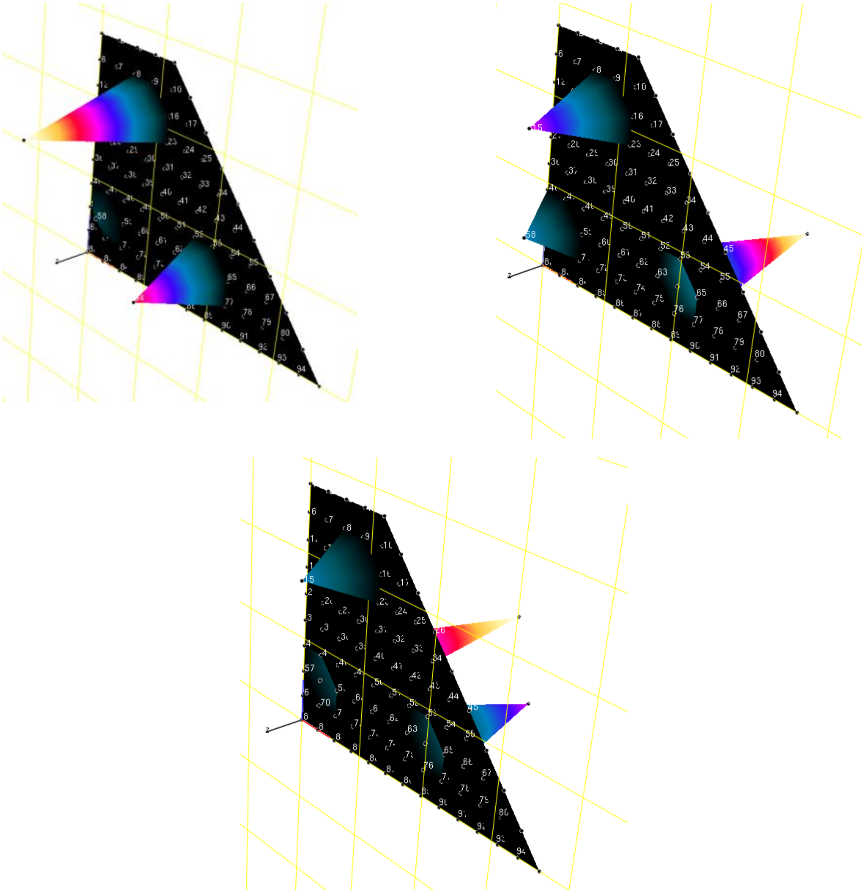

(f)

Figure 21 Total Error - Configuration G (a) Configuration Obtained from Optimization (b) Configuration in B&K Modal Test Consultant (c) Accelerance FRF (d) Test Setup (e) Resonance Frequencies Obtained (f) Mode Shapes Observed from One Measurement

The most expensive case of optimization of total errors was validated by the test and results are shown in Figure 21. Only three accelerometers were selected and all of them were the most expensive ones which are also the lightest. These accelerometers were located in a triangular shape to capture the first bending, the first torsion and the second bending mode shapes. Also, an impact hammer was selected in order not to increase the mass loading error.

CHAPTER 7

UNMANNED AERIAL WING MODELLING

Unmanned aerial vehicles (UAV) are a kind of drones which are mainly controlled in two ways which are remotely controlled (RC) and computer controlled (Autonomous). Endurance and range of these drones are the most important performance goals in design stage. Therefore they are very light weight and flexible which makes them more prone to vibration borne problems. In order to solve these problems ground vibration tests (GVT) are usually performed on UAVs to find dynamic characteristics of aircraft before going airborne. Using these GVTs, a structural design engineer is able to modify structure in a way which leads to lower vibrational problems. This is strongly dependent on quality and reliability of GVTs. To have that it is required to perform a pre-test analysis before those modal tests. In this study wing of an UAV which is shown in Figure 22 was used as test specimen. This UAV was designed and manufactured in a project which was funded by TÜBİTAK institute (TÜBİTAK 107M103 [28]).

Figure 22 Unmanned Aerial Vehicle Designed and Manufactured In TÜBİTAK 107M103 Project [28]

7.1 Numerical Model of UAV Wing

7.1.1 Finite Element Modelling and Analysis

UAV wing is modelled and meshed using MSC©PATRAN [15] (Figure 23). Modal characteristics of the wing (i.e. the natural frequencies and the corresponding mode shapes) are determined by MSC©NASTRAN using SOL103 module and are shown in Figure 24.

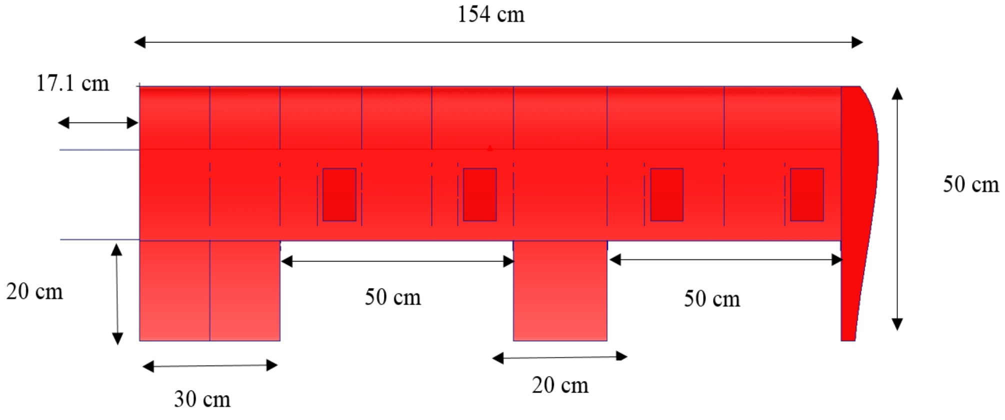

(a)

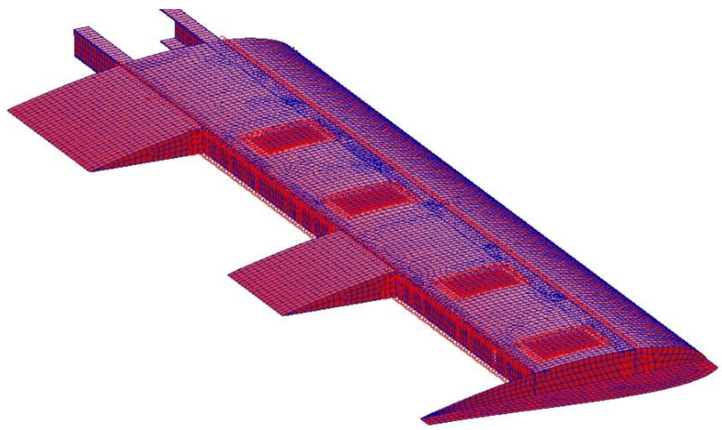

(b)

Figure 23 (a) Dimensions of UAV wing [28] (b) and the mesh used in MSC©PATRAN.

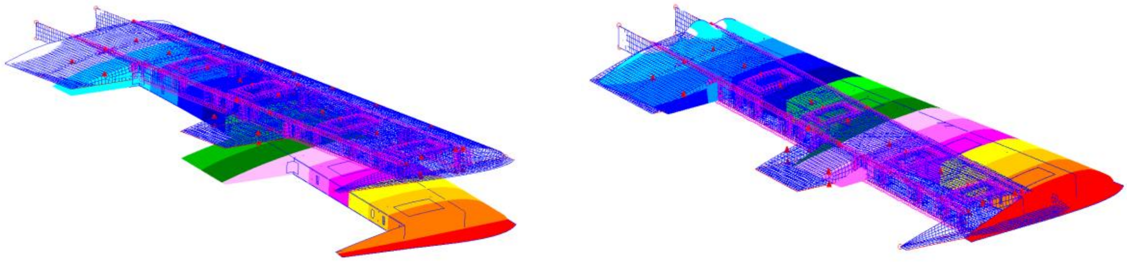

(a) (b)

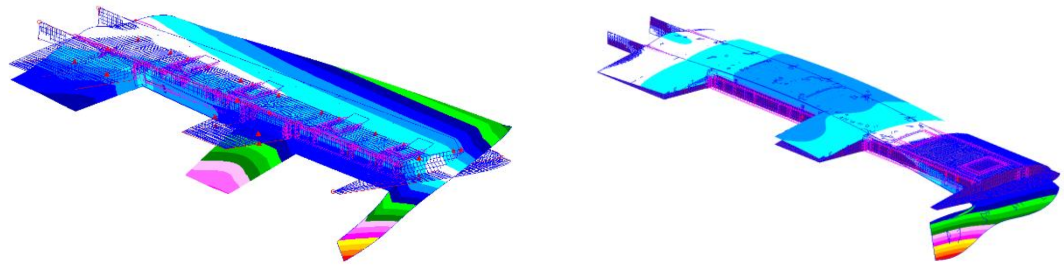

(c) (d)

Figure 24 Mode Shapes obtained via FEA (a) 1st Out-of-Plane Bending [14.99 Hz], (b) 1st In-Plane Bending [49.87 Hz], (c) 1st Torsion [62.68 Hz] (d) 2nd Out-of-Plane Bending [94.86 Hz]

7.1.2 Mesh Convergence Analysis

A mesh convergence analysis is also performed to obtain a fine enough mesh density with reasonable accuracy and computing time. Different mesh densities are depicted in Figure 25 and mesh convergence analysis results are tabulated in Table 9.

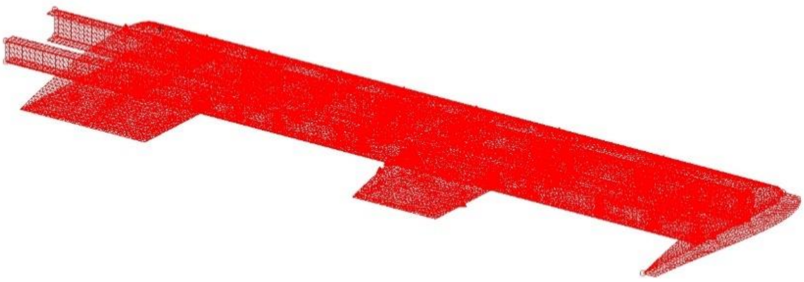

(a)

Figure continues on next page

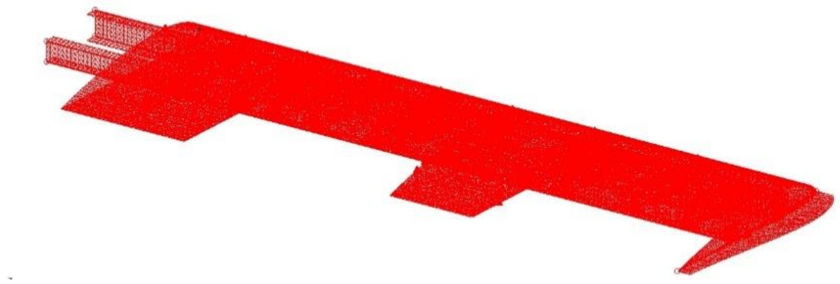

(b)

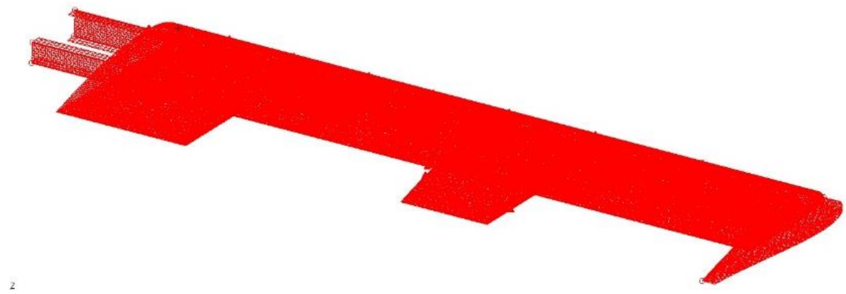

(c)

Figure 25 Mesh Densities (a) 0.01 m (b) 0.005 m (c) 0.0025 m.

Table 9 Mesh Convergence Analysis for UAV Wing.

Mode Shape (Element Edge Length)	**1st Mesh (0.01 m)**	**2nd Mesh (0.005 m)**	**3rd Mesh (0.0025 m)**
1st Out-of-Plane Bending [Hz]	15.43	15.13	14.99
1st In-Plane Bending [Hz]	50.51	50.12	49.87
1st Torsion [Hz]	64.41	63.15	62.68
2nd Out-of-Plane Bending [Hz]	97.05	95.35	94.86
# of Elements	35580	70491	140313
# of Nodes	18764	37575	73993

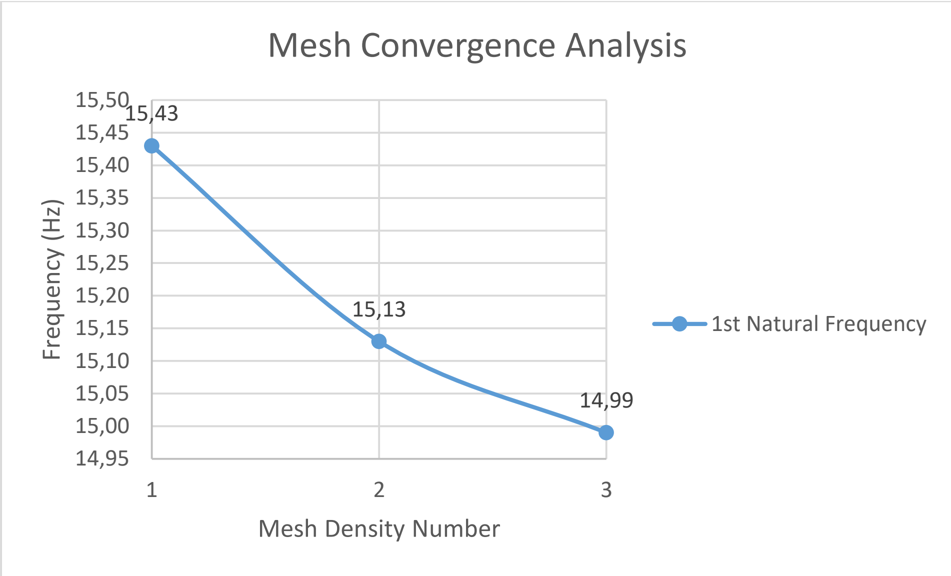

(a)

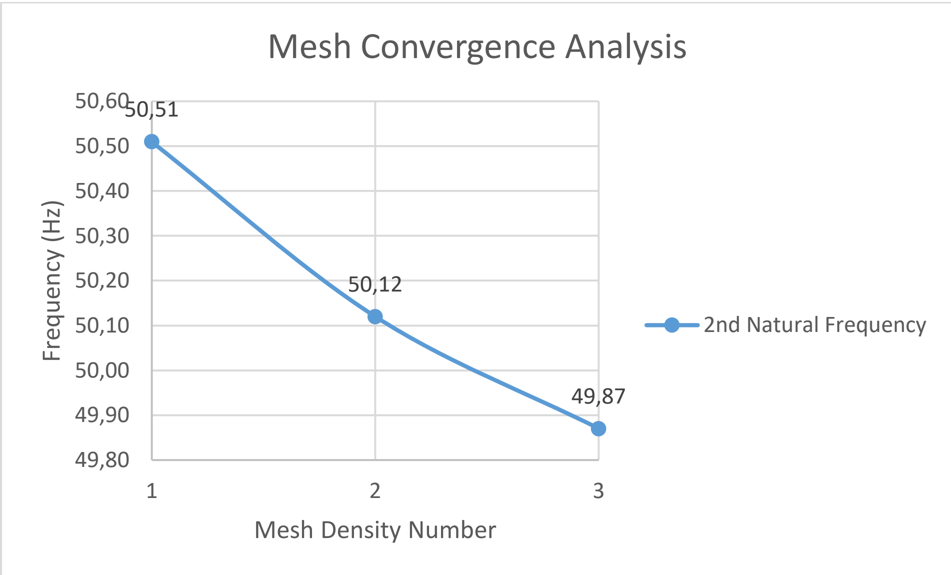

(b)

Figure continues on next page

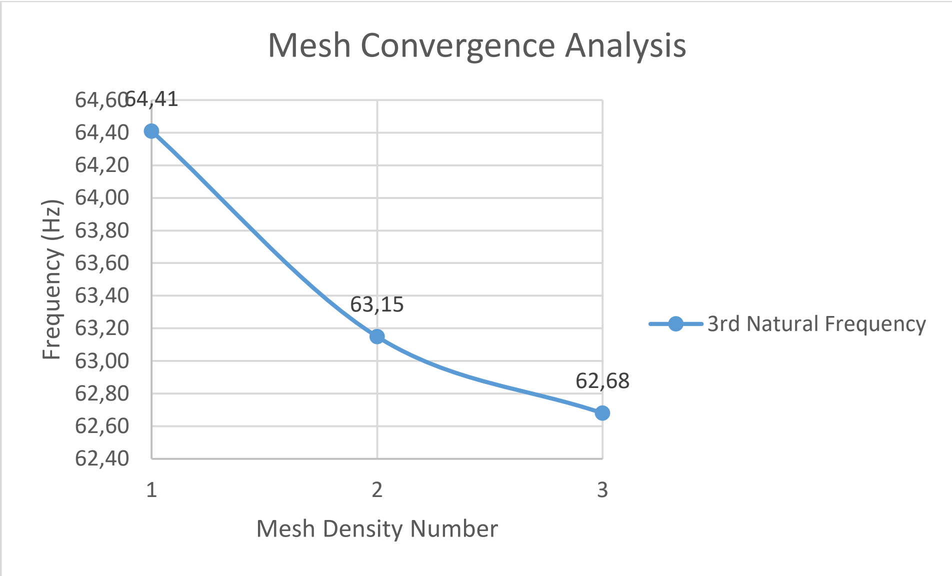

(c)

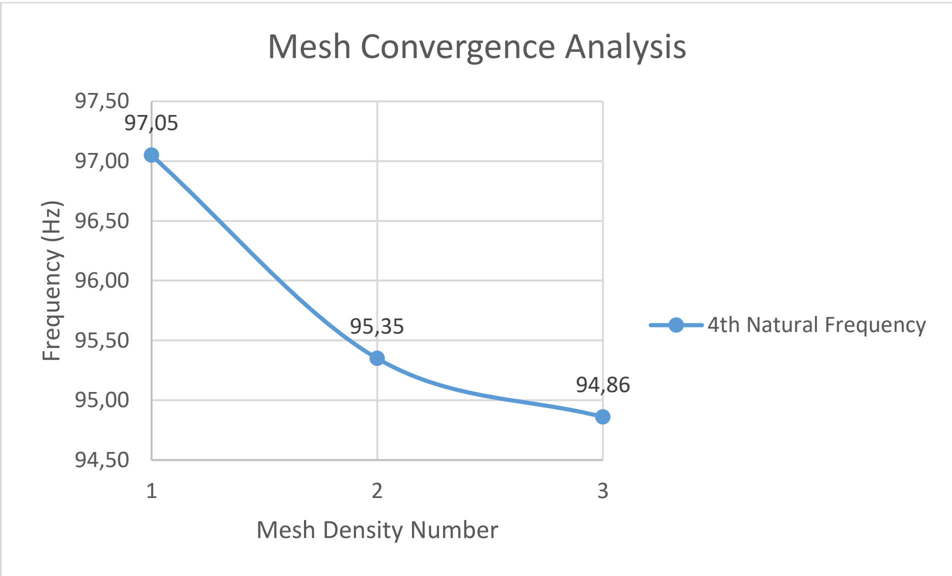

(d)

Figure 26 Mesh Convergence Analysis Diagrams of UAV Wing. (a) 1st Natural Frequency (b) 2nd Natural Frequency (c) 3rd Natural Frequency (d) 4th Natural Frequency

It can interpreted from Table 9 and Figure 26 that increase in mesh density over 0.0025 (3rd Mesh Density) results in differences in frequencies smaller than

0.3% (set as stopping criteria before) in predictions, therefore 3rd mesh density (0.0025 m) is decided to be used in this study.

7.2 Parametric Model of UAV Wing

During optimization, a new set of locations of transducers in each iteration is generated. To determine the new modal characteristics of the fin-like plate, re-meshing of existing finite element model is mandatory. Re-meshing is performed using a MATLAB script by changing existing finite element model mesh. This script first creates zero dimensional point elements on candidate transducer's locations, and then assigns a lumped mass property to these locations which carry mass information of transducers. It also selects these locations as master degrees of freedom (ASET) to use in Guyan model reduction.

Since genetic algorithm mimics nature evolutionary behavior, it evolves in each iteration. Therefore, there must be an automated process which evaluates objective and constraint functions for each solution of population. The objective function related with the error in prediction of the modal characteristics of the plate is evaluated by re-meshing and re-analysis of baseline FEM. A distributed computing cluster was setup using parallel computing toolbox of MATLAB and 6 computers were selected as workers. Therefore by help of cluster, a fourfold increase in computation power is observed.

Global optimization toolbox of MATLAB was used for optimization. Genetic algorithm code sends out design variables of each member to objective and constraint functions by taking into account limits of design variables. In these objective and constraint functions there are calls to external finite element solver (MSC©NASTRAN). Result from solver is fed back into these functions by help of regular expression library in MATLAB. At the end these functions return objective values and constraint violations of each member to genetic algorithm main code.

7.3 Test Model of UAV Wing

In order to obtain dynamic test model of the UAV wing, experimental modal analysis (EMA) is performed. Impact Hammer (B&K 8206) [16] with aluminum tip is used as an exciter (hammer figures in Figure 27) and a miniature accelerometer (B&K 4517-002) [17] (red arrow in Figure 27) is attached to tip of the wing and the Frequency Response Functions (FRFs) are calculated by roving hammer process. B&K Pulse©LABSHOP [18] software is used to gather experimental data from data acquisition device (B&K Modal Test Consultant 7753 with 6 channels) [19] and B&K Pulse/Reflex [22] software was used to perform the modal analysis by using obtained accelerance FRFs (Figure 28). The experimentally obtained resonance frequencies and the corresponding mode shapes are shown in Figure 29.

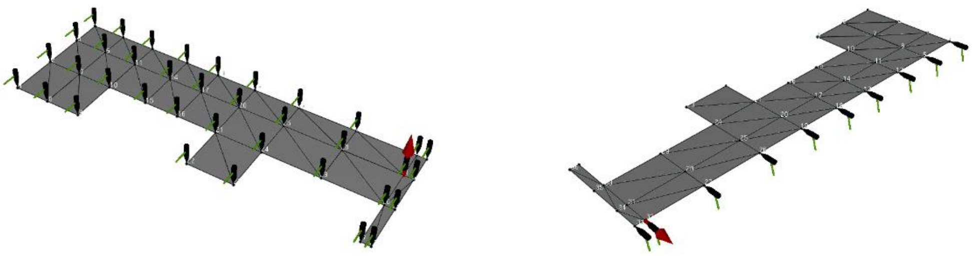

(a) (b)

Figure 27 Measurement Locations (a) Out-of-Plane, (b) In-Plane (Roving Hammer Test)

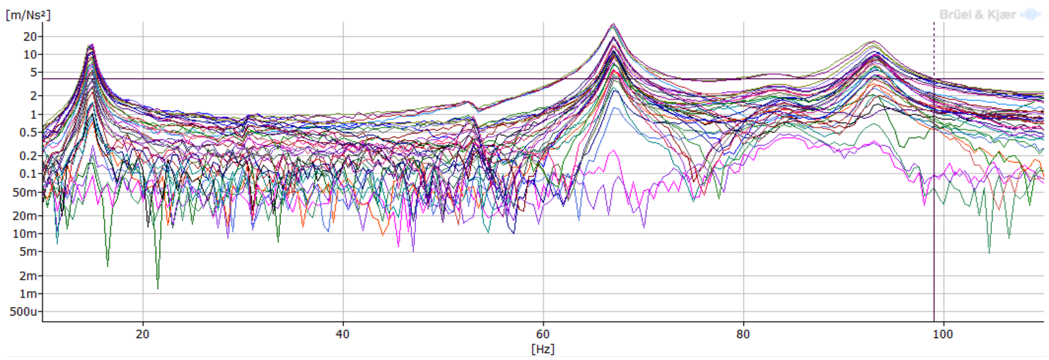

(a)

Figure continues on next page

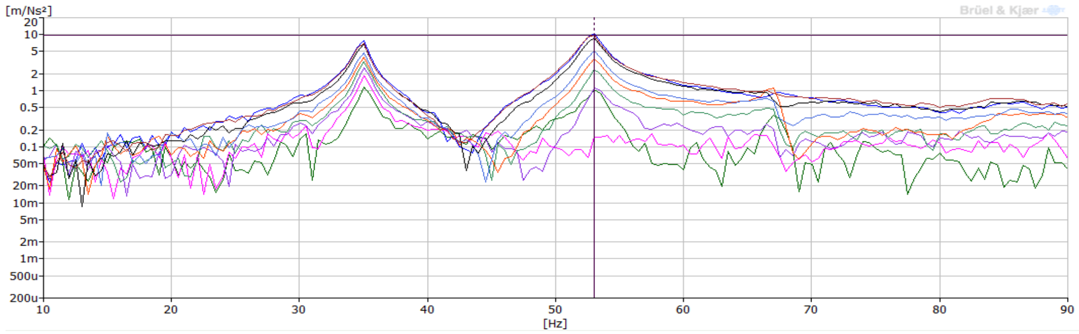

(b)

Figure 28 Accelerance FRFs Plots (a) Out-of-Plane, (b) In-Plane (Roving Hammer Test)

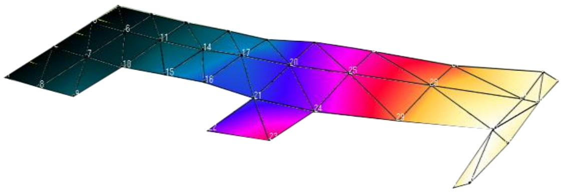

(a)

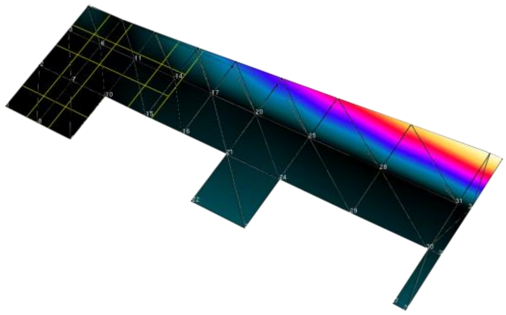

(b)

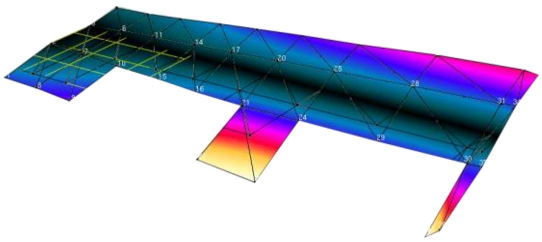

(c)

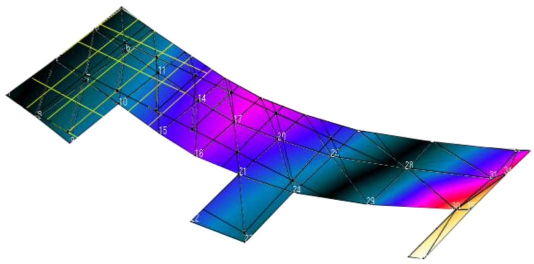

(d)

Figure 29 Mode Shapes obtained via EMA. (a) 1st Out-of-Plane Bending [14.99 Hz], (b) 1st In-Plane Bending [49.87 Hz], (c) 1st Torsion [62.68 Hz] (d) 2nd Out-of-Plane Bending [94.86 Hz]

7.3.1 Validation and Model Updating

Before model updating a correlation analysis is performed to make a comparison between the modal characteristics of two different models, namely FEM and the test model. The model updating is done using FEMTools [21] software. Since exact material properties of UAV wing are not known while modelling, standard values of aluminium were used. Therefore, in model updating wing's global material properties (i.e. stiffness [68.9-73.1 GPa], density [2660-2851 kg/m3]) are chosen as changing parameters in the ranges gives and the natural frequencies are chosen as response parameters. After several iterations, the obtained natural frequencies of FE model are closer to those of test model. The results of the model updating are tabulated in Table 10.

Table 10 Model Updating Results For UAV Wing.

Mode Shape	**FE Natural Frequencies – Before (Hz)**	**FE Natural Frequencies – After (Hz)**	**EMA Resonance Frequencies(Hz)**	**% $\Delta\omega$ Before**	**%$\Delta\omega$ After**
1st Out-of Plane Bending	14.99	14.88	14.85	0.93	0.21
1st In-Plane Bending	49.87	50.34	52.50	-5.27	-4.29
1st Torsion	62.67	63.12	67.29	-7.37	-6.61
2nd Out-of Plane Bending	94.86	94.23	94.03	0.87	0.21

During optimization, a new set of locations of transducers in each iteration is generated. To determine the new modal characteristics of the UAV wing, re-meshing of existing finite element model is mandatory. Re-meshing is performed using a MATLAB script by changing existing finite element model mesh. This script first creates zero dimensional point elements on candidate transducer's locations, and then assigns a lumped mass property to these locations which carry mass information of transducers. It also selects these locations as master degrees of freedom (ASET) to use in Guyan model reduction.

Since genetic algorithm mimics nature evolutionary behavior, it evolves in each iteration. Therefore, there must be an automated process which evaluates objective and constraint functions for each solution of population. The objective function related with the error in prediction of the modal characteristics of the wing is evaluated by re-meshing and re-analysis of baseline FEM. A distributed computing cluster was setup using parallel computing toolbox of MATLAB and 6 computers were selected as workers. Therefore by help of cluster, a fourfold increase in computation power is observed.

Global optimization toolbox of MATLAB was used for optimization. Genetic algorithm code sends out design variables of each member to objective and constraint functions by taking into account limits of design variables. In these objective and constraint functions there are calls to external finite element solver (MSC©NASTRAN). Result from solver is fed back into these functions by help of regular expression library in MATLAB. At the end these functions return objective values and constraint violations of each member to genetic algorithm main code.

CHAPTER 8

MULTI-OBJECTIVE GENETIC ALGORITHM OPTIMIZATION OF UAV WING

Optimization problem setup of UAV wing is exactly same as fin-like plate. But there are a few differences in design variables and constraint functions which are explained in following parts. Objective function in UAV wing case considers first four natural frequencies not three as in the case of fin-like plate.

8.1 Design Variables

There are fifteen available transducers used in this study. In Table 5, transducers' type, model, number, image, price, mass and channel usage are listed. For each of these transducers two design variables are assigned. One variable is a binary variable that shows the use of that transducer and its measurement direction which is either zero, one or two. (0: not selected, 1: selected and in-plane, 2: selected and out-of-plane). The other variables is a discrete variable which is node number of corresponding transducer. Therefore, there are 30 discrete design variables which are used in this optimization problem. There are 18,904 grid points (Figure 30) in wing FE model but transducers must located on exterior grid points not interior ones. Also to avoid capturing local mode shapes (Usually on skin between spars and ribs), only exterior points which are located over ribs and spars are chosen as candidate transducer location (Figure 31). This reduces the number of grids to 1,511, which in return reduces FEA calculations runtime tremendously.

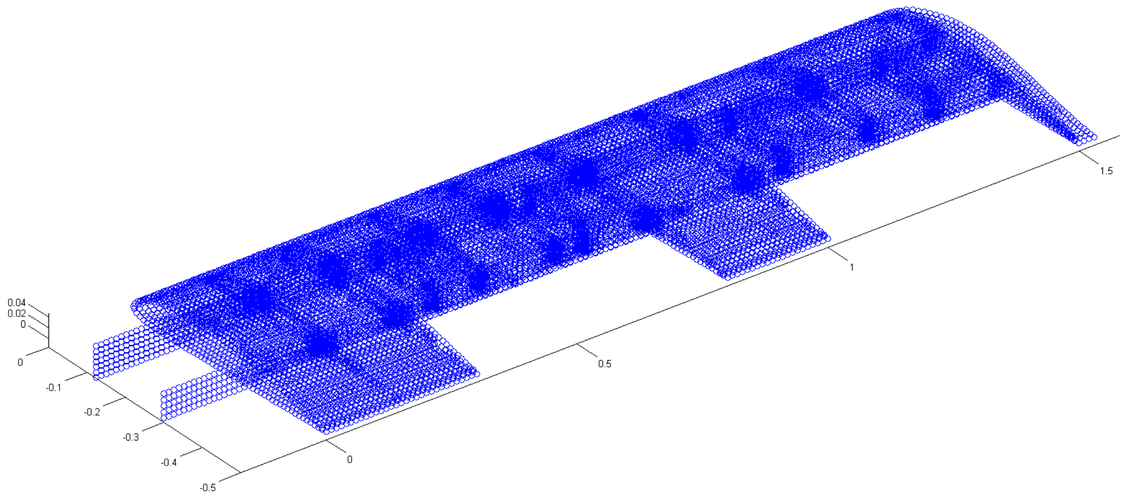

Figure 30 Candidate Transducers Locations (All Grid Points)

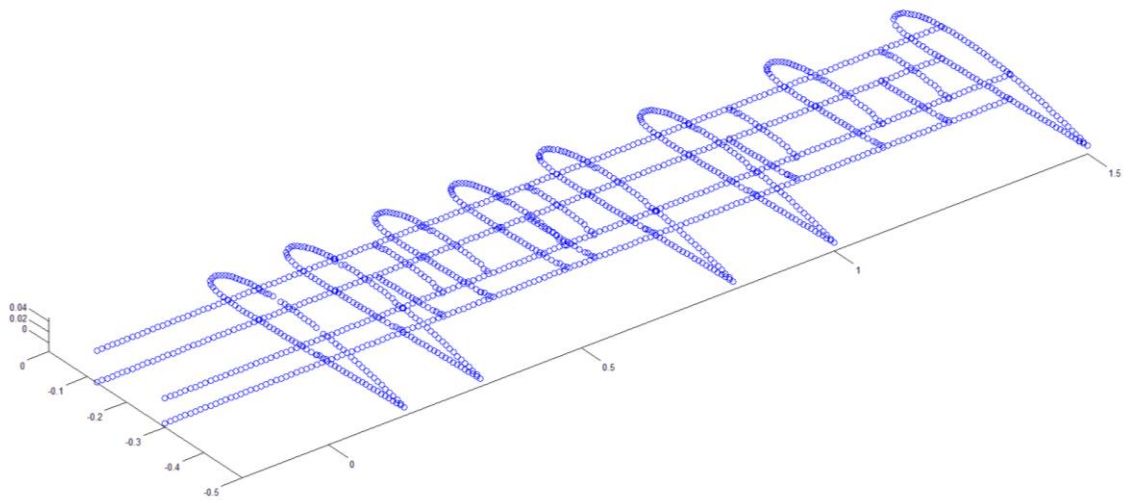

Figure 31 Candidate Transducers Locations (Selected Grid Points)

Figure continues on next page

8.2 Constraint Function

Seven constraints which are used in all of optimizations are listed below.

$$AVAIL_i = its\ elements\ shows\ whether$$
$$that\ specific\ transducers\ is\ selected\ or\ not$$ and whether

It is in in-plane or out-of-plane direction

(0: not selected, 1: in-plane, 2: out-of-plane)

$$i = 1,..,15\ (number\ of\ available\ tranducers)$$

$$ACC_i = its\ elements\ shows\ whether$$
$$that\ specific\ transducers\ is\ accelerometer\ or\ not$$
$$i = 1,..,15\ (number\ of\ available\ tranducers)$$

$$FT_i = its\ elements\ shows\ whether$$
$$that\ specific\ transducers\ is\ force\ transducer\ or\ not$$
$$i = 1,..,15\ (number\ of\ available\ tranducers)$$

$$CH_i = its\ elements\ shows\ number$$
$$of\ occupied\ channels\ in\ data\ aquisition\ device\ by\ that\ transducer$$
$$i = 1,..,15\ (number\ of\ available\ tranducers)$$

In case of impedance head, FT and ACC are both one.

i. Transducers must not located on areas near clamped part of wing which has no skin.

$$v_i \geq L$$

$$v_i = 1..15 \begin{pmatrix} \text{spanwise distance from middle of transducer to clamp side} \\ 15 = \text{ number of available transducers} \end{pmatrix}$$

$$L = \ unskined\ spars\ length$$

ii. At least one accelerometer and one force transducer must be selected.

$$\sum_{i=1}^{15} step\_function(AVAIL_i - 1) * (ACC_i + FT_i) \geq 2$$

iii. Minimum distance between transducers must not exceed diameter of largest transducer.

$$\sum_{\substack{i=1 \\ j=1}}^{\substack{i=15 \\ j=15}} \sqrt{\left(x_i - x_j\right)^2 + \left(y_i - y_j\right)^2 \left(z_i - z_j\right)^2} \geq D_{Largest}$$

$$x_{i,j} = x\ coordinate\ of\ center\ of\ transducer$$

$$y_{i,j} = y\ coordinate\ of\ center\ of\ transducer$$

$$z_{i,j} = z\ coordinate\ of\ center\ of\ transducer$$

$$D_{Largest} = \ largest\ transudcer\ diameter$$

iv. Number of occupied channels by transducers must not exceed six. (data acquisition device has maximum of six channels)

$$\sum_{i=1}^{15} step\_function(AVAIL_i - 1) * \ CH_i \ \leq 6$$

v. Only one force transducer must be selected, because the test setup (roving hammer) is a SIMO (single-input and multiple-output) system.

$$\sum_{i=13}^{15} step\_function(AVAIL_i - 1) \ \leq 1$$

$$i = 13{,}14{,}15\ are\ indices\ of\ force\ transducers$$

vi. At least one accelerometer in both in-plane and out-of-plane directions to capture both in plane and out of plane mode shapes.

$$at\ least\ one\ AVAIL_i\ with\ value\ of\ one\ and\ another\ AVAIL_i\ with\ value\ of\ 2$$
$$i = 1, \ldots, 15\ (number\ of\ available\ tranducers)$$

vii. In order to make modal test easier for test engineer, impact hammer location must be on areas over upper skin and modal shaker location must be on areas over lower skin of wing.

$$impact\ hammer\ vertical\ distance\ from\ wing\ midsurface > 0$$
$$modal\ shaker\ vertical\ distance\ from\ wing\ midsurface < 0$$

8.3 Optimization Results

In multi-objective optimization problem, there is no single optimum solution, instead there is a range of solutions in which several optima can reside. In this range, some solutions are dominated by other solutions (has higher values in all of objectives). Solutions which are not dominated by any other solutions (has lower values in all of objectives) are called non-dominant solutions. A curve passing through these non-dominant solutions is called Pareto frontier curve.

8.3.1 Case 1: Minimization of the MLE and the Total Cost

The Pareto frontier curve obtained for Case 1 is shown in Figure 32. Three representative Pareto optimal solutions are chosen for depiction and listed in Table 11. It is observed from Table 11 and Figure 32 that the mass loading error is very small for the chosen representative Pareto optimal solutions. When the optimum configurations A and B are analyzed (see *Figure 33*) it is observed that transducers are placed very close to the region with minimum modal constant in all modes of interest (near root area). In configuration C and D, force transducer is located far from root because the selected transducers are impact hammers. Their location do not affect modal masses of wing because they are not attached to structure like shakers' force transducer. Another important concept is that with increasing cost limit, the optimizer still chooses only two accelerometer and force transducer and that is because to keep mass loading as minimum as possible. With increasing price only type (therefore mass) of transducers is changed.

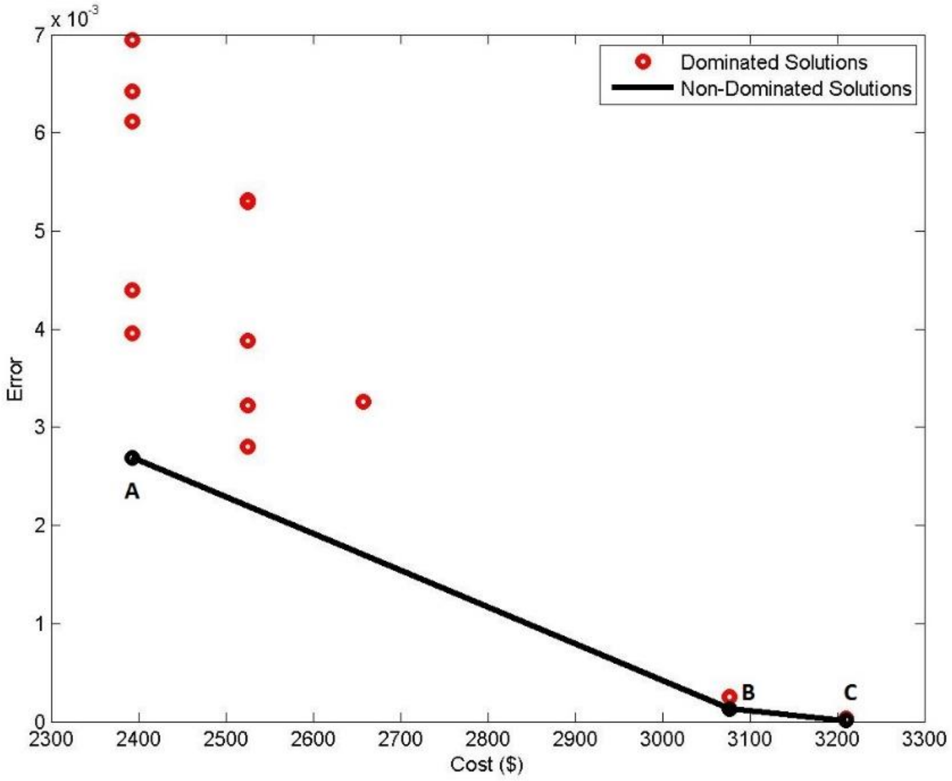

Figure 32 Pareto Frontier Curve and Selected Non-dominant Solutions (ML Error Only).

Table 11 Total Error and Cost of Pareto Frontier Solutions (ML Error Only) For UAV Wing.

Configuration	*ML Error	Cost ($)
A	0.00269	2392
B	0.00013	3076
C	0.00001	3209

* *ML: Mass Loading*

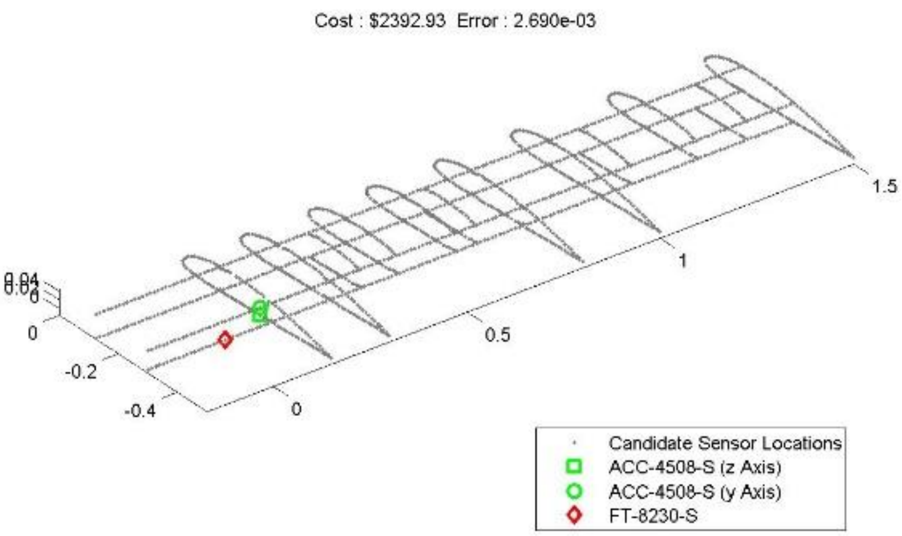

(a)

Figure continues in next page

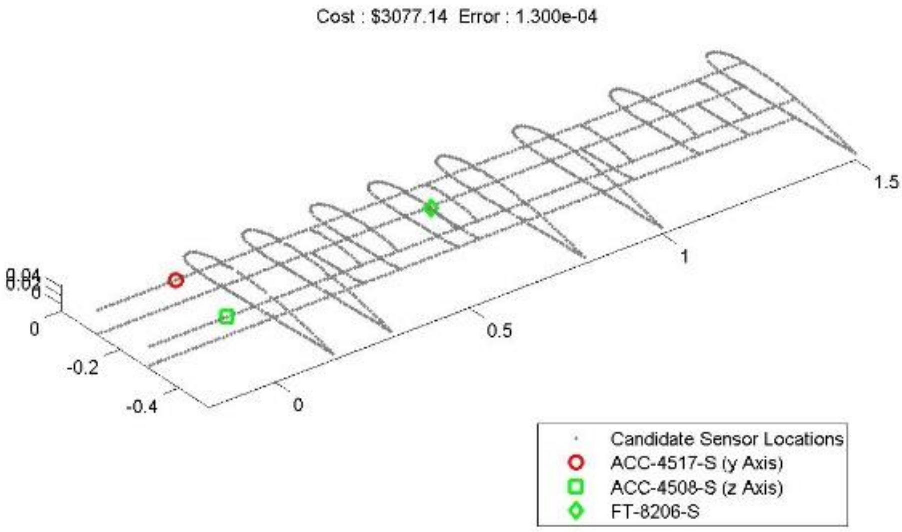

(b)

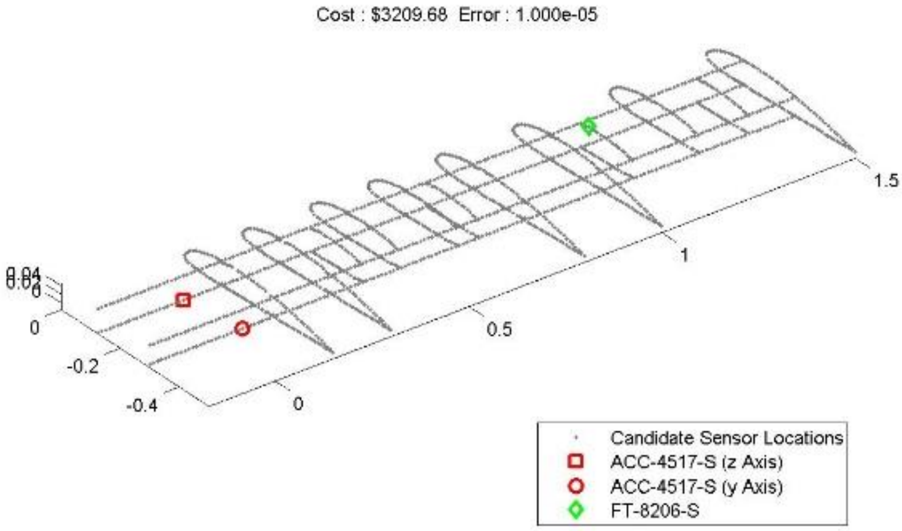

(c)

Figure 33 Locations of Transducers in Candidate Configurations from Pareto Frontier (ML Error Only).Configuration A (b) Configuration B (c) Configuration C

8.3.2 Case 2: Minimization of the MSOE and the Total Cost

The Pareto frontier curve obtained for Case 2 is shown in Figure 34. Three representative Pareto optimal solutions are chosen for depiction and listed in Table 12. It is evident from results that increase in number of accelerometers will lead to better mode shape observability. Figure 35 shows that in configuration A, because of cost limit only three single axis accelerometers were selected. Two of them are pointed in out of plane direction and one in in-plane direction. All of accelerometers are placed over nodal line of fourth mode which is out of plane 2nd bending mode and that is due to minimum modal mass change (at least for fourth mode). These two out of plane accelerometers are able to capture 1st, 2nd out of plane bending and 1st torsion mode shapes. Single in-plane accelerometer will also capture 1st in-plane bending mode shape. As it is expected with increasing price more accelerometers are added and they are usually placed in regions with high acceleration (at least in one mode shape). This optimization shows that for mode shape observability the more accelerometer you use, mode shapes are more distinguished with only one SIMO test (not roving) and of course their location has a vital importance in observability of mode shapes. For example with three accelerometers you can capture all four or just three mode shapes and that depends on how you arrange accelerometers to capture torsion mode

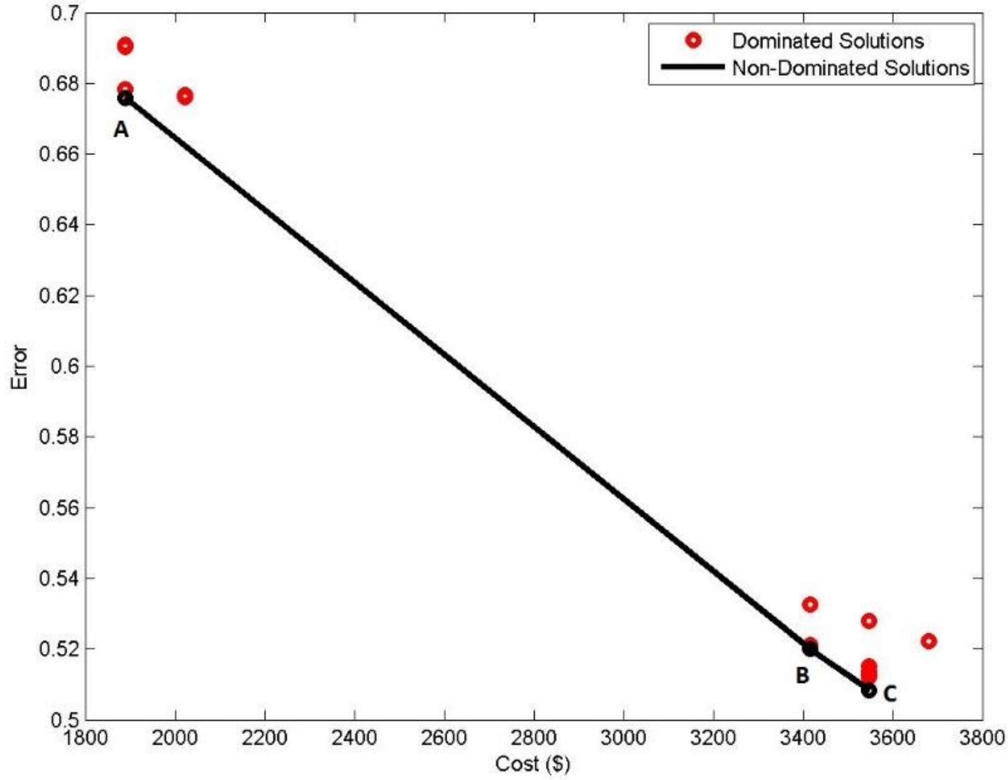

Figure 34 Pareto Frontier Curve and Selected Non-dominant Solutions (MSO Error Only).

Table 12 Total Error and Cost of Pareto Frontier Solutions (MSO Error Only) For UAV Wing.

Configuration	***MSO Error**	**Cost ($)**
A	0.6759	1890
B	0.5199	3415
C	0.5084	3547

**MSO: Mode Shape Observability*

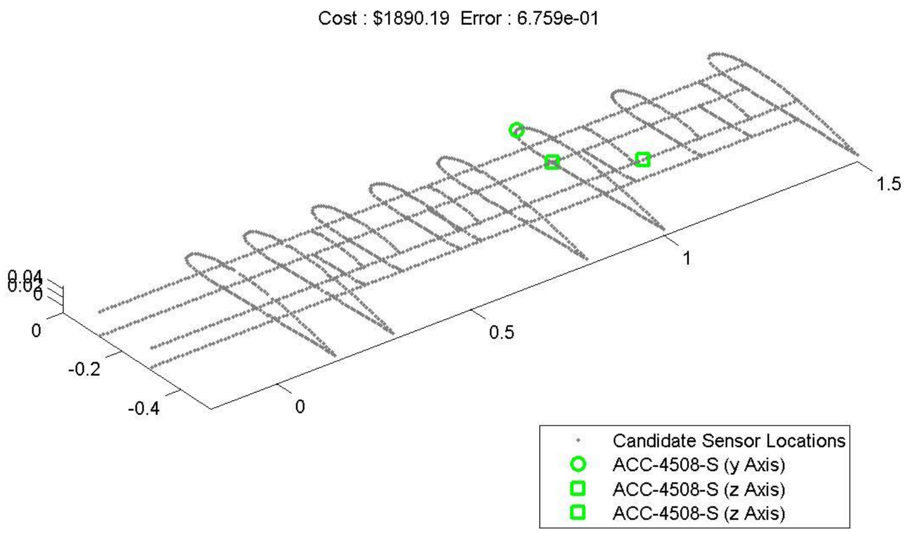

(a)

Figure continues in next page

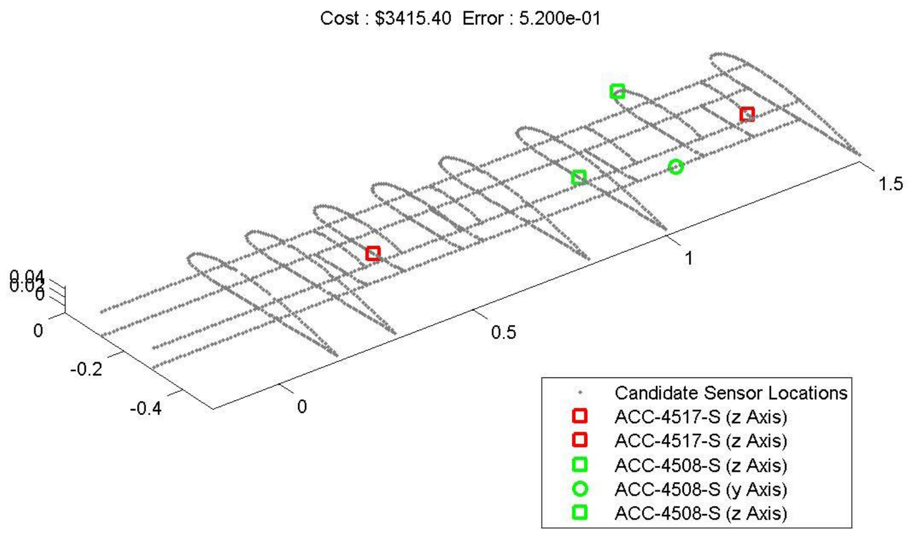

(b)

Figure continues in next page

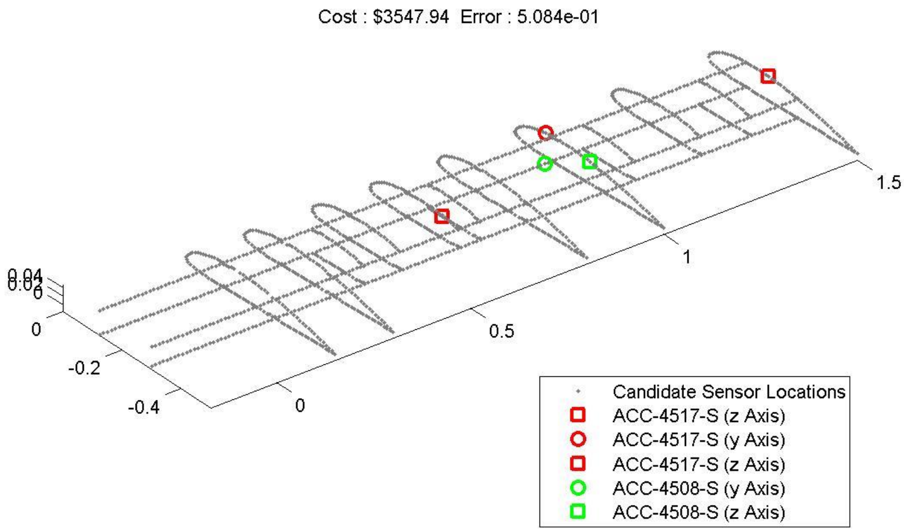

(c)

Figure 35 Locations of Transducers in Candidate Configurations from Pareto Frontier (MSO Error Only). (a) Configuration A (b) Configuration B (c) Configuration C

8.3.3 Case 3: Minimization of the ODPE and the Total Cost

When objective function is only dependent on optimum driving point error, the optimization problem reduces to the selection of the most appropriate location for the impact hammer or modal shaker. Since the shakers' force transducer is less expensive than the impact hammer, the optimum choice is the use of the shaker. It is found that the optimum solution is attaching the shaker to a point with minimum acceleration (Figure 36). The ODP error for this configuration is computed as 0.000653.

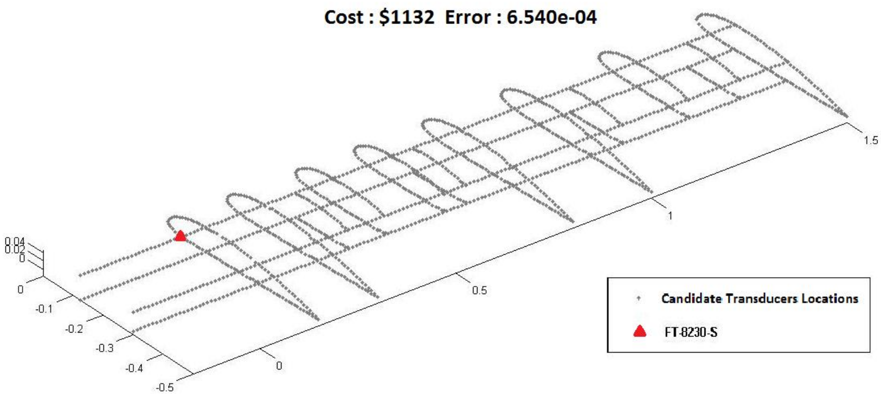

Figure 36 Optimum Location of the Shaker for minimum ODPE

8.3.4 Case 4: Minimization of the Overall Equivalent Error and the Total Cost

The Pareto frontier curve obtained for Case 4 is shown in Figure 37. Six representative Pareto optimal solutions are chosen for depiction and listed in Table 13. Figure 38 shows that for configurations of all optimum solutions. When all of errors are combined together it can be concluded that all errors are tried to get minimized or kept at a minimum level. Since there is no weighting used in summation of errors, dominant error (MSO Error) is always tried to get minimized further as price increases. Also the other two non-dominant ones (ML and ODP Errors) are kept at a minimum level with increasing price. In configuration A, because of constraint limit minimum two accelerometers were selected and price limit forced to choose cheapest ones (heavy ones). Also the cheapest force transducer (shaker) was selected. Both in-plane and out of plane accelerometers are selected to capture at least 1st in-plane and out of plane bending mode shapes. In configuration B, with a price limit increase one more accelerometer (4517-002) is selected. In configuration C, instead of one of three accelerometers, two of them are chosen as 4517-002 (expensive one). As it was expected with another price increase instead of shaker force transducer an impact hammer transducer (more expensive) is selected. This trend goes on until configuration

F which is the most expensive one but minimum error. In this configuration three out of plane miniature accelerometers are located in a triangular shape (like the fin-like plate). This triangular shape will capture 1st out of plane bending, 2nd out of plane bending and 1st torsion mode shapes. Two in-plane accelerometers were also selected to capture first in-plane bending mode shape. For excitation impact hammer is selected. Since these results may be are local minimums. Performing further optimizations may provide better local minima or even global minimum.

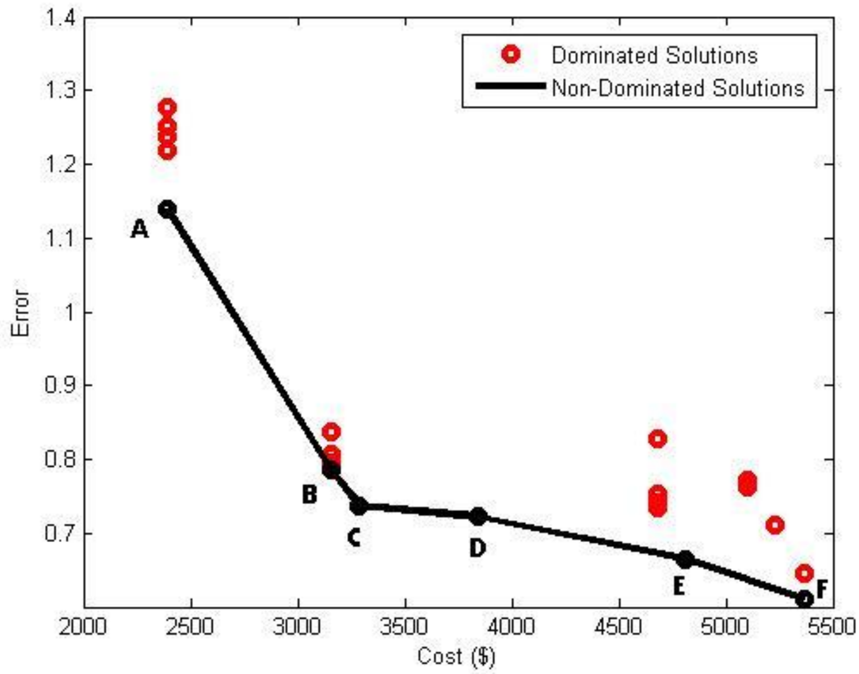

Figure 37 Pareto Frontier Curve and Selected Non-dominant Solutions (Total Error).

Table 13 Total Error and Cost of Pareto Frontier Solutions (Total Error) For UAV Wing.

Configuration	***ML Error**	***MSO Error**	***ODP Error**	**Total Error**	**Cost ($)**
A	0.0836	1.0538	0.0020	1.1394	2392
B	0.0754	0.7086	0.0017	0.7857	3155
C	0.0405	0.6941	0.0030	0.7376	3288
D	0.0400	0.6803	0.0022	0.7225	3839
E	0.1301	0.5317	0.0028	0.6645	4813
F	0.0594	0.5382	0.0134	0.6110	5364

** ML: Mass Loading MSO: Mode Shape Observability ODP: Optimum Driving Point*

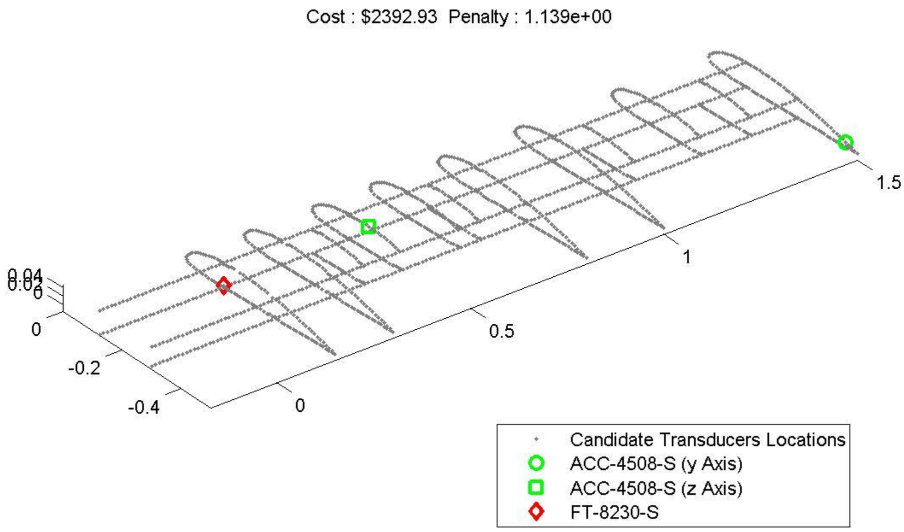

(a)

Figure continues in next page

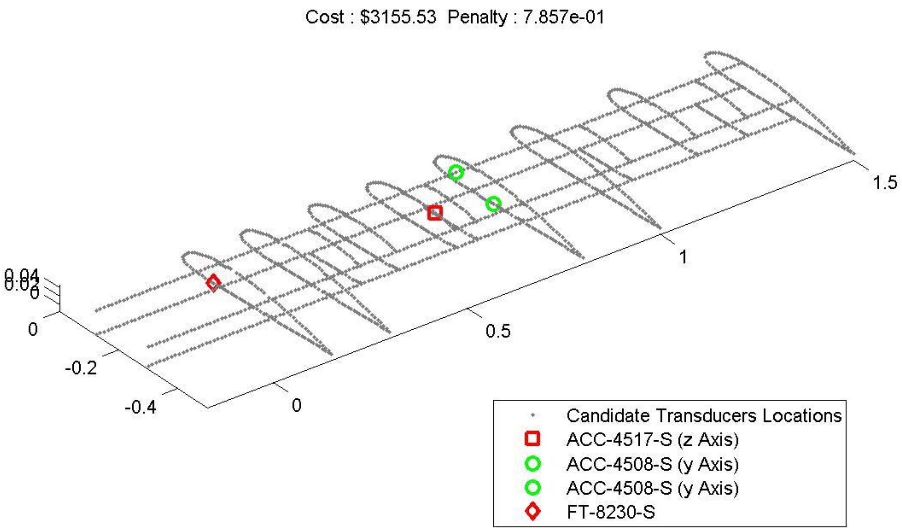

(b)

Figure continues in next page

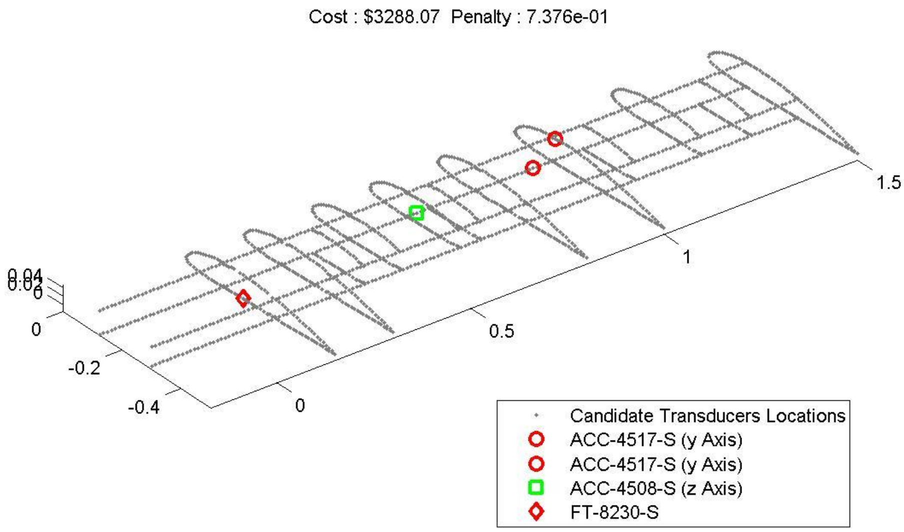

(c)

Figure continues in next page

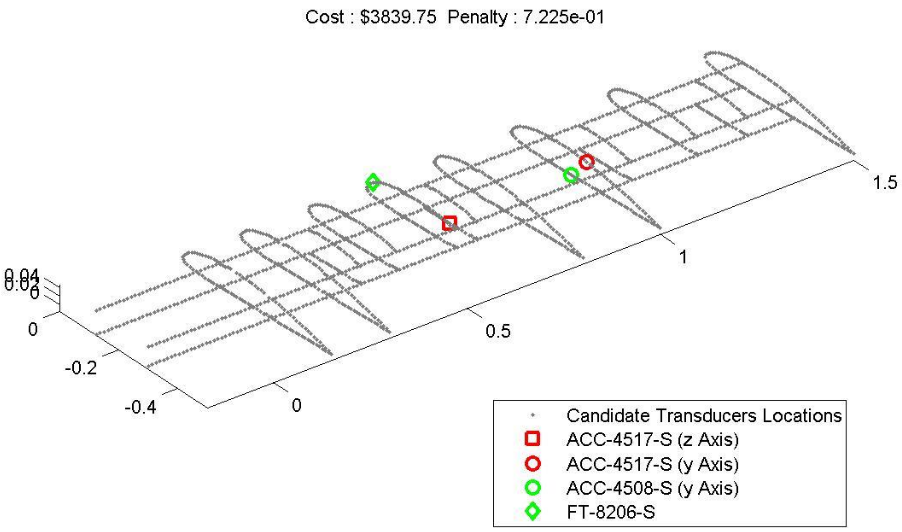

(d)

Figure continues in next page

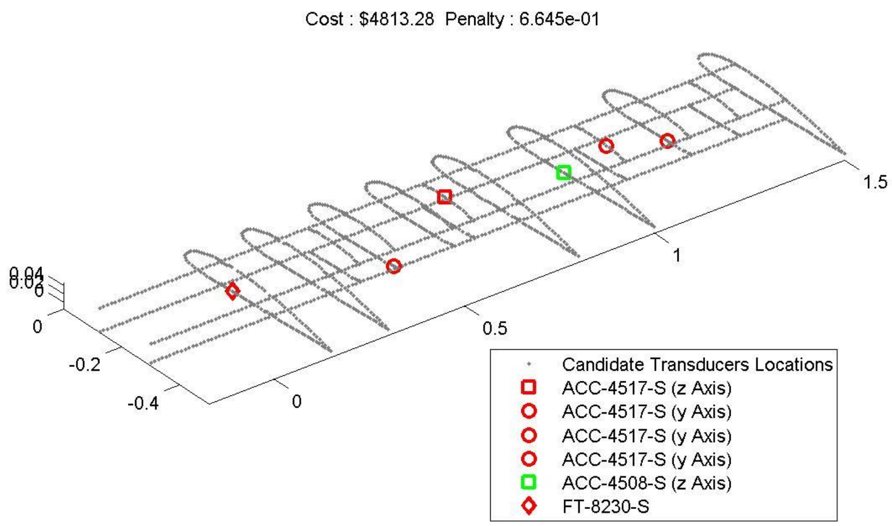

(e)

Figure continues in next page

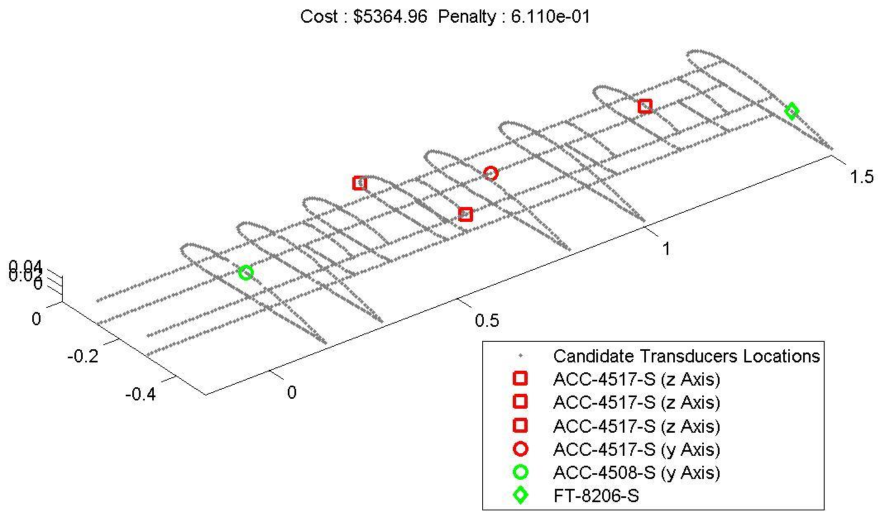

(f)

Figure 38 Locations of Transducers in Candidate Configurations from Pareto Frontier (Total Error). (a) Configuration A (b) Configuration B (c) Configuration C (d) Configuration D (e) Configuration E (f) Configuration F

CHAPTER 9

VALIDATION OF THE OPTIMIZATION RESULTS VIA MODAL TEST

In this part of the study, configurations of Pareto optimum set in all optimizations are verified using experimental modal analysis technique. The previously obtained optimal results are taken into consideration and the experimental modal analysis setups are designed. The sensor(s)/actuator pairs are selected from Table 3 and the FRFs are calculated for various configurations by using B&K Modal Test Consultant 7753 software with 6 channel spectrum analyzer. The configurations are selected in such a way that one corresponding to a minimum-error (the most expensive) and one for the maximum-error (the cheapest). In (Figure 39 till Figure 50) all of results are presented in terms of the configuration obtained from the optimization analyses (the upper left figure), corresponding B&K Modal Test Consultant wing configuration (the upper right figure), accelerance FRF in the frequency range of interest, photo of the experimental setup regarding sensor(s)/actuator pairs and test results for the first four modes. Additionally, figures showing whether the modes of interests are captured by the performed experimental analyses or not are also presented if there are more than one accelerometer in corresponding direction (the bottom figure).

9.1 Case 1: Minimization of the MLE and the Total Cost

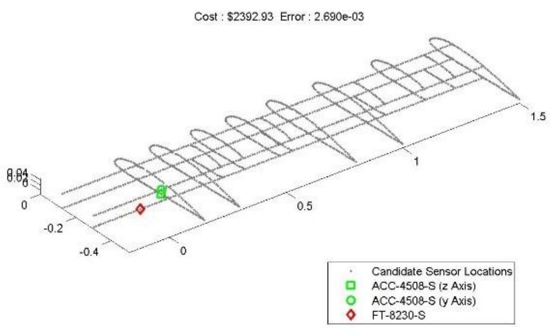

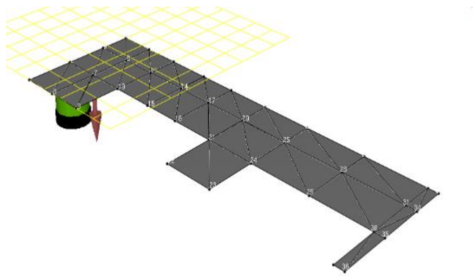

(b)

(a)

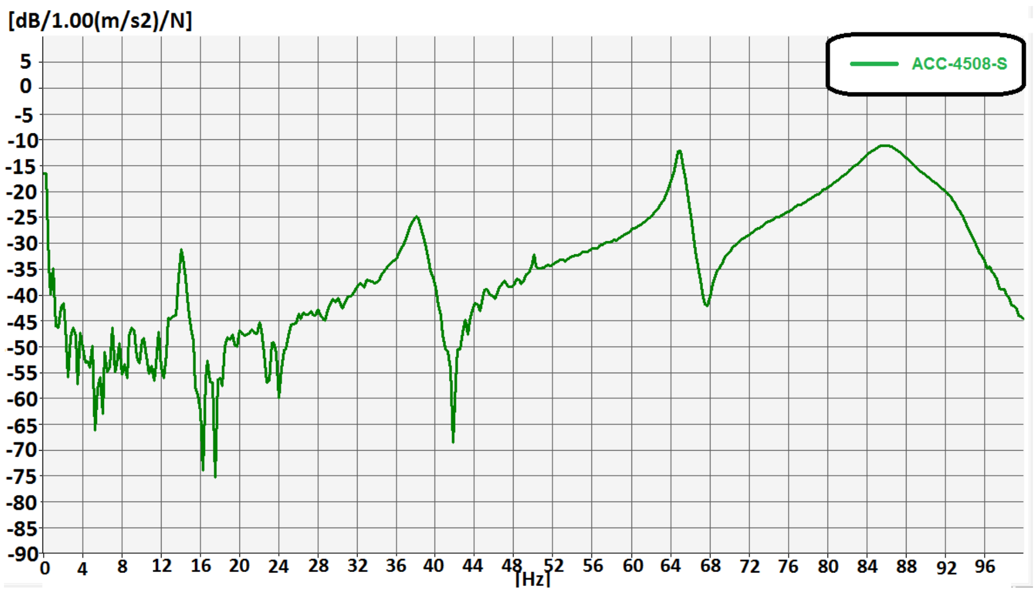

(c)

Figure continues in next page

Configuration	Resonance Frequencies[Hz]		
	1. Mode	2. Mode	3. Mode
ML (A)	14.00	65.00	85.75

(d) (e)

Figure 39 Mass Loading - Configuration A [Out of Plane] [UAV Wing] (a) Configuration Obtained from Optimization (b) Configuration in B&K Modal Test Consultant (c) Accelerance FRF (d) Test Setup (e) Resonance Frequencies Obtained

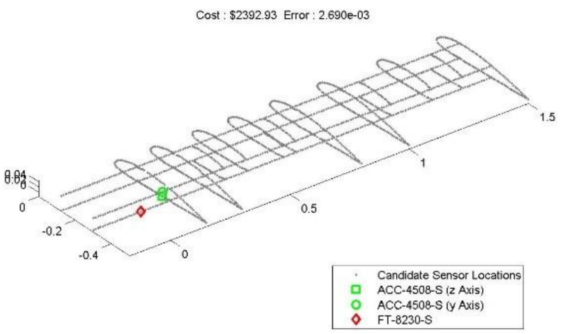

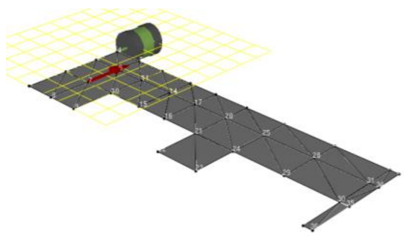

(a) (b)

Figure continues in next page

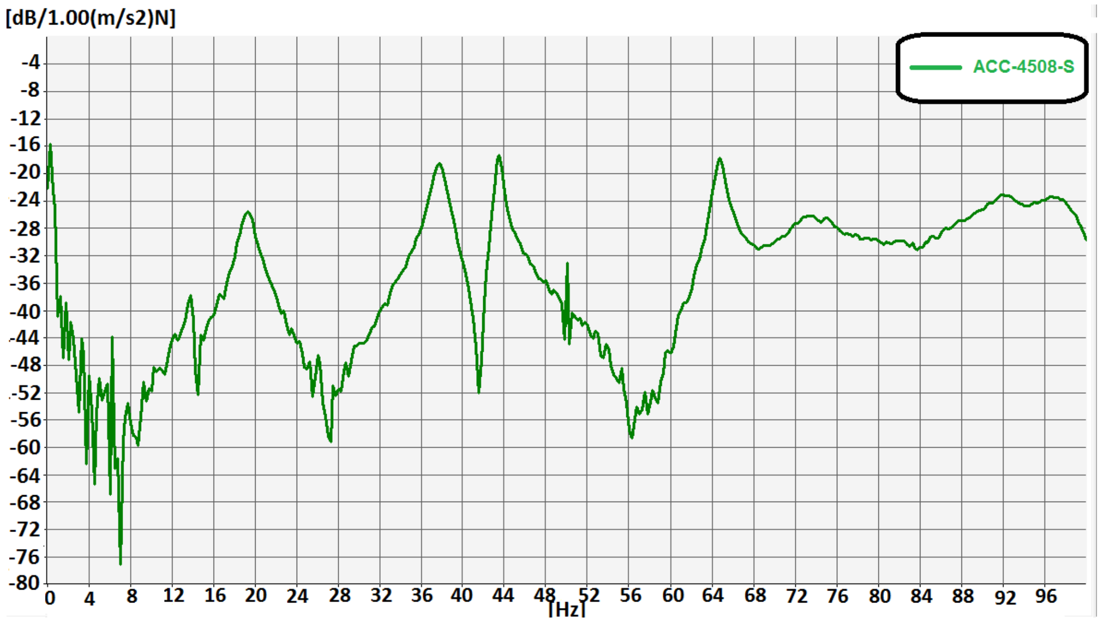

(c)

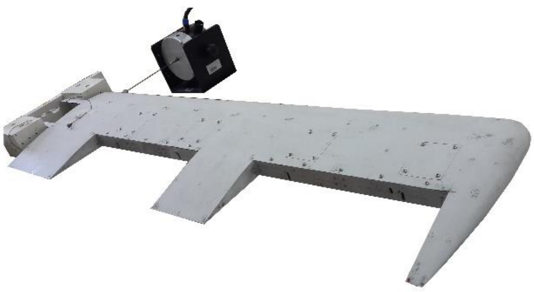

(d)

Configuration	Resonance Frequencies[Hz]
	1. Mode
ML (A)	43.50

(e)

Figure 40 Mass Loading - Configuration A [In Plane] [UAV Wing] (a) Configuration Obtained from Optimization (b) Configuration in B&K Modal Test Consultant (c) Accelerance FRF (d) Test Setup (e) Resonance Frequencies Obtained

As it is expected in the cheapest configuration (Figure 39 and Figure 40) of mass loading error optimization, two cheap accelerometers are selected and located near the clamp area to minimize mass loading error. Therefore, one accelerometer is located in the in-plane and other one is in the out-of-plane direction. Also, because of being the cheapest configuration, a modal shaker is located closer to the clamp area making shaker-structure interaction minimum.

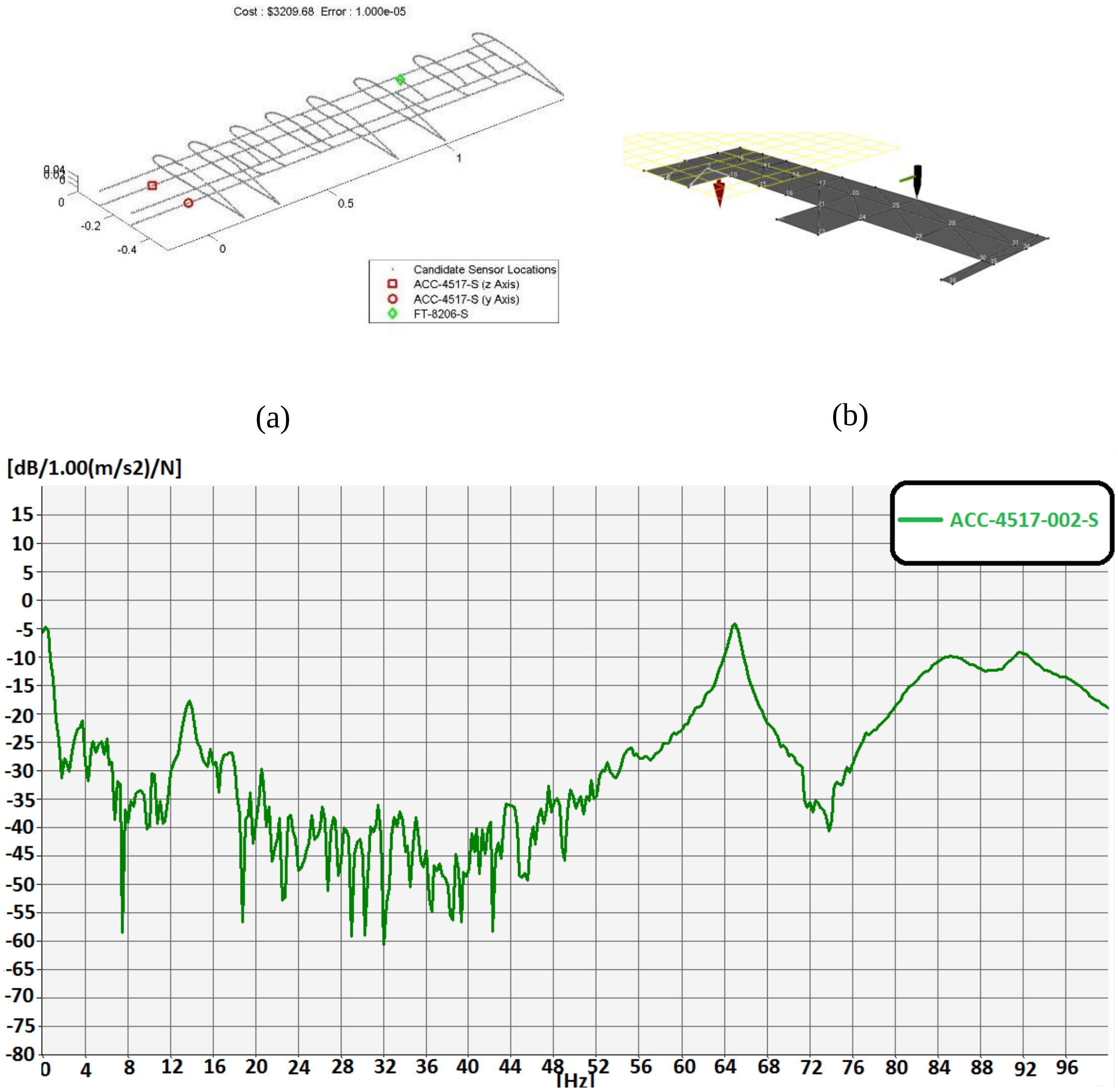

(a) (b)

(c)

Figure continues in next page

(d)

Configuration	Resonance Frequencies[Hz]		
	1. Mode	2. Mode	3. Mode
ML (C)	13.75	65.00	91.75

(e)

Figure 41 Mass Loading - Configuration C [Out of Plane] [UAV Wing] (a) Configuration Obtained from Optimization (b) Configuration in B&K Modal Test Consultant (c) Accelerance FRF (d) Test Setup (e) Resonance Frequencies Obtained

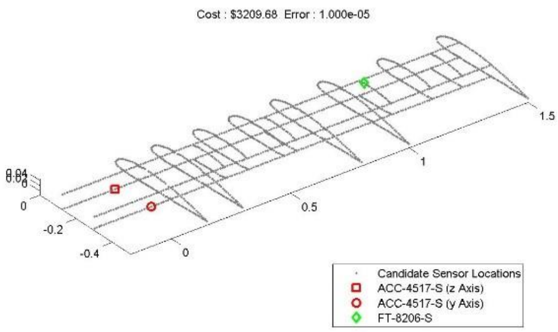

(a)

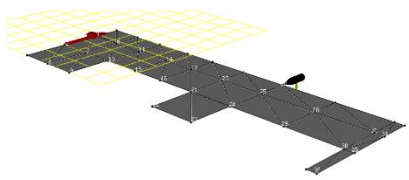

(b)

Figure continues on next page

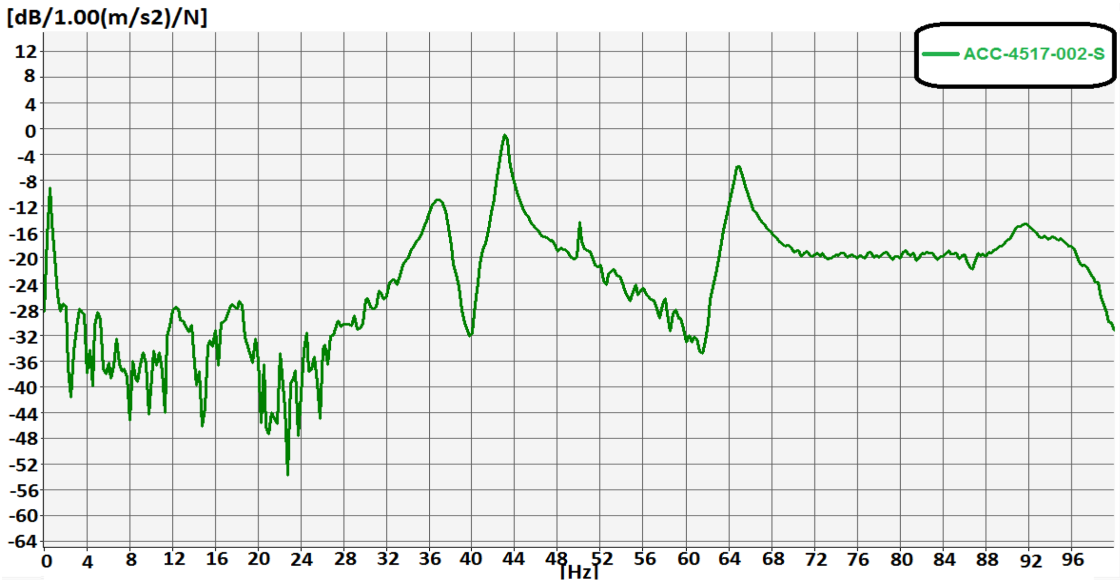

(c)

Configuration	Resonance Frequencies[Hz]
	1. Mode
ML (C)	43.00

(e)

(d)

Figure 42 Mass Loading Configuration C [In-Plane] [UAV Wing] (a) Configuration Obtained from Optimization (b) Configuration in B&K Modal Test Consultant (c) Accelerance FRF (d) Test Setup (e) Resonance Frequencies Obtained

In the most expensive case (Figure 41 and Figure 42) of mass loading optimization, two lightweight accelerometers are selected and located near the clamp area of the wing. One accelerometer is located in in-plane and other is in out-of-plane direction to capture both in- and out- of plane mode shapes. Also, impact hammer is selected by the algorithm in order to minimize mass loading error. Since accelerometers are placed near the areas having minimum acceleration, a low signal to noise ratio data was recorded. This is because of the sole purpose of this part of optimization which was to reduce mass loading error not the mode shape observability.

9.2 Case 2 and 3: Minimization of the MSOE and ODP and the Total Cost

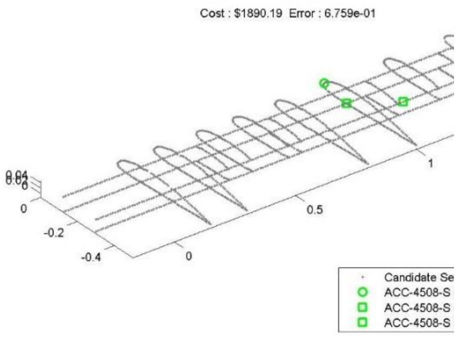

(a)

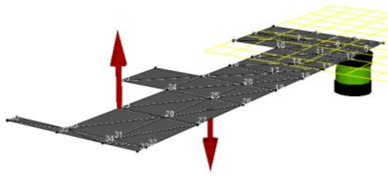

(b)

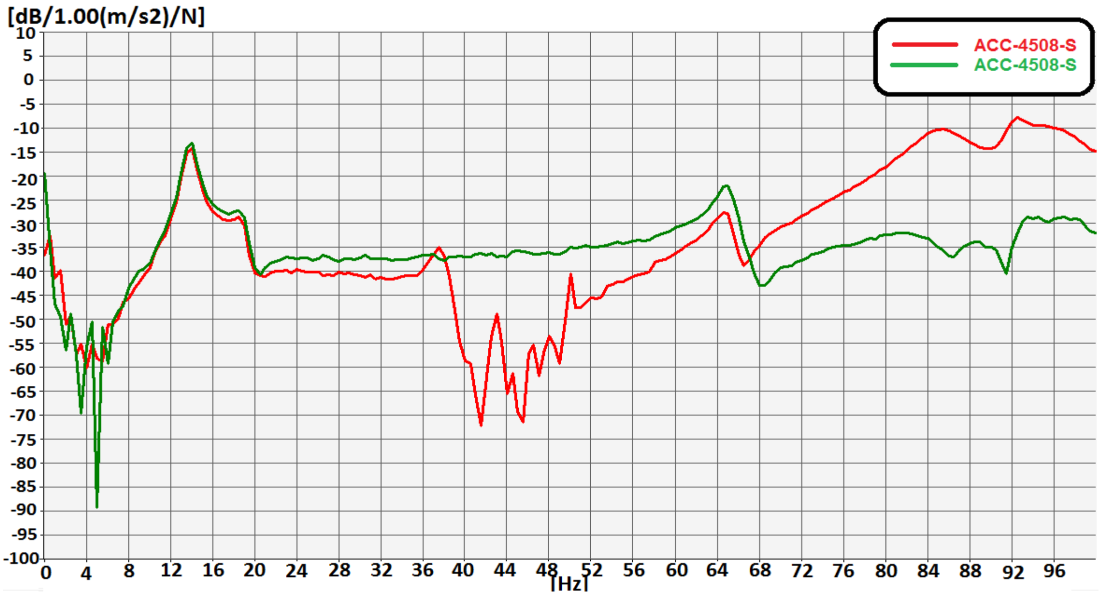

(c)

Figure continues in next page

Configuration	Resonance Frequencies[Hz]		
	1. Mode	2. Mode	3. Mode
MSO (A)	14.00	65.00	93.50

(d) (e)

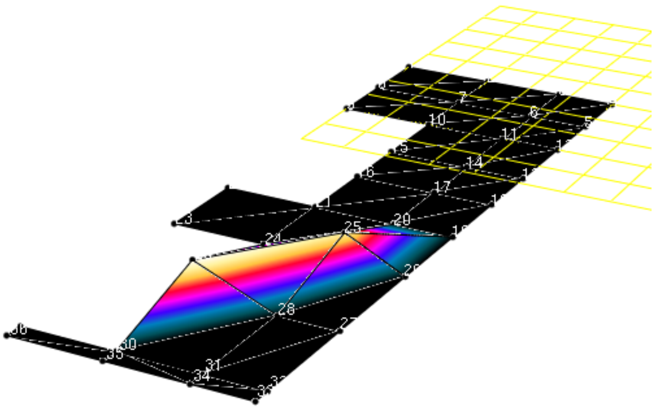

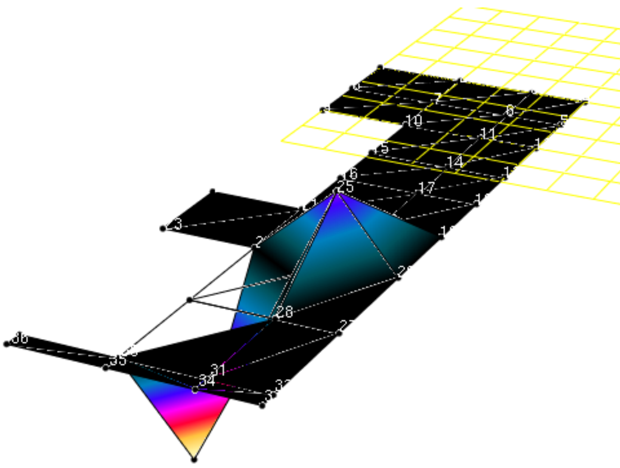

Figure continues in next page

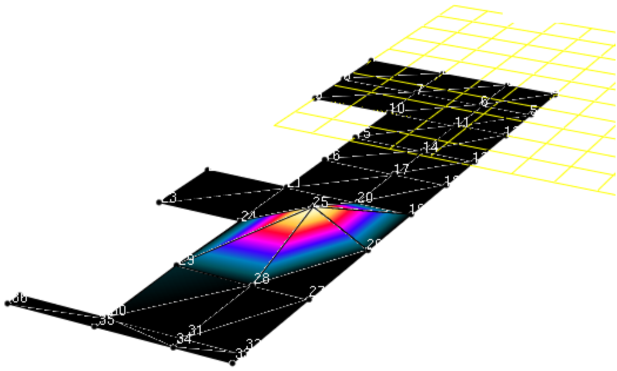

(f)

Figure 43 Mode Shape Observability - Configuration A [Out of Plane] [UAV Wing] (a) Configuration Obtained from Optimization (b) Configuration in B&K Modal Test Consultant (c) Accelerance FRF (d) Test Setup (e) Resonance Frequencies Obtained (f) Mode Shapes Observed from One Measurement

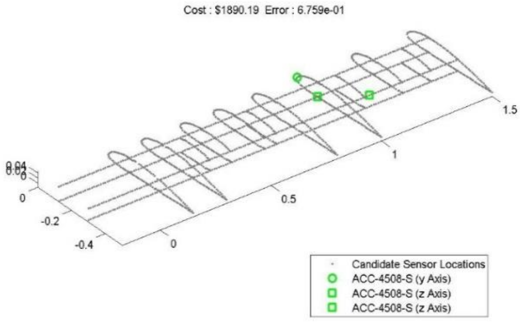

(a)

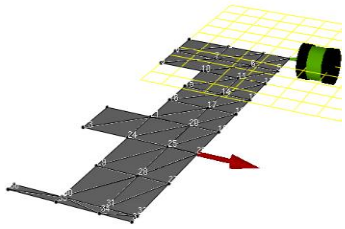

(b)

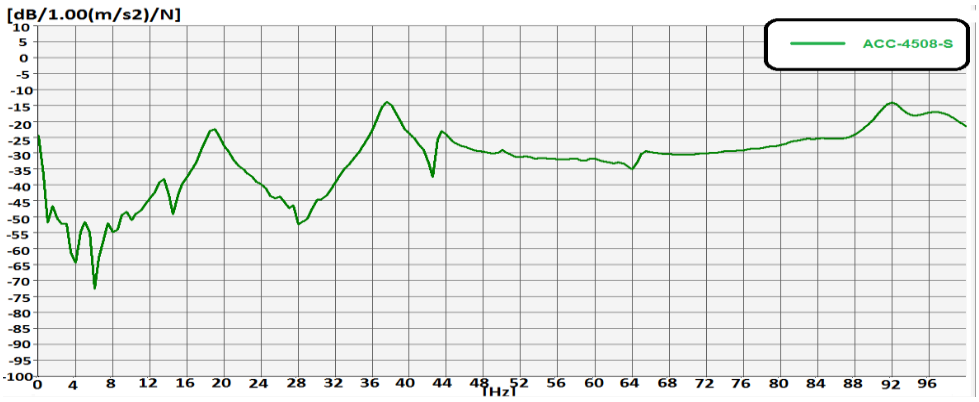

(c)

(d)

Configuration	Resonance Frequencies[Hz]
	1. Mode
MSO (A)	43.50

(e)

Figure continues in next page

Figure 44 Mode Shape Observability - Configuration A [In-Plane] [UAV Wing] (a) Configuration Obtained from Optimization (b) Configuration in B&K Modal Test Consultant (c) Accelerance FRF (d) Test Setup (e) Resonance Frequencies Obtained

In Figure 43 and Figure 44, it is shown that in the cheapest configuration of mode shape observability, only three heavy but cheap accelerometers were selected. Two of the accelerometers are placed in a way to captured 1st out of plane bending and 1st torsion mode shapes and one accelerometer was selected in the in-plane direction to capture 1st in-plane mode shape. As it was expected that the modal shaker was selected by optimization because of the price limit. It was shown in above figures that this configuration, which is the cheapest, was not able to capture the out of plane modes in a good fashion because of insufficient number of accelerometers.

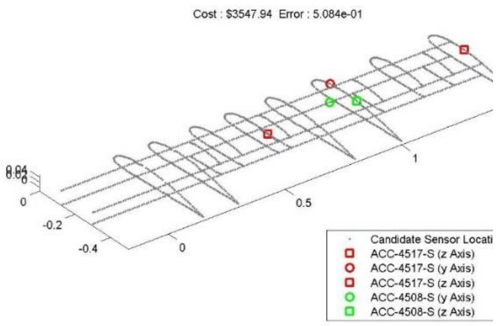

(a)

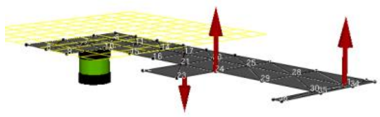

(b)

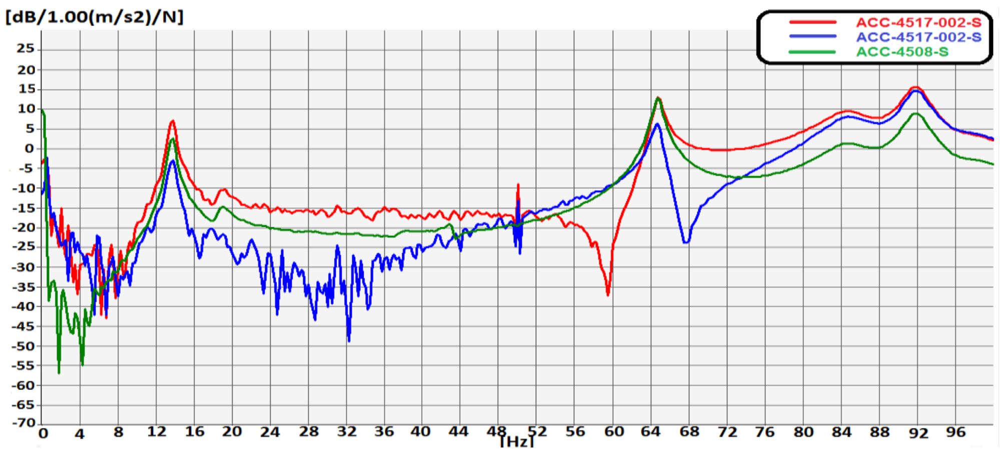

(c)

Figure continues on next page

(d)

Configuration	Resonance Frequencies[Hz]		
	1. Mode	2. Mode	3. Mode
MSO (C)	13.75	64.75	91.75

(e)

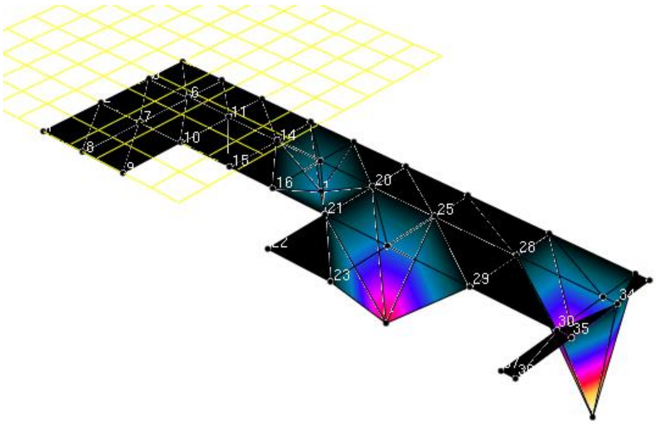

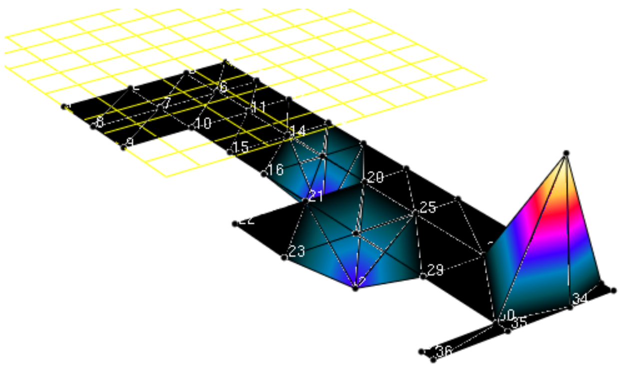

Figure continues on next page

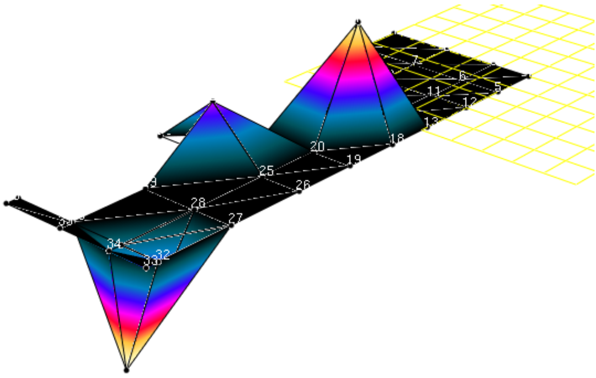

(f)

Figure 45 Mode Shape Observability - Configuration C [Out of Plane] [UAV Wing] (a) Configuration Obtained from Optimization (b) Configuration in B&K Modal Test Consultant (c) Accelerance FRF (d) Test Setup (e) Resonance Frequencies Obtained (f) Mode Shapes Observed from One Measurement

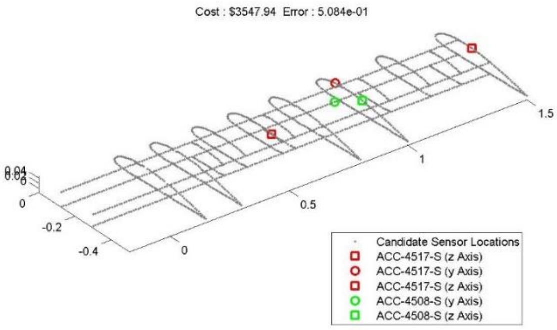

(a)

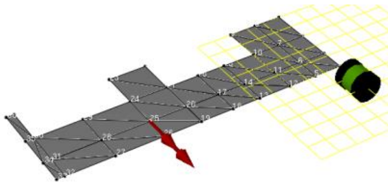

(b)

Figure continues on next page

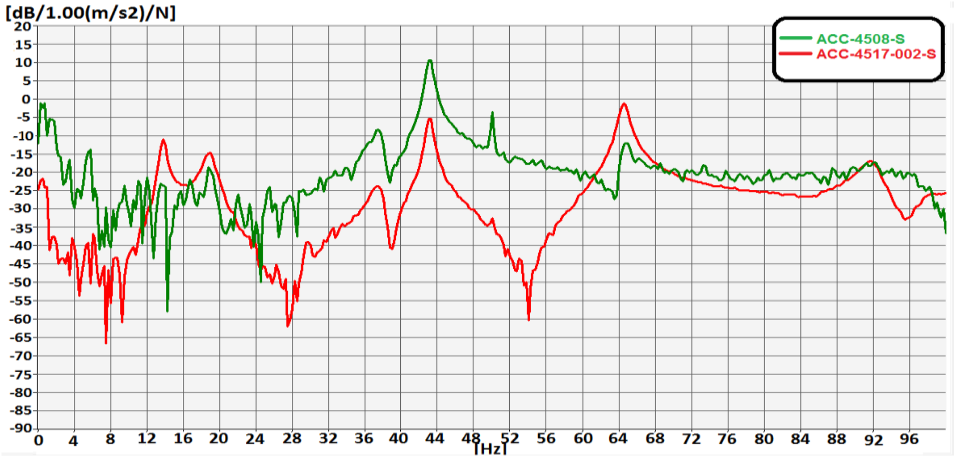

(c)

(d)

Configuration	Resonance Frequencies[Hz]
	1. Mode
MSO (C)	43.50

(e)

Figure continues on next page

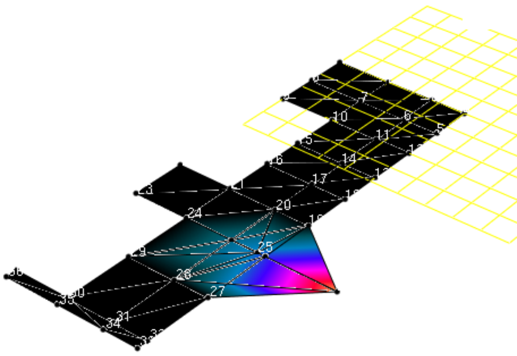

(f)

Figure 46 Mode Shape Observability - Configuration C [In-Plane] [UAV Wing] (a) Configuration Obtained from Optimization (b) Configuration in B&K Modal Test Consultant (c) Accelerance FRF (d) Test Setup (e) Resonance Frequencies Obtained (f) Mode Shapes Observed from One Measurement

In Figure 45 and Figure 46, the most expensive mode shape observability was shown. As it is evident from the results that all three out-of-plane and one in-plane mode shapes were successfully captured. Three out-of-plane accelerometers were selected and placed in a triangular shape (just like in the fin-like plate) to capture all out-of-plane mode shapes. Two accelerometers were also placed in the in-plane direction to capture in-plane bending mode shape.

9.3 Case 4: Minimization of the Overall Equivalent Error and the Total Cost

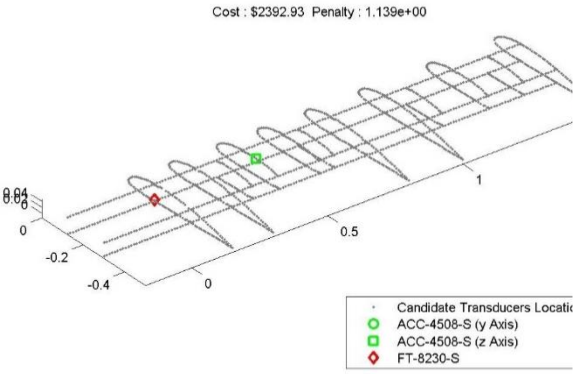

(a)

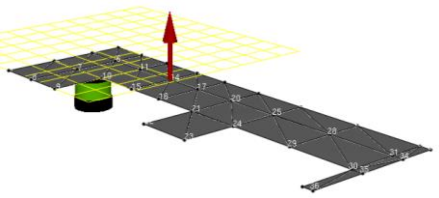

(b)

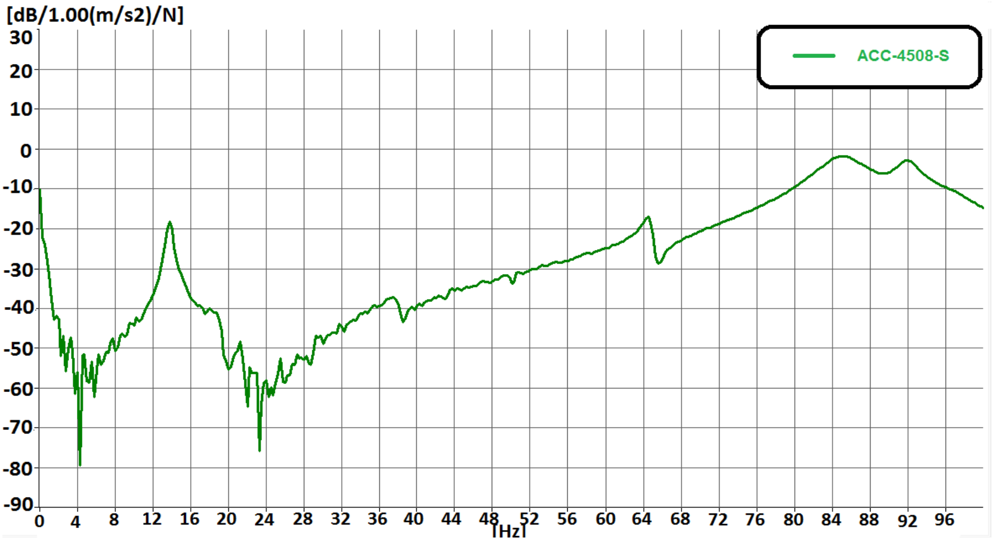

(c)

Figure continues on next page

(d)

Configuration	Resonance Frequencies[Hz]		
	1. Mode	2. Mode	3. Mode
Total Error (A)	13.75	64.50	92.00

(e)

Figure 47 Total Error - Configuration A [Out of Plane] [UAV Wing] (a) Configuration Obtained from Optimization (b) Configuration in B&K Modal Test Consultant (c) Accelerance FRF (d) Test Setup (e) Resonance Frequencies Obtained

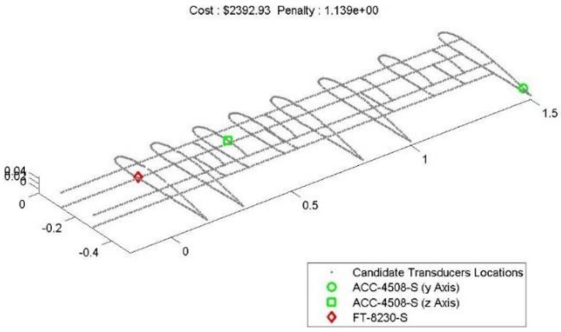

(a)

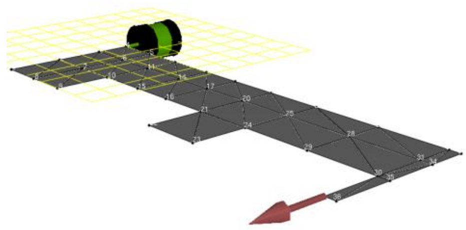

(b)

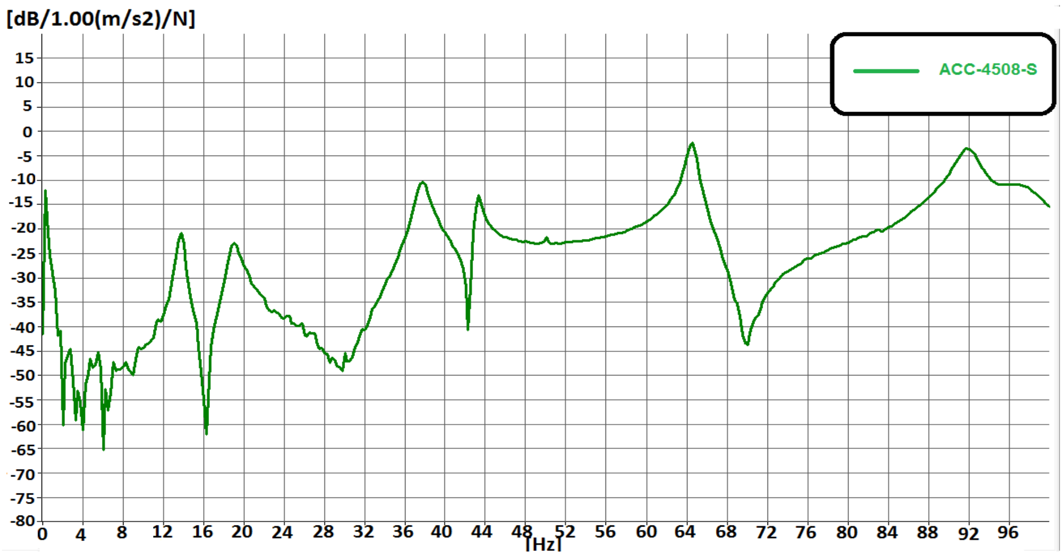

(c)

Figure continues on next page

(d)

Configuration	Resonance Frequencies[Hz]
	1. Mode
Total Error (A)	43.25

(e)

Figure 48 Total Error - Configuration A [In-Plane] [UAV Wing] (a) Configuration Obtained from Optimization (b) Configuration in B&K Modal Test Consultant (c) Accelerance FRF (d) Test Setup (e) Resonance Frequencies Obtained

In Figure 47 and Figure 48, the test results of the cheapest configuration of total error optimization are depicted. As it was expected that two heavy accelerometers were selected and they were located near the clamp area of the wing just like in the case of mass loading error but this time they are slightly away from the clamp part to be able capture the 1st in-plane and 1st out-of-plane bending mode shapes. Again, the modal shaker was selected to minimize the shaker-structure interaction error.

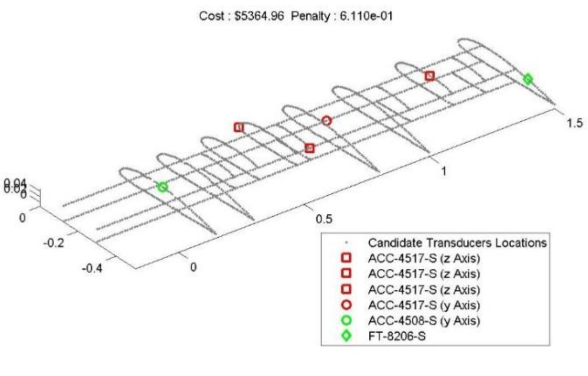

(a)

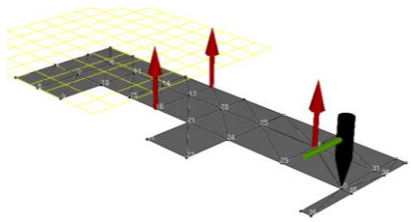

(b)

Figure continues on next page

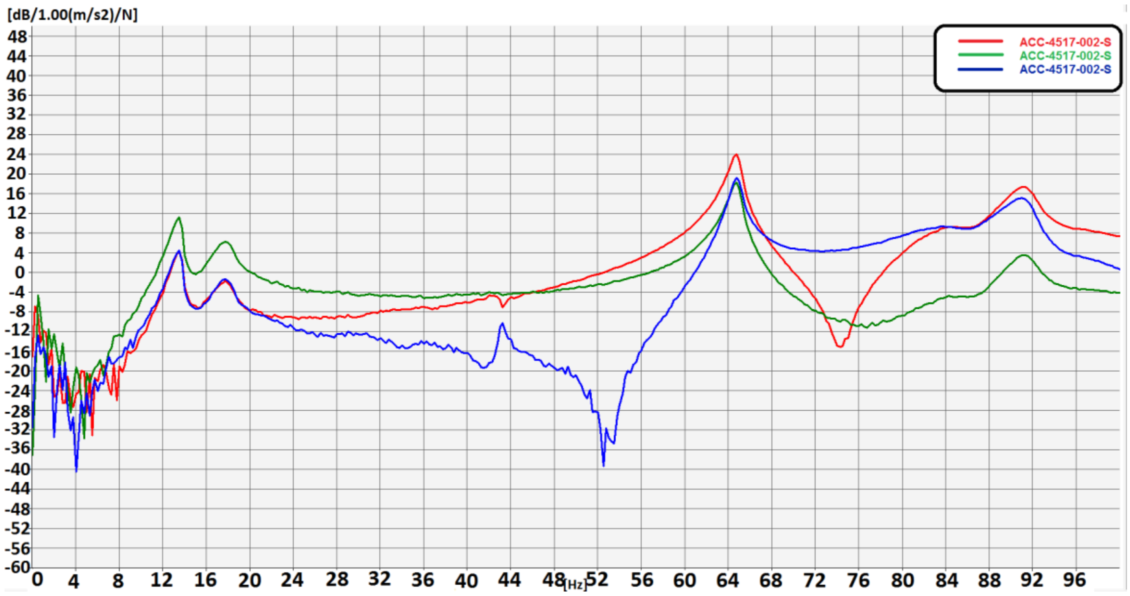

(c)

(d)

Configuration	Resonance Frequencies[Hz]		
	1. Mode	2. Mode	3. Mode
Total Error (F)	13.50	64.75	91.25

(e)

Figure continues on next page

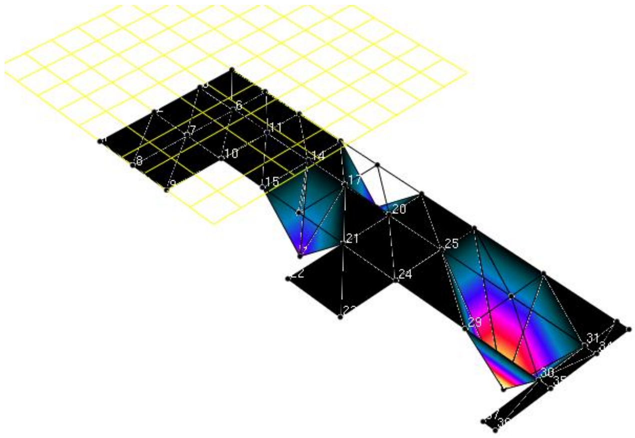

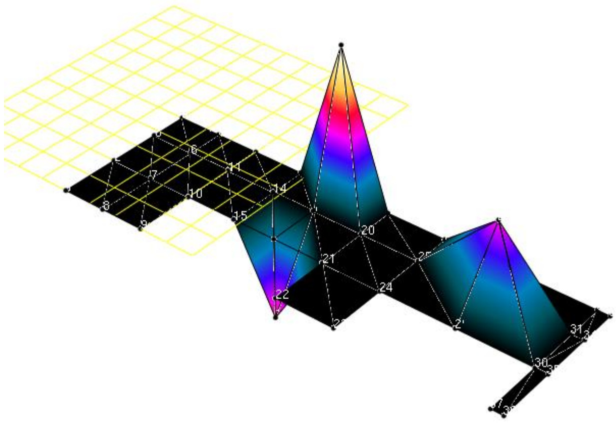

Figure continues in next page

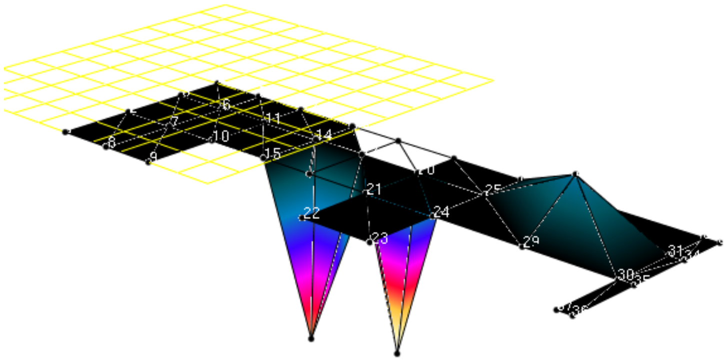

(f)

Figure 49 Total Error - Configuration F [Out of Plane] [UAV Wing] (a) Configuration Obtained from Optimization (b) Configuration in B&K Modal Test Consultant (c) Accelerance FRF (d) Test Setup (e) Resonance Frequencies Obtained (f) Mode Shapes Observed from One Measurement

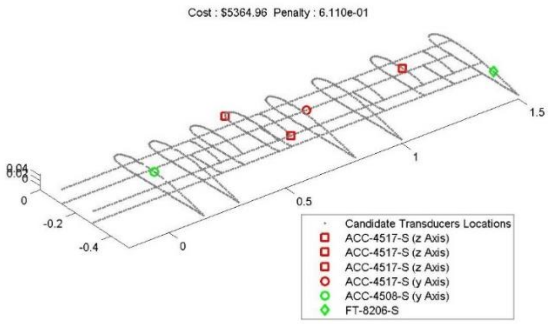

(a)

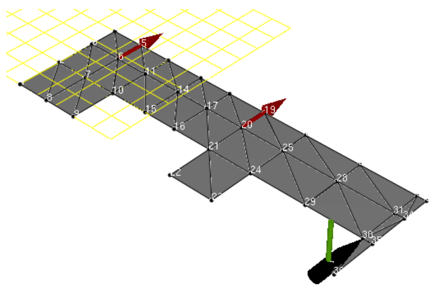

(b)

Figure continues in next page

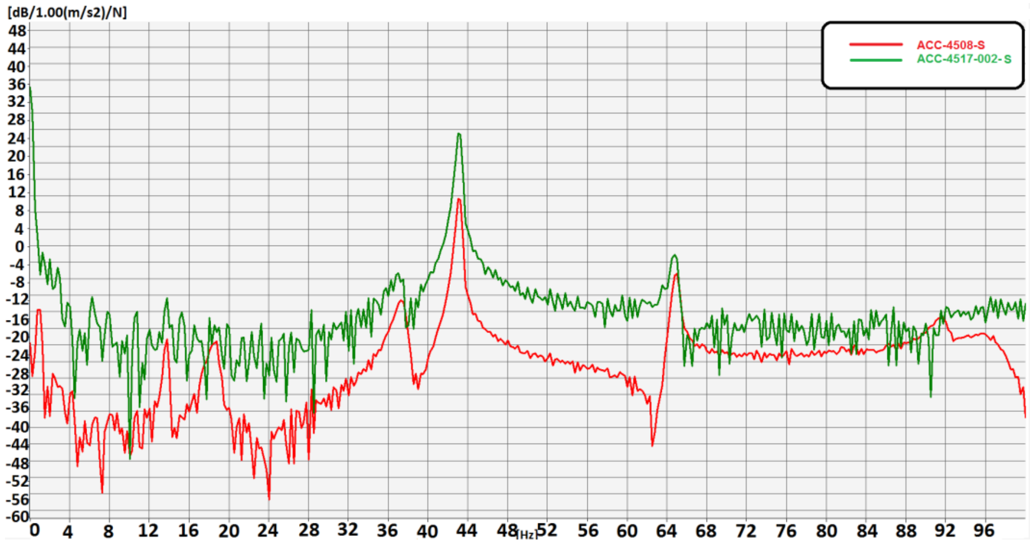

(c)

(d)

Configuration	Resonance Frequencies[Hz]
	1. Mode
Total Error (F)	43.00

(e)

Figure 50 Total Error - Configuration F [In-Plane] [UAV Wing] (a) Configuration Obtained from Optimization (b) Configuration in B&K Modal Test Consultant (c) Accelerance FRF (d) Test Setup (e) Resonance Frequencies Obtained

In Figure 49 and Figure 50, the test results of the most expensive case of total error optimization are shown. In this configuration, three lightweight accelerometers sensitive to the out of plane modes were selected and placed in a triangular shape (as in the fin-like plate case) to capture all out-of-plane mode shapes. Two accelerometers were also located on the area closer to the leading edge of wing in order to capture the 1st and the 2nd in-plane bending mode shapes.

CHAPTER 10

CONCLUSION

10.1 Concluding Marks of This Thesis

Before performing any experimental modal test, a pre-test analysis is an important step to reduced time, cost of test and increase quality of data gathered during modal test. In this study [29][30][31] a multi optimization based on genetic algorithm was done in which types, numbers and locations of transducers used in modal test of trapezoidal fin-like plate were optimized. Three different problems which test engineers are faced with during a modal test are considered in this research which were mass loading, mode shape observability and optimum driving point. Mass loading (ML) is an error which is caused by addition of extra mass of transducers to the original structure. This will interfere with results of original structure and to avoid this it was tried to place transducers near areas close to nodal lines or close to clamped side of the plate (because those areas will have minimum effect on modal masses). Mode shape observability (MSO) is a measure of distinguishability of mode shapes of interest with one SIMO test. In some cases it is just required to have a general idea about mode shapes without performing a roving impact hammer or accelerometer test. Considering mode shape observability is of profound importance in those cases.

Optimum driving point (ODP) is also an indicator which was used to locate areas with minimum velocity and acceleration. Because areas with high velocity have higher probability of double hit when using impact hammer and areas with high acceleration will have more interference from attached shaker at point of connection (local stiffening). There were four different multi objective optimizations in which all of these problems were formulated as an error in objective functions. Using multi-objective genetic algorithm optimization toolbox of MATLAB, MSC©NASTRAN finite element solver and some extra MATLAB scripts, a Pareto frontier set was found for all optimization cases. These Pareto frontier sets are of great help to a test engineer during modal test. As it was expected with higher cost algorithm did not chose lots of accelerometers and that is because of mass loading error. In all of Pareto solutions, it was tried to capture all three mode shapes of interest with minimum mass loading error. Usually three accelerometers suffice for that purpose (lightest ones selected for higher cost). ODP also forced optimization to place excitation location near clamped area of plate which has lowest velocity and acceleration respect to other areas of plate.

Moreover, the following conclusions can be drawn from the experimental modal analyses results. In the Mass Loading Error - Configuration A (the cheapest option) case, due to having a sensor and an actuator transducer very close to nodal lines and/or to clamped side of the plate, the first out-off-plane bending mode is not captured and disappeared from the FRF. When the excitation location is changed and the sensor is replaced in the Mass Loading Error - Configuration C case (the most expensive option), this particular mode is detected. When the Mode Shape Observability Error - Configuration A (the cheapest option) case is compared with that of Configuration G case (the most expensive option), the second-out-off plane bending mode is also observed. Finally, in the case of Total Error, both the Configuration A (the cheapest option) and the Configuration G case (the most expensive option) provide quite high values for the accelerance responses at the each resonance by also providing a better observability in each mode as well. Finally, it is observed from the optimisation and the experimental verification results that the proposed approached is a realizable one which could be used in the ground vibration tests of aircraft structures.

10.2 Future Work

In this study the main focus was on finding a test setup which leads to cheapest and accurate enough results to get an overall idea about modal characteristics of structure. This research can be further developed by focusing on pipeline or workflow of test. For example, in case of modal test of large structures like airplane, to reduce the distance a test engineer needs to walk to access all of excitation locations can be minimized by adding an extra objective function similar to traveling salesman problem (TSP).

This algorithm can be generalized and automated to perform this optimization over any structure by just importing mesh data and available transducers and data acquisition channel limitation. Another improvement could be also taking into account the direct and cross sensitivities of accelerometers rather than just their weight, measuring directions and price.

REFERENCES

[1] P. C. Shah and F. E. Udwadia, “A Methodology for Optimal Sensor Locations for Identification of Dynamic Systems,” J. Appl. Mech., vol. 45, p. 188, 1978.

[2] D. C. Kanner, “*Sensor Placement for On-Orbit Modal Identification and Correlation of Large Space Structures,”* Am. Control Conf., vol. 14, pp. 251–259, 1990.

[3] L. Yao, W. a. Sethares, and D. C. Kammer, “Sensor placement for on-orbit modal identification of large space structure via a genetic algorithm,” IEEE Int. Conf. Syst. Eng., vol. 31, pp. 1922–1928, 1992.

[4] F. E. Udwadia, *“Methodology for Optimum Sensor Locations for Parameter Identification in Dynamic Systems,”* J. Eng. Mech., vol. 120, no. 2, pp. 368–390, 1994.

[5] P. H. Kirkegaard and R. Brincker, “*On the optimal location of sensors for parametric identification of linear structural systems,”* Mech. Syst. Signal Process., vol. 8, pp. 639–647, 1994.

[6] J. E. T. Penny, M. I. Friswell, and S. D. Garvey, *“Automatic choice of measurement locations for dynamic testing,”* AIAA J., vol. 32, pp. 407–414, 1994.

[7] R. M. Rao and G. Anandakumar, “*Optimal placement of sensors for structural system identification and health monitoring using a hybrid swarm intelligence technique,”* Smart Mater. Struct., vol. 16, no. 6, pp. 2658–2672, 2007.

[8] T. Van Langenhove and M. Brughmans, *"Using MSC/Nastran and LMS/Pretest to find an optimal sensor placement for modal identification and correlation of aerospace structures.,"* in LMS International Belgium, 1999, Belgium

[9] I. T. J. Peck, "*A DMAP Program for the selection of accelerometer locations in MSC/ NASTRAN,"* in Proceedings of the 45th AIAA/ASME/ASCE/AHS/ASC Structures, 2004.

[10] "MATLAB." [Online]. Available: http://www.mathworks.com/products/matlab/., Accessed on Dec 2015

[11] "MSC®NASTRAN." *[Online]. Available: http://www.mscsoftware.com/product/msc-nastran.*, Accessed on Dec 2015

[12] N. Imamovic a, "*Validation of large structural dynamics models using modal test data,"* 1998, Imperia College, UK

[13] Chen, X., Zhang, Y., Zhang, Y., and Jiang, M., *"Hanger Location Design and Vibration Isolation of an Exhaust System,"* SAE Technical Paper 2014-01-1708, 2014, USA

[14] W. Gressick, John T. Wen," *Order Reduction of Large Scale Finite Element Models: a System Perspective"*,pp. 337 -362, Multi Scale Computational Engineering, 2005, USA

[15] Evgenii B. Rudnyi and Jan G. Korvink,*" Model order reduction for large scale finite element engineering models"*, TU Delft, 2006, Netherland

[16] Z.-Q. Qu, "*Model Order Reduction Techniques with Applications in Finite Element Analysis," pp. 47–50.*, *Springer*, 2004, USA

[17] Z.-Q. Qu, *Model Order Reduction Techniques with Applications in Finite Element Analysis*. pp. 151–162., Springer, 2004, USA

[18] D. J. Ewins, "*Modal testing: theory, practice, and application"* pp. 425-426, Wiley, 1984, USA

[19] "MSC®PATRAN." *[Online]. Available: http://www.mscsoftware.com/product/patran.* ., Accessed on Dec 2015

[20] "8206 – Impact hammer." *[Online]. Available: http://www.bksv.com/P*roducts/transducers/vibration. ., Accessed on Dec 2015

[21] "4517 - Miniature tear-drop CCLD accelerometer." *[Online]. Available: http://www.bksv.com/.*., Accessed on Dec 2015

[22] "B&K Pulse Labshop." *[Online]. Available: http://www.bksv.com/products/pulse-analyzer/pulse-platform/pulse-labshop.aspx.* ., Accessed on Dec 2015

[23] "7753 – Modal test consultant." *[Online]. Available: http://www.bksv.com/products/analysis-software/vibration/structural-dynamics/classical-modal-analysis/modal-test-consultant-7753.* ., Accessed on Dec 2015

[24] "B&K Pulse Reflex." *[Online]. Available: http://www.bksv.com/Products/pulse-analyzer/pulse-platform/pulse-reflex-core.aspx.* ., Accessed on Dec 2015

[25] "FEMTools." *[Online]. Available: http://www.femtools.com/.* ., Accessed on Dec 2015

[26] M. Mitchel, "*An Introduction to Genetic Algorithms*", MIT Press, 1998, USA

[27] K. Deb,"*Multi-Objective Optimization Using Evolutionary Algorithms*", Wiley, 2001, USA

[28] Y. Yaman et al *“Aeroservoelastic Analysis of the Effects of Camber and Twist on Tactical Unmanned Aerial Vehicle Mission-Adaptive Wings”* TÜBİTAK 107M103, 2007

[29] N. Pedramasl, M. Şahin, E. Acar, "*Multi-Objective Optimization of Types, Numbers and Locations of Transducers used in Modal Test of a Fin-Like Structure",* Tokyo International Conference on Engineering and Applied Science, December 2014, Tokyo, Japan

[30] N. Pedramasl, M. Şahin, E. Acar, "*Multi-Objective Optimization of Transducers used in Modal Test of an Unmanned Aerial Vehicle Wing",* International Conference on Advances in Vibrations, 30 March -1 April 2015, Porto, Portugal

[31] N. Pedramasl, M. Şahin, E. Acar, "*Simulation-Based Optimal Sensor/Actuator Positioning on a Fin-Like Structure ",*16th AIAA/ISSMO Multidisciplinary Analysis and Optimization Conference,22-26 June 2015, Dallas, TX, USA